



UNIVERSITY OF BERGAMO

DEPARTMENT OF ENGINEERING AND APPLIED SCIENCES

Sustainable Alkali-Activated Slag mortars: Study of durability and smart properties

Doctoral Dissertation of

Elena Crotti

Supervisor:

Prof. Luigi Coppola

Tutor:

Prof. Tommaso Pastore

XXXIV Cicle – 2018/2021

Ringraziamenti

Questa tesi di dottorato è il risultato del supporto di diverse persone alle quali sono estremamente grata. Prima di tutto ringrazio il mio supervisor Luigi Coppola sia per la sua eccellente e straordinaria professionalità che, cosa più importante, per la grande attenzione che personalmente mi ha riservato. Sono anche grata per la collaborazione, il supporto e i consigli del mio tutor Tommaso Pastore con Marina Cabrini e Sergio Lorenzi.

Ringrazio di cuore tutti i colleghi del Laboratorio dell'Università di Bergamo per la loro partecipazione attiva alla ricerca presentata in questa tesi.

Sono anche profondamente riconoscente per il duro lavoro di revisione del mio collega Denny Coffetti che ha contribuito con le sue idee e le sue intuizioni a migliorare gli studi presentati in questa tesi. A Denny e Gabriele Gazzaniga anche il merito di aver sempre promosso un ambiente amichevole e piacevole dove lavorare.

Abstract

Alkali-activated materials (AAM) are a category of inorganic binders that involve the reaction of a substance containing alkali metals with a solid powder substance, containing alumino-silicates, with different levels of calcium oxide. Such reactive powders can be of natural origin, such as metakaolin, or a by-product of other processes, such as fly ash and ground granulated blast furnace slag. A sub-category of these materials are the “geopolymers”, in which the reactive powder consists of alumino-silicates and low percentage of calcium. There is an area in which alkali-activated binders have certainly higher performances if compared with their Ordinary Portland Cement (OPC) counterparts: the reduction of the carbon footprint and the energy saving. However, the reduction of the amount of CO₂ generated, energy used and natural raw materials consumed is an efficient strategy with a view to sustainability but it could be totally ineffective if durability and performance are not also evaluated. The use of concrete defined as “smart” is fully part of the concept of sustainability, in fact, thanks to the addition of nanoparticles can improve mechanical and physical performance, improve durability and reduce environmental impact. The study of alternative and sustainable materials is also a fundamental concept with regard to the conservation of historical building heritage, as it is possible to realize materials that are chemically and physically compatible with historical masonry.

This thesis presents the research carried out on the development and characterization of one-part alkali-activated slag mortars for traditional and innovative application. The mortars were tested and compared in terms of specific mass, workability, air content, dynamic modulus of elasticity and compressive strength. Freezing and thawing resistance, calcium chloride resistance, magnesium sulphate attack resistance, carbonation resistance, sulfuric acid resistance, water permeability, self-sensing capacity and self-cleaning ability were also investigated. The experimental results show that the key parameter that governed most of the properties both in fresh and hardened state of this materials is the alkali content: the higher the alkali content, the higher the strength and the resistance to severe conditions. In particular, high alkali-content AAS mortars evidence a freeze-thaw resistance similar to that of blast furnace-based mixtures. Furthermore, the use of AEA enhances the freezing and thawing resistance of alkali-activated slag-based mortars without any strong reduction in compressive strength. The AAS mixtures are quasi-immune to expansive calcium oxychloride formation in presence of CaCl₂-based deicing salts due to the negligible calcium hydroxide content. On the other hand, these conglomerates suffer from severe damages and high strength loss as a consequence of

semi-immersion in 10 wt% Mg_2SO_4 solution due to decalcification of C-S-H gel and gypsum formation. The resistance to carbonation of the AAS is related to its strength: the higher the compressive strength, the greater the carbonation resistance. Also, alkali-activated slag show higher acid corrosion resistance compared to Portland cement, due to the absence of portlandite and low Ca/Si ratio in the binder. Moreover, alkali-activated mortars seem to be a reasonable alternative to traditional plaster for rehabilitation or restoration of ancient masonry buildings and existing concrete structures. Finally, alkali-activated slag mortars are also suitable to produce intelligent mixtures: it is possible to manufacture self-cleaning or self-sensing mortars with the addition of nanoparticles of titanium dioxide and carbon-based nanofillers, respectively.

Contents

RINGRAZIAMENTI	I
ABSTRACT	III
CONTENTS	V
TABLE OF FIGURES	IX
TABLE OF TABLES	XIII
PREFACE	1
CHAPTER 1.	5
ALKALI-ACTIVATED SLAG	5
1.1 STRUCTURE AND CHEMISTRY OF ALKALI-ACTIVATED SLAG	7
1.2 EFFECT OF THE ALKALINE ACTIVATORS	8
1.2.1 <i>Effect of OH⁻</i>	9
1.2.2 <i>Effect of Silicates</i>	10
1.2.3 <i>Effect of carbonates</i>	11
1.2.4 <i>Effect of sulfates</i>	12
1.3 BINDERS PROPERTIES OF ALKALI-ACTIVATED SLAG	13
1.3.1 <i>Fresh properties</i>	13
1.3.1.1 Setting time.....	13
1.3.1.2 Workability.....	14
1.4 MECHANICAL PROPERTIES	15
1.4.1 <i>Compressive strength</i>	16
1.4.2 <i>Tensile strength</i>	18
1.4.3 <i>Elastic modulus</i>	18
1.5 CURING CONDITIONS	20
1.6 APPLICATIONS OF ALKALI-ACTIVATED SLAG	20
1.6.1 <i>AAM for repair of existing masonry buildings and concrete structures</i>	21
1.7 CO₂ EMISSIONS	22
CHAPTER 2.	23
SUSTAINABILITY	23
2.1 CLIMATE CHANGE, POPULATION GROWTH AND CONCRETE INDUSTRY	23
2.2 STRATEGIES TO SUSTAINABLE CONCRETE	27

2.2.1	<i>Alternative binders to OPC-replacement</i>	27
2.2.2	<i>Smart and multifunctional concrete</i>	28
2.3	EDUCATION AND STANDARD	29
CHAPTER 3.		31
DURABILITY OF AAS.....		33
3.1	INTRODUCTION.....	33
3.1.1	<i>Resistance to freeze-thaw</i>	33
3.1.2	<i>Chloride penetration</i>	35
3.1.3	<i>Sulphate attack</i>	36
3.1.4	<i>Carbonation resistance</i>	37
3.1.5	<i>Acid attack</i>	39
3.1.6	<i>Permeability</i>	40
3.1.7	<i>Resistance to high temperature and fire</i>	41
3.1.8	<i>Alkali-silica reaction</i>	43
3.2	EXPERIMENTAL RESEARCH ON AAS MORTARS	44
3.2.1	<i>Materials</i>	44
3.2.2	<i>Mixtures, preparation and samples curing</i>	45
3.2.3	<i>Experimental methods</i>	46
3.2.3.1	Fresh state and elasto-mechanical properties	46
3.2.3.2	Freezing and thawing resistance	47
3.2.3.3	Calcium chloride resistance	47
3.2.3.4	Magnesium sulphate attack resistance	47
3.2.3.5	Carbonation resistance	48
3.2.3.6	Sulfuric acid resistance.....	48
3.2.3.7	Permeability	49
3.2.4	<i>Results and discussion</i>	50
3.2.4.1	Fresh state and elasto-mechanical properties	50
3.2.4.2	Freezing and thawing resistance	53
3.2.4.3	Calcium chloride resistance	57
3.2.4.4	Magnesium sulphate attack resistance	59
3.2.4.5	Carbonation resistance	61
3.2.4.6	Sulfuric acid resistance.....	63
3.2.4.7	Permeability	68
3.2.5	<i>Conclusions</i>	71

CHAPTER 4.	73
CEMENT-FREE ALKALI-ACTIVATED SLAG PLASTER	73
4.1 INTRODUCTION	73
4.2 EXPERIMENTAL PROGRAM	76
4.2.1 <i>Materials</i>	76
4.2.2 <i>Experimental methods</i>	77
4.2.2.1 Screening test	77
4.2.2.2 Improvement of rheological properties	78
4.2.2.3 Development of the plaster	79
4.2.3 <i>Results and discussion</i>	80
4.2.3.1 Screening test	80
4.2.3.2 Improvement of rheological properties	82
4.2.3.3 Development of the plaster	86
4.2.4 <i>Conclusions</i>	90
CHAPTER 5.	93
SMART AND MULTIFUNCTIONAL MORTARS	93
5.1 INTRODUCTION	93
5.2 EXPERIMENTAL RESEARCH ON SELF-SENSING CAPABILITY OF ALKALI-ACTIVATED SLAG MORTARS	94
5.2.1 <i>Materials</i>	95
5.2.2 <i>Mixtures, preparation and samples curing</i>	96
5.2.3 <i>Experimental methods</i>	97
5.2.4 <i>Results and Discussion</i>	99
5.2.4.1 General characterization of mortars	99
5.2.4.2 Electrical tests	100
5.2.4.3 Sensing tests	101
5.2.5 <i>Conclusions</i>	105
5.3 EXPERIMENTAL RESEARCH ON SELF-CLEANING CAPABILITY OF ALKALI-ACTIVATED SLAG MORTARS	106
5.3.1 <i>Materials</i>	108
5.3.2 <i>Mixtures, preparation and samples curing</i>	109
5.3.3 <i>Experimental Setup</i>	110
5.3.3.1 Fresh and Elasto-Mechanical Properties	110
5.3.3.2 Accelerated photocatalyst tests	110

5.3.3.3	Outdoor natural exposure	111
5.3.4	<i>Results and Discussion</i>	111
5.3.4.1	Fresh state and Elasto-Mechanical Properties.....	111
5.3.4.2	Accelerated photocatalyst test	115
5.3.4.3	Outdoor natural exposure	119
5.3.5	<i>Conclusions</i>	122
CONCLUSIONS		123
REFERENCES		125
ANNEX A		153
ANNEX B		157

List of figures

Figure 1-1. Number of papers published per year (2021)	6
Figure 1-2. Solubility of soluble silica in slag versus pH and amount of dissolved silica in aluminosilicates versus pH [10]	10
Figure 1-3. Viscosity of sodium silicate solutions versus mass ratio $\text{SiO}_2/\text{Na}_2\text{O}$	11
Figure 1-4. 1-day compressive strength of AAS manufactured with different activators (alkali content fixed). Data from [36].....	12
Figure 1-5. Influence of activator dosage in initial setting time of alkali-activated slag [38] .	14
Figure 1-6. Effect of modulus of sodium silicate in mini-slump of alkali activated slag cement pastes ($w/s = 0.4$)[8]	15
Figure 1-7. Compressive strength at 1 day of one-part alkali activated slag (the letter N represents the value of the module M_n and the letter M denotes the value of the M_s module) [44].	17
Figure 1-8. Splitting tensile strength of alkali activated slag concrete under different alkaline concentration [51]	18
Figure 1-9. Young's moduli and ultimate compressive strength of alkali-activated Materials[55]	19
Figure 2-1 Population evolution and estimation from 1950 to 2050. Data re-elaborated from [88]	25
Figure 2-2 - Embodied CO_2 and energy for construction materials. The radius of bubbles represents the worldwide production per year. Data re-elaborated from [90–92]	26
Figure 3-1 Elastic modulus loss of mortars as a function of number of freezing/thawing cycles [123]	34
Figure 3-2 Chloride diffusion coefficient (D_{nssd}) values measured for AAS concrete mixes (the first number indicated the percentage of Na_2O and the second the M_s ratio) [129].	35
Figure 3-3 Compressive strength reduction of AAS and OPC samples subjected to sulfate attack in 5% MgSO_4 or in 5% Na_2SO_4	37
Figure 3-4 Natural carbonation depths of aged silicate-activated slag concretes, as a function of mix design [139].....	38

Figure 3-5 Compressive strength of OPC and AAS mortars as a function of the time of exposure to pH 4.5 acetic acid [141]	40
Figure 3-6 Effect of liquid/solid ratio on permeability of AAS binders [66]	41
Figure 3-7 Residual compressive strength [152]. = ordinary Portland cement paste, 50/50 =blended 50% OPC/50% slag paste, AASP=alkali activated slag paste).	(OPCP 42
Figure 3-8 ASR expansion of the AAS mortars containing different alkali dosages, the numbers represents the weight percentage of activators [157]	43
Figure 3-9 XRD pattern of GGBFS	45
Figure 3-10 Schematic procedure for evaluating the durability of mortars in sulphate-rich aqueous solution	48
Figure 3-11 Ratio η between the compressive strengths of air-entrained mortars and mixtures produced without AEA at different ages	53
Figure 3-12 Superficial deterioration of specimens after 150 cycles	53
Figure 3-13 Mass loss of mortars as a function of numbers of freezing/thawing cycles	54
Figure 3-14 Strength loss of mortars as a function of numbers of freezing/thawing cycles	55
Figure 3-15 Elastic modulus loss of mortars as a function of numbers of freezing/thawing cycles	56
Figure 3-16 Optical microscopy observation of AAS8 before freeze/thaw cycles	56
Figure 3-17 PC specimen after 42 days in CaCl ₂ -rich solution	57
Figure 3-18 Mass change of specimens exposed to CaCl ₂ -rich solution	57
Figure 3-19 Compressive strength loss of specimens exposed to CaCl ₂ -rich solution	58
Figure 3-20 Efflorescence formation after 130 days in sulphate-rich solution	59
Figure 3-21 Efflorescence amount after 130 days in sulphate-rich solution	59
Figure 3-22 Compressive strength loss after 130 days in sulphate-rich solution	61
Figure 3-23 Carbonation depths of the alkali-activated mortars and Portland cement mortars	62
Figure 3-24 Effect of carbonation on variation of compressive strength	63

Figure 3-25 Minutes necessary for a sulfuric acid solution at pH=4 to reach a pH value equal to 7, as a function of volumetric ratio	64
Figure 3-26 pH variation of the 5% of sulfuric acid solution as a function of time	64
Figure 3-27 Superficial deterioration of specimens after 28 days in 5% of sulfuric acid	65
Figure 3-28 Mass change of specimens exposed to 5% sulfuric acid solution	66
Figure 3-29 Variation of compressive strength of specimens exposed to 5% sulfuric acid solution	67
Figure 3-30 Depth of lost alkalinity of specimens under 5% sulfuric acid attack	68
Figure 3-31 Capillary sorptivity curves of mortars as a function of time of curing. A) after 28 days of curing, B) after 90 days of curing	69
Figure 3-32 Water penetration depth	70
Figure 4-1 Ratio η between the compressive strength of air-entrained mortars and mixtures produced without AEA at different ages	84
Figure 4-2 Application test: Support (left), application of plaster S8 4:1 MEF (middle) and application of plaster S8 4:1_def	85
Figure 4-3 Free shrinkage of plaster up to 126 days	87
Figure 4-4 Test on a brick: S8 4:1 detached and S8 4:1_def adherent	87
Figure 4-5 Capillary water absorption of plaster	88
Figure 4-6 Raw material stored for 1 month in the paper bags	89
Figure 5-1 Nano-modified sample's preparation: dispersion of nano-fillers (a and b), mortar's preparation (c and d), curing (e)	97
Figure 5-2 Setup of electromechanical tests: (a) Sketch and (b) detail of sample and LVDTs	98
Figure 5-3 Compressive strength development of mortars	100
Figure 5-4 The 28-day compressive strength of mortars vs specific mass	100
Figure 5-5 Electrical tests: (a) sample during the tests, (b) electrical resistance of mortars ..	101
Figure 5-6 Electromechanical tests: (a) an instrumented sample during the tests; (b) load and stress history	102
Figure 5-7 Results of the electromechanical tests on normal and nano-modified samples: outputs of normalized variation of electrical resistance (a); strain variation (b)	103

Figure 5-8 Gauge factors obtained from electromechanical tests on all the samples	103
Figure 5-9 Analysis of the linearity of the signals	104
Figure 5-10 Fractional change in electrical resistance vs. applied strain for loading and unloading phase under cyclic compression loads for samples: (a) NEAT, (b) with carbon black (CB), (c) with graphite nanoplatelets (GNP), (d) with carbon nanofibers (NF)	105
Figure 5-11 Initial and final setting time of mortars	113
Figure 5-12 a% (extent of degradation) of RhB solution, previously deposited and dried on sample, under UV irradiation on standard and photoactive samples	115
Figure 5-13 b% (extent of degradation) of MB solution, previously deposited and dried on samples, under UV irradiation on standard and photoactive samples.....	116
Figure 5-14 Comparison of the results obtained for both dyes in samples	117
Figure 5-15 Difference in brightness (ΔL) between the part of mortar which was immersed in the carbon black solution and that not immersed	118
Figure 5-16 Correlation between water absorption and difference in brightness of mortars. .	119
Figure 5-17 Optical micrograph of S8	119
Figure 5-18 Lightness percent variation recorded on mortars during the 6 months	120
Figure 5-19 b* variation of specimens	122

List of tables

Table 3-1	Chemical composition and physical properties of binders	44
Table 3-2	Physical properties of aggregates	45
Table 3-3	Composition of mortars. PC: Portland cement-based mortars; BFC: Blast furnace cement-based mortars; AAS: Alkali activated slag-based mortars (the number indicates the activator to slag ratio by mass); AE: mortars containing AEA	46
Table 3-4	Summary of tested properties and sample details.....	49
Table 3-5	Fresh and hardened properties of mortars manufactured without AEA	51
Table 3-6	Fresh and hardened properties of mortars manufactured with AEA	52
Table 3-7	Capillary absorption coefficient k and total porosity at 28 and 90 days.....	69
Table 3-8	Karsten tube results.....	70
Table 4-1	Physical properties of aggregates	77
Table 4-2	Properties of admixtures	77
Table 4-3	Composition of mortars (nomenclature: S8: Alkali-Activated Slag plaster with alkaline reagents/binder ratio in mass equal to 8, the following number represents the aggregates/binder ratio) (GGBFS:ground granulated blast furnace slag).....	78
Table 4-4	Costs of the materials used	78
Table 4-5	Composition of mortars (M:methylcellulose + Modified starch, E: Air-entraining agent, F: fibers)	79
Table 4-6	Composition of mortars (M:methylcellulose + Modified starch, E: Air-entraining agent, F: fibers)	80
Table 4-7	Mortar's specimens manufactured for each test.....	80
Table 4-8	Properties of mortars at fresh state	80
Table 4-9	Properties of mortars at hardened state (** the mixture is not hardened enough to be demolded).....	81
Table 4-10	Costs of plasters	82
Table 4-11	Properties of mortars at fresh state	83

Table 4-12 Properties of mortars at hardened state	84
Table 4-13 Elastic modulus of plasters	85
Table 4-14 Properties of plaster at fresh and hardened state.....	86
Table 4-15 Properties of mortars at fresh and hardened state after 1 month of storage (IN:store in laboratory, OUT:stored outdoors, P: paper bag, PL:plastic bag, ** the mixture is not hardened enough to be demolded)	89
Table 4-16 Properties of mortars at fresh and hardened state after 2 months of storage (IN:store in laboratory, OUT:stored outdoors, P: paper bag, PL:plastic bag, ** the mixture is not hardened enough to be demolded)	90
Table 4-17 Costs of plasters	90
Table 5-1 Properties of aggregates	95
Table 5-2 Carbon fillers' characteristics (data provided by suppliers)	96
Table 5-3 Composition of mortars	97
Table 5-4 General properties of mortars	99
Table 5-5 Initial resistance R ₀ , Gauge Factor GF, Sensor Response SR and linearity of the tested samples.....	104
Table 5-6 Physical properties of aggregates	109
Table 5-7 Composition of mortars. WC: White cement-based mortars; GC: Portland cement-based mortars; S: Alkali-activated slag-based mortars (The number indicates the activator to slag ratio by mass; the number after the hyphen indicates the percentage of TiO ₂)......	109
Table 5-8 Fresh properties of mortars manufactured	112
Table 5-9 Hardened properties of mortars manufactured	114
Table 5-10 Elastic modulus of mortars manufactured	114
Table B - 1 Color intensity coordinates of WC specimens exposed South.....	157
Table B - 2 Color intensity coordinates of WC specimens exposed North.....	157
Table B - 3 Color intensity coordinates of GC specimens exposed South	158
Table B - 4 Color intensity coordinates of GC specimens exposed North	158
Table B - 5 Color intensity coordinates of S8 specimens exposed South.....	159

Table B - 6 Color intensity coordinates of S8 specimens exposed North.....	159
Table B - 7 Color intensity coordinates of S12 specimens exposed South.....	160
Table B - 8 Color intensity coordinates of S12 specimens exposed North.....	160
Table B - 9 Color intensity coordinates of S16 specimens exposed South.....	161
Table B - 10 Color intensity coordinates of S16 specimens exposed North.....	161

Preface

The production of Portland cement has a very strong environmental impact, since non-renewable resources are used and large quantities of carbon dioxide are emitted, the main greenhouse gas responsible for global warming of the planet and climate change that is felt today. For these reasons, the international scientific community is focusing on the search for alternative binders, with similar properties of Portland cement, but with a lower environmental impact.

Even with a basic knowledge of the concrete technology, it is quite simple to drastically reduce the environmental impact of a concrete. However, in many cases this would involve a strong reduction in the service life of the element made and/or a marked penalty of elasto-mechanical performance, with consequent failure to improve the sustainability of the material, but simply causing an extension of the environmental impact over time. For this reason, reducing the amount of carbon dioxide produced, the energy used and the natural raw materials consumed is an efficient sustainability strategy, but it could be completely ineffective if the durability and performance of the materials used are not also evaluated. The use of concrete defined as “smart” is fully part of the concept of sustainability, in fact, thanks to the addition of nanoparticles, mechanical and physical performance can be improved, as well as the durability and the environmental impact can be reduced. The study of alternative and sustainable materials is also a fundamental concept with regard to the conservation of historical building heritage, as it is possible to produce materials that are chemically and physically compatible with historical masonry.

The thesis deals with the study of the durability of sustainable conglomerates manufactured with alkali-activated slag, with the aim of identifying mixtures that ensure a resistance in aggressive environments comparable to that shown by traditional cements. The experimental tests were carried out in order to assess the behavior of the alkali-activated mixtures in different aggressive environments. Moreover, a Portland-free structural plaster has been studied in order to ensure elasto-mechanical compatibility with the historic masonry. The thesis also deals with the study of conglomerates defined “smart and multifunctional concrete”, a series of mixtures manufactured with the addition of

nanoparticles able to possess properties of “self-cleaning” or able to monitor the state of stress, evaluating the variations in electrical resistivity of the material.

In particular, in the third chapter the physical attack due to cycles of freeze and thaw has been studied. The resistance to freeze and thaw cycle is an important factor influencing the durability of structures in cold regions. The deterioration of concrete structures appears with internal cracks, expansions, surface scaling and mass loss, that thereby reduce the service life of the buildings. In addition, resistance to calcium chloride-based deicing salts has been investigated, due to the fact that during the winter season on road, highway and airport thawing salts based on CaCl_2 are applied for the removal of ice. Resistance to aggression by chemicals agents present in soil and water and/or produced by bacterial action, such as magnesium sulphate and sulphuric acid has also been studied. In fact, of all the chemically aggressive agents for concrete structures, sulphate are undoubtedly among the most important both for the frequency with which the sulphate attack may occur and for the extremely negative consequences which they are capable of causing, like cracks, swelling and mass loss. Also sulphuric acid, a substance produced by the transformation of hydrogen sulphide, present in swamp or sewage waters, by aerobic bacteria can also severely degrade the concrete structures. Finally, since the chemical attack can be accelerated or aggravated by high water absorption, the penetration of water in these alternative mixtures has also been studied.

In the fourth chapter, the applicability of a structural plaster manufactured with alkali activated slag was studied. This plaster is able to overcome the structural problems of historic masonry, using a material that is physically, chemically and mechanically compatible and, at the same time, sustainable.

Finally, the last chapter deals with the study of conglomerates defined as “smart and multifunctional concrete”. In particular, photocatalytic mixtures have been manufactured with the addition of titanium dioxide nanoparticles to verify the self-cleaning capacity of these systems. The self-cleaning materials have the advantage of keeping the building surface clean, with a significant reduction in maintenance. In addition, the self-sensing capacity of alkali activated materials manufactured with the addition of several carbon-based nanofillers (nanotubes, nanofibers, carbon black and graphene nanoplatelets) was also assessed. In particular, carbon nanofillers can give the

mixtures piezoresistive properties, able to monitor the state of stress, evaluating the variations of electrical resistivity of the material.

CHAPTER 1.

ALKALI-ACTIVATED SLAG

Alkali-activated materials (AAM) are a category of inorganic binders that involve the reaction of a substance containing alkali metals (KOH, NaOH, Na_2SiO_3) with a solid powder substance, containing aluminosilicates, with different levels of calcium oxide. Such reactive powders can be of natural origin, such as metakaolin, or a by-product of other processes, such as fly ash and ground granulated blast furnace slag (GGBFS). A sub-category of these materials are the “geopolymers”, in which the reactive powder consists of aluminosilicates and low percentage of calcium.

The first use of alkali activation of aluminosilicate precursors in order to obtain an ordinary Portland cement alternative material is a patent of Kuhl in 1908. But it is only thanks to the studies of Glukhovsky in the 1950s that scientists and researchers began to talk about alkaline cements. Relevant changes took place in the 1970s with the finding of Davidovits [1] who coined the term “geopolymer” in 1979 having patented several aluminosilicate formulations. In 2009 Provis and van Deventer [2] summarized the state of art describing the process of transition from natural or synthetic powders to geopolymer-alumina-silicates. This is because in previous years more than one hundred research centers had been involved in the study of the AAMs, which, however, had coined different terms to indicate the same materials, making it difficult to uniform the acquired knowledge. In particular, some names that have been used to describe alkali-activated materials are “mineral polymers”, “soil cements”, “soil silicates”, “SKJ-binders”, “F-concretes”, “hydroceramics”, “zeoceramics”, “zeocements”, “inorganic polymers”, “inorganic polymer glass” and others.

Actually, there are a great number of scientific papers available in the literature which report the chemistry and properties of alkali-activated binder manufactured with

different raw materials. Figure 1-1 shows a quantification of the published memories per year in alkali activated materials and geopolymers and the impact they have generated in the scientific community. Research was made taking into account title, abstract and keywords in Scopus. Results are subdivided as a function of the precursor's nature: ground granulated blast furnace slag, fly ash (FA) and metakaolin (MK).

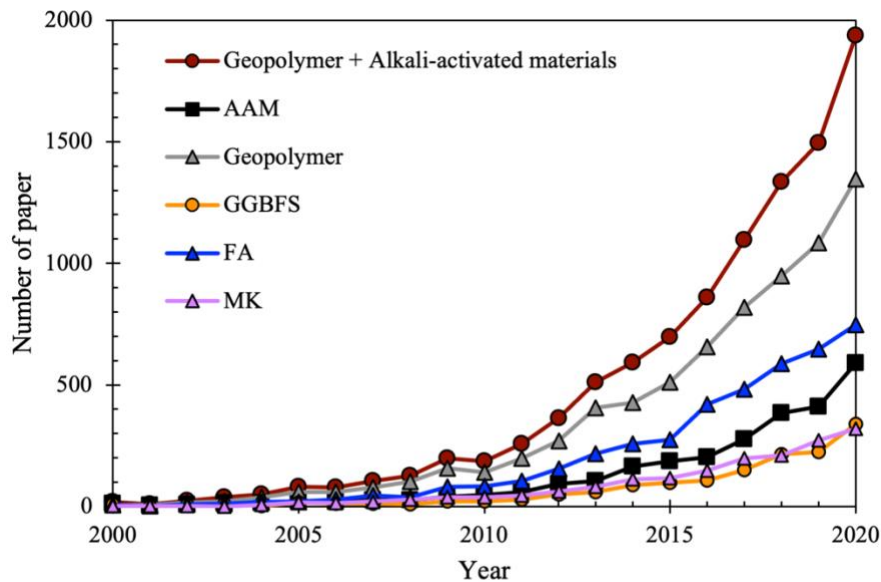


Figure 1-1. Number of papers published per year (2021)

Alkaline cements are cementitious materials formed as the result of an alkaline attack on the amorphous or vitreous aluminosilicates. When mixed with alkaline activators, these materials set and harden, yielding a material with good binding properties. The structural development of AAS mortars is a highly heterogeneous reaction process that is mainly governed by four mechanisms: dissolution of the glassy precursor particles, nucleation and growth of the initial solid phases, interactions and mechanical binding at the boundaries of the phases formed, and ongoing reaction via dynamic chemical equilibria and diffusion of reactive species through the reaction products formed at advanced times of curing [3–5]. The main reaction product, a C-S-H type gel, forms along with a series of secondary products. The type of secondary product generated depends on starting material composition, activator type and concentration, curing conditions and pH, among other [6,7].

1.1 Structure and chemistry of Alkali-Activated Slag

The material most commonly used to prepare calcium-rich alkaline cements and concrete is ground granulated blast furnace slag. This vitreous steel industry waste is formed when the acid oxides (SiO_2 and Al_2O_3) from the mix of acid clay gangue present in iron ore and sulfur ash in coke combine with the basic oxides (CaO and MgO) present in limestone or dolomite used as fluxes during high temperature (1600°C) smelting followed by abrupt cooling to temperatures of 800°C [8]. The majority components in slag are CaO (35-40%), SiO_2 (25-35%), MgO (5-10%) and Al_2O_3 (5-15%), while its minor constituents include S, Fe_2O_3 , MnO and K_2O (with percentages below 1%) as reported by Provis and van Deventer [9]. Generally, 90-95% of the GGBFS is vitreous (a depolymerized calcium silicate) and the rest of solid solution is formed by minor crystalline phases, such as gehlenite and akermanite [10]. Li et al. [11] affirmed that the vitreous phase content influences the reactivity of the slag in alkaline activation processes, and recommends values higher than 90%. Nevertheless, also slag with low vitreous phase contents (30-65%) could also deliver good results as reported by Pal et al. [12].

The hydraulic activity of ground granulated blast furnace slag is measured through parameters such as the basicity coefficient (K_b) and the quality coefficient (K_q):

$$K_b = \frac{\text{CaO} + \text{MgO}}{\text{SiO}_2 + \text{Al}_2\text{O}_3}$$

$$K_q = \frac{\text{CaO} + \text{MgO} + \text{Al}_2\text{O}_3}{\text{SiO}_2 + \text{TiO}_2}$$

The ideal values for basicity coefficient K_b are between 1.0 and 1.3, while quality coefficient K_q should be higher than 1.0 as reported by Pal et al. [12].

The optimal characteristics for having a blast furnace slag that can be used as a binder for mortars are as listed below:

- Vitreous phase content higher than 85-95% [13];
- CaO/SiO_2 ratio between 0.5 and 2.0 [14];
- $\text{Al}_2\text{O}_3/\text{SiO}_2$ ratio between 0.1 and 0.6 [15];

- Specific surface area equal to 400-600 m²/kg [16,17].

The chemical composition of the original raw material and its mineralogical characteristics are determinants in the formation of the C-S-H gels which strongly condition the mechanical properties and the durability of alkali-activated slag mortars and concretes. The characteristics of the gel formed can be evaluated and system performance predicted a priori by measuring the $(\text{CaO}/\text{SiO}_2)_{\text{reactive}}$ ratio [18]. This gel is similar to the product generated in normal Portland cement hydration, although its C/S ratio is lower than in latter. C-S-H gel ratios usually range from 0.9 to 1.2. The silica content of gels conditions their polymerization: the higher the silica content (lowering the C/S ratio) the longer the silica chains. The method to modifying the CaO/SiO₂ ratio is by adding soluble silica, with the alkaline activator, to the system. In particular, a rise in silica content leads to more densely packed, more polymerized gels with excellent mechanical properties (>80 MPa at 28 days [19,20]).

1.2 Effect of the Alkaline activators

The most critical role of the alkaline activator in an alkali-activated slag is therefore to accelerate this reaction to take place within a reasonable timeframe for the production of an engineering material, and this is most readily achieved by the generation of an elevated pH. In fact, by mixing GGBFS with water in the absence of alkaline activators, Taylor et al. reports that after 20 years of hydration only 22% of a rather coarsely -ground blast furnace slag proved to be sufficient reactive components for binder gel formation [21]. The alkaline activators normally used are alkaline salts or caustic solutions. Glukhovsky [22] classified activators by their chemical composition, identifying six groups: caustic solutions (MOH), slightly acid (M₂CO₃, M₂SO₃, M₃PO₄, MF), silicates (M₂O_xnSiO₂), aluminates (M₂O_xnAl₂O₃), aluminosilicates (M₂O_xAl₂O₃xSiO₂) and non-siliceous (M₂SO₄).

Cations and anions play distinctly different role in alkaline activation. The first ones play a significant role in alkaline activation, since they can be absorbed into the system, maintaining the pH values of the aqueous phase or forming part of the gel structure. The anions in the activating solution play an important role in the reactions taking place in the

systems and consequently in the mineralogical and microstructural characteristics of the materials synthesized. The anions that are normally mixed with the raw materials used to prepare alkaline cements are hydroxides, silicates, carbonates and, to a lesser extent, sulfates [10].

1.2.1 Effect of OH⁻

The presence of OH⁻ ions catalyzes the hydrolytic reactions and raises the pH to the values required for initial precursor dissolution and the subsequent condensation reactions. Figure 1.2 plots the percentage of soluble silica in slag versus pH: for pH between 3 and 11 silica solubility is low, but rises steeply at values below 3 and over 11 [23]. While slag solubility rises in acid media, the hydrates formed are unstable and form no consistent structures. On the contrary, basic pH not only favors slag dissolution but also the formation of stable hydrates, gradually raising the cementitious properties of the material. Very high OH⁻ concentrations are not favorable when slag is the raw material, however, unlike silica and alumina, calcium becomes less soluble with rising pH. In general, alkaline hydroxides are effective GGBFS activators at concentration ranging from 2M to 4M. Moreover, such high doses of alkalis may be detrimental, increasing efflorescence and rendering the material more brittle. In particular, the alkali activated slag with sodium activators shows more severe damage from efflorescence since increasing Na₂O in unreacted state causes a relatively easy movement of sodium ions in the aluminosilicate structure, as reported by Kang et al. [24]. However, Tang et al [25] report that the addition of Ca(OH)₂ decreases the concentration of Na⁺ from powder leaching of hardened AAS mortars.

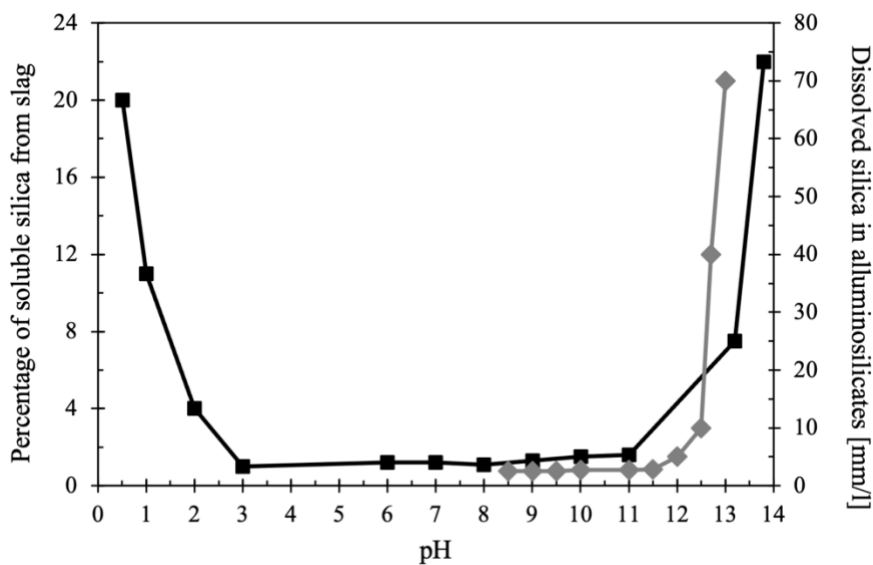


Figure 1-2. Solubility of soluble silica in slag versus pH and amount of dissolved silica in aluminosilicates versus pH [10]

1.2.2 Effect of Silicates

The availability of soluble silica is of cardinal importance in these systems, because it affects the workability, setting and mechanical strength development and modifies both gel composition and microstructure of the material formed. The general formula for these soluble silicate is: $x\text{SiO}_2/\text{R}_2\text{O}$, where $\text{R} = \text{Na}, \text{K}$ or Li and x = molar ratio. The most frequently used in alkaline activator is sodium silicate and the silicate solution can be modified by dilution in deionized water or by adding extra alkalis to change the molar ratio. At values of pH lower than 10, the solution begins to gel. The method most commonly deployed to control the $\text{SiO}_2/\text{Na}_2\text{O}$ ratio and raise the solution pH is to add alkalis, normally in the form of an NaOH solution, the result is known as waterglass ($x\text{SiO}_3 \cdot y\text{Na}_2\text{O} \cdot n\text{H}_2\text{O}$). In slag activation, waterglass is believed to make a dual contribution to strength development: as an alkaline activator and an inducer of the formation of high-silica primary gel. Depending on slag nature and fineness and curing conditions, the optimal Na_2O content is regarded to be around 4% of slag weight and the optimal SiO_2/NaO molar ratio on the order of 0.75 – 1.25 for acid slag, 0.9 – 1.3 for neutral slag and 1.0 – 1.5 for basic slag [26].

Several studies [27–29] have addressed the poor rheological properties of sodium-silicate AAS cementitious systems, that worsen with the increase of siliceous modulus and alkali concentration. Figure 1.3 presents the viscosities of sodium silicate solution as

a function of composition, at room temperature [30]. Due to the high viscosity, the finishing freshly placed sodium silicate-activated mortars can thus be problematic, because the sodium-containing AAM pastes tend to stick to concrete finishing equipment, and also to the sand and aggregate particles. Yang et al. [31] showed that the viscosities of sodium silicate solutions decrease markedly with increasing temperature. However, the solubility of some sodium metasilicate phases begin to decrease at elevated temperature, meaning that heating doesn't favor the preparation of activating solutions from solid metasilicates. Palacios et al. [32] showed that lengthening mixing time decreased the viscosity and improved the workability of sodium-silicate alkali-activated mortars.

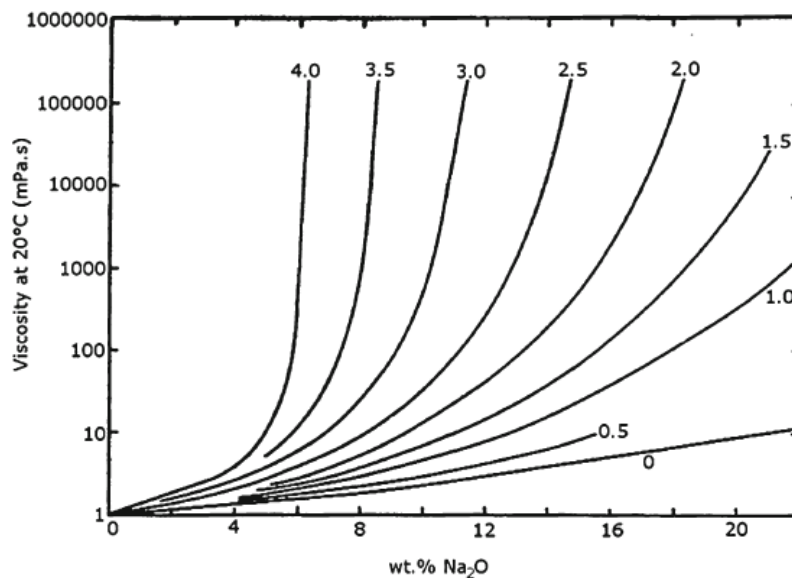


Figure 1-3. Viscosity of sodium silicate solutions versus mass ratio $\text{SiO}_2/\text{Na}_2\text{O}$

1.2.3 Effect of carbonates

The use of carbonates in the alkali-activated slag has gained interest because the production of these compounds has a lower environmental impact than that hydroxide or silicate solutions. This activator induces a lower pH than found in many alkali-activated binders systems, a potentially beneficial effect in terms of occupational health and safety [8]. At early age (< 4 days) there is a preferential reaction of Ca^{2+} with the CO_3^{2-} from the activator, forming calcium carbonate and gaylussite, while the aluminosilicate component of slag reacts separately with sodium ions from the activator to form zeolite NaA. These

phases do not give the high degree of cohesion necessary for development of high early mechanical strength (Figure 1-4), and the reaction is relatively gradual due to the slow dissolution of the slag under moderate pH conditions introduced by Na_2CO_3 as activator [33]. Xu et al. [34] assessed older GGBFS concretes activated with Na_2CO_3 and $\text{Na}_2\text{CO}_3/\text{NaOH}$ blends that had been gaining strength for years or decades. Moreover, provided that in Na_2CO_3 -activated slag, the long-term activation reaction is a cycles hydration process in which the Na_2CO_3 creates a buffered alkaline environment. The level of CO_3^{2-} available in the system would be maintained by the gradual dissolution of CaCO_3 in which the Ca released would react with the dissolved silicate from the GGBFS. The viscosities of Na_2CO_3 and NaHCO_3 solutions are unlikely to be problematic in handling or production; these do not exceed the viscosity of water by more than a factor of 5 up to saturation concentrations [35].

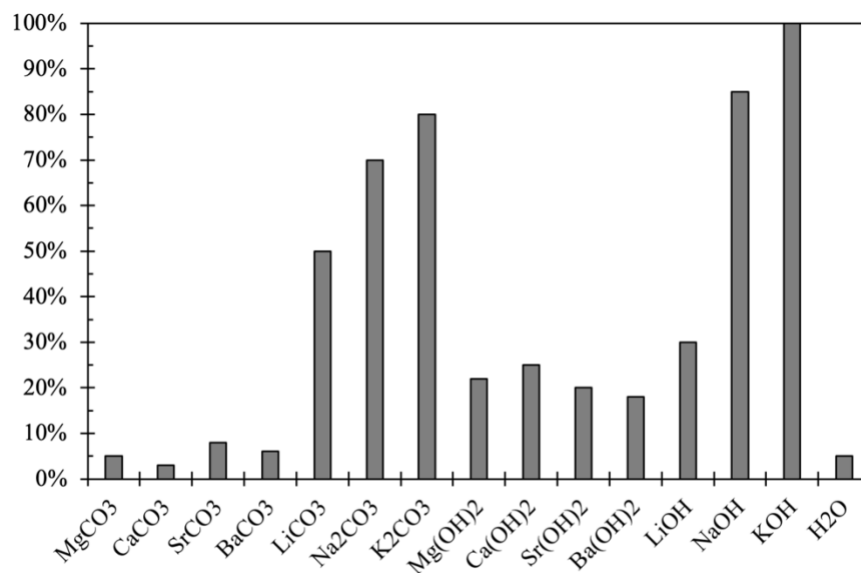


Figure 1-4. 1-day compressive strength of AAS manufactured with different activators (alkali content fixed). Data from [36]

1.2.4 Effect of sulfates

While sulfates are less commonly applied as activators, a few papers have been published on their use in slag activation [8]. Sulfate ions induce a less basic alkaline medium, lowering the amount of soluble silica released by the slag. Slag can be activated with a saturated Na_2SO_4 solution with a relatively low pH (≈ 7), although the process is slow. As when gypsum is the activator, a sufficient source of hydroxyl ions is needed to

accelerate activation. At a sufficiently high pH, bonds are broken in the slag structure and the ettringite formed stabilizes. Activation with a combination of gypsum and NaOH yields Na₂SO₄. While this procedure calls for five times more activation than needed in calcium activation, it yields double the amount of hydration product. The viscosities of aqueous sodium sulfate solutions are also not more than a factor of ≈ 5 times higher than that of water at in the room temperature.

1.3 Binders properties of Alkali-Activated Slag

During the alkali activation process, the vitreous phase of slag dissolves, forming C-S-H gel. This reaction depends on a whole series of parameters such as particle size distribution, chemical composition and amount of vitreous phase in raw materials, as well as the nature, concentration and pH of activators. Conditions of the reaction, i.e. curing conditions, also show a great influence on the development of microstructure and thereafter on the physical and elasto-mechanical properties of AAS mixtures.

1.3.1 Fresh properties

The knowledge of the fresh behavior of AAS mixtures is of primary important because it allows to optimize the mixing, placing and finishing operations of alkali-activated slag-based concretes and mortars. Several researches have been conducted on these issues, however some fresh properties of AAS mixtures have not yet been fully investigated (e.g. bleeding, segregation, workability retention).

1.3.1.1 Setting time

Initial setting time is of practical importance since it is an indicator of the time available for transit, placing, compacting (if required) and finishing. Setting times are defined as times when the material will just withstand a prescribed pressure or resist penetration to a prescribed depth. Setting characteristics of alkali-activated materials depend strongly on the characteristics and the composition/formulation of the systems. In particular, the Blaine fineness of the slag does not appear to affect the setting times of the alkali-activated slag cement greatly in the range of 350-530 m²/kg [37]. However, a very sharp reduction in setting times is noted when the slag fineness increases from 530 to 670

m²/kg. Setting time of alkali activated slag is also influenced by the basicity $[(CaO+MgO)/SiO_2]$ of the slag: higher basicity will likely result in shorten setting times regardless of the nature of activators used [10]. Furthermore, waterglass-activated slag cements tend to exhibit shorter setting time than either NaOH- or Na₂CO₃-activated slag cements. As shown in Figure 1.5, setting time usually decreases with increased activator dosage or silica modulus Ms. In general, the combination of two or more activators can drastically change the setting characteristics of alkali-activated slag.

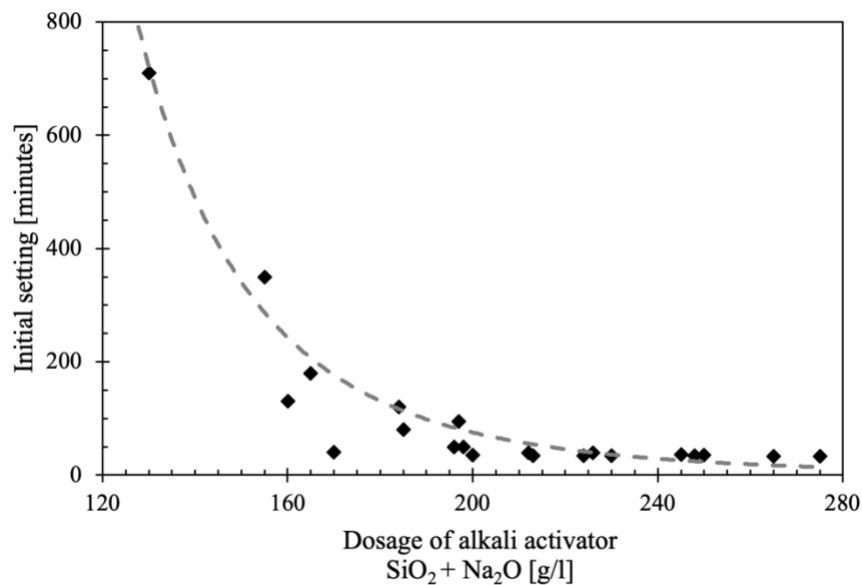


Figure 1-5. Influence of activator dosage in initial setting time of alkali-activated slag [38]

1.3.1.2 Workability

Many factors such as the nature of slag and activators, dosage of activators, fineness of slag, chemical admixtures, addition of lime, mineral admixtures and timing for the addition of activators have an effect on the workability of alkali-activated slag cement pastes. In particular, the nature of activator affects the rheological properties of alkali-activated slag cement pastes. Shi et al. [39] reported that the water requirement for normal consistency for waterglass-activated slag cement paste was 0.28, lower than that for NaOH and Na₂CO₃-activated slag cement paste – 0.30. Furthermore, for waterglass-activated slag cement, the modulus Ms has a significant effect on workability (Figure 1-6). When the modulus is lower than 0.5, the workability is low and similar to that of NaOH-activated cement pastes. The workability is very high and the slump loss with time is minimal when modulus is between 0.5 and 1.0. As the modulus of sodium silicate is

greater than 1, the workability of the paste decreased markedly with the increase of the modulus of silicate and when the modulus is 2, the workability is lost within few minutes after mixing.

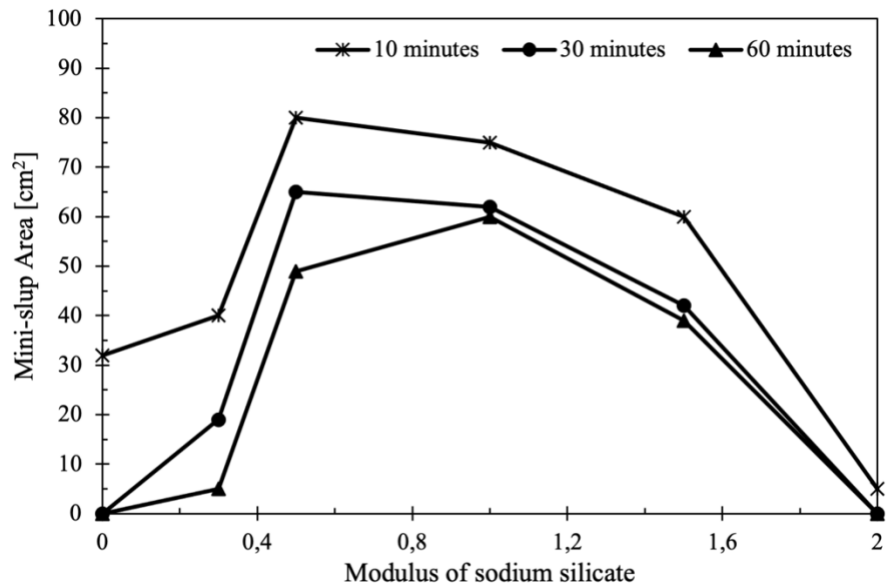


Figure 1-6. Effect of modulus of sodium silicate in mini-slip of alkali activated slag cement pastes ($w/s = 0.4$)[8]

1.4 Mechanical properties

The knowledge of the mechanical properties of AAS mixtures is of primary important because it allows to understand in which fields it is possible to use alkali-activated slag-based concretes and mortars. During the alkali activation process, the vitreous phase of raw materials dissolves, forming calcium silicate or aluminosilicate gel afterwards. This reaction depends on a whole series of parameters such as: particle size distribution, chemical composition, amount of vitreous phase in prime materials, as well as the nature, concentration, and pH activators. Conditions of the reaction, i.e. the curing conditions (temperature, relative humidity, curing time), also show a great influence on the development of microstructure, and thereafter on the mechanical properties of alkali-activated slag.

1.4.1 Compressive strength

Fernandez-Jimenez et al. [40] have studied the influence of several factors on the development of mechanical performance in AAS cements, concluding that the order of the most significant effects on the development of compressive strength is: nature of alkali activator >> activator concentration > curing temperature \approx specific surface of slag.

The strength depends on the basicity (CaO/SiO_2 or $\text{CaO} + \text{MgO}/\text{SiO}_2 + \text{Al}_2\text{O}_3$ ratio) of the slag. Under the same reaction conditions basic slag develops much higher strength compared to acid and neutral slag [13]. Furthermore, higher MgO content of slag resulted in a faster reaction and higher mortars compressive strength (50-80% increase after 28 days) of silicate-activated GGBFS, but in the case of hydroxide-activated slag the strength increase was quite limited [41]. Higher Al_2O_3 content of the slag resulted in a slower reaction and a lower compressive strength during the first days. At 28 days and longer, no significant effects of slag Al_2O_3 content on the compressive strengths were observed [42]. On the other hand, small addition of Al_2O_3 powder to sodium silicate-activated slag concrete resulted in significant compressive strength increase [43]. After 28 days of curing at room temperature the strength of alkali-activated slag concrete was ≈ 65 MPa, compared to ≈ 45 MPa for concrete without Al_2O_3 addition.

Particle size or fineness is a key physical factor influencing the mechanical properties of alkali-activated slag (Figure 1-7). Reactivity of raw materials increases as fineness increases (particle size decreases). However, increase of fineness over a certain threshold value may have an adverse effect on strength due to the higher water demand. Higher (mortar or paste) compressive strength can be achieved by increasing fineness of GGBFS, especially at early ages [44].

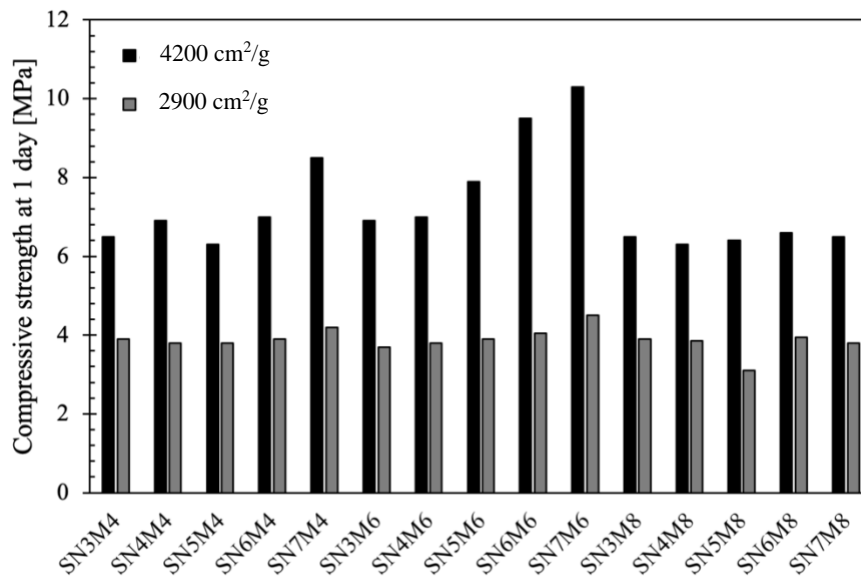


Figure 1-7. Compressive strength at 1 day of one-part alkali activated slag (the letter N represents the value of the module M_n and the letter M denotes the value of the M_s module) [44].

The compressive strength of alkali-activated slag is highly affected by the nature and the concentration of activators [45]. Furthermore, there is an optimum dosage to obtain the best mechanical performance, but it varies according to the nature of the slag and alkali activators used, and the curing conditions [46] and therefore it is difficult to find the optimal dosage for each individual mixture. Ben Haha et al. [47] found that the activation of slag using NaOH results in high early (day 1) strength, but strength at 7 days and longer is lower than for the waterglass-activated slag. Sodium silicate-activated slag mortars most commonly develop the highest strength, unfortunately usually accompanied by undesirable side effects, such as fast setting and/or high shrinkage [10]. Activation of GGBFS with KOH gave higher early (1 day) strength than for sodium silicate activation, but the subsequent strength development and strengths at later ages were much lower for the KOH systems.

The strength development of alkali-activated slag is strongly influenced by the curing temperature, with significant retardation at 5°C and significant acceleration at 40°C, as compared with the strength development while curing at 20°C [48]. Heat treatment was found to be very effective in promoting high early strength of alkali-activated slag concrete, and reducing drying shrinkage as well [49].

1.4.2 Tensile strength

Alkali-activated slag concrete (AASC) showed greater tensile strain capacity than OPC concrete due to the greater creep, lower elastic modulus and higher tensile strength of AASC [50]. Generally, the tensile strength of the OPC concrete is only 1/10 – 1/20 of its compressive strength. Similar to OPC concrete, the tensile strength of alkali-activated slag concrete agrees well with compressive strength [51]. Ryu et al. [52] examined the relationship between splitting tensile strength and compressive strength of alkali-activated concrete, and analyzed the difference between the measured data and those calculated by empirical formulas, and then they proposed a more precise equation with the coefficient of determination of 0.983. The most essential factor that influences the tensile strength is the nature of raw materials. Zhang et al. [53] found that the tensile strength increased with GGBFS content, while decreased with the increasing amount of additional water. Also, high concentration activator showed the considerable improvement of tensile strength (Figure 1-8).

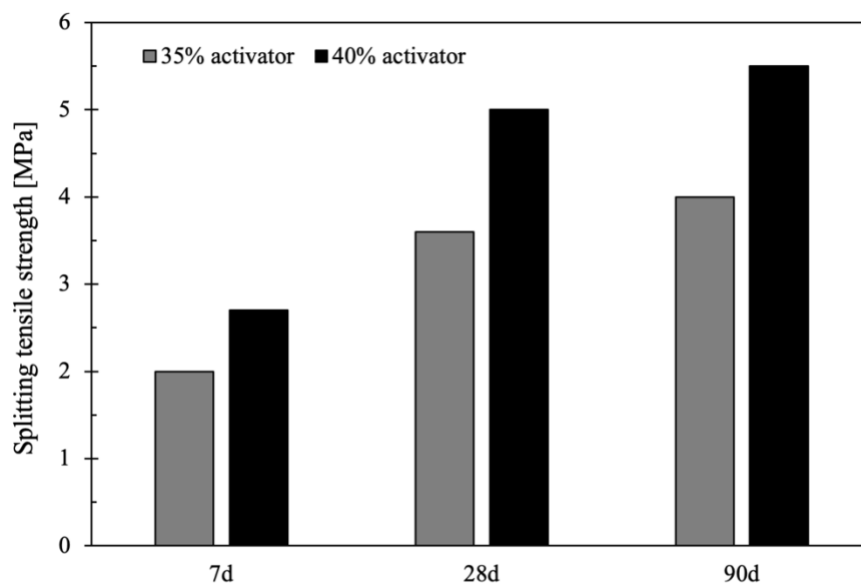


Figure 1-8. Splitting tensile strength of alkali activated slag concrete under different alkaline concentration [51]

1.4.3 Elastic modulus

Collins and Sanjiayan [54] found that the elastic modulus of alkali-activated slag concrete with the use of different alkali activators was marginally lower than that of Ordinary Portland cement concrete. The elastic modulus of alkali-activated mixtures is

also influenced by the mix design of the conglomerate. For example, Duxson et al. [55] observed an increase in elastic modulus, from 2.3 to 5.2 GPa, when increasing the Si/Al ratio of alkali-activated pastes from 1.15 to 1.90; in those data, a decrease in modulus with Si addition was only observed beyond Si/Al = 2.0 (Figure 1-9). Wongpa et al. [56] found that the elastic modulus decreases with increasing curing time, and Talling and Krivenko also found that the modulus of elasticity is reduced by initial steam curing of high-strength AAS [57]. Also the nature of the activator greatly influenced the elastic modulus values, in particular, Puertas et al. [19] found modulus values between 28 and 50 GPa for the C-A-S-H gel binder in alkali silicate-activated BFS specimens and 12-42 GPa in alkali hydroxide-activated BFS. Oh et al. [58] also showed that Al substitution in C-S-H has little influence on its basic mechanical properties, including elastic modulus. Finally, Douglas et al. [59] found a slight increase in the elastic modulus of alkali-activated GGBFS concretes from 28 to 91 days, and obtained elastic moduli of around 30-35 GPa for their samples, which agree very well with the ACI 318 model, as do the available data for alkali-activated BFS.

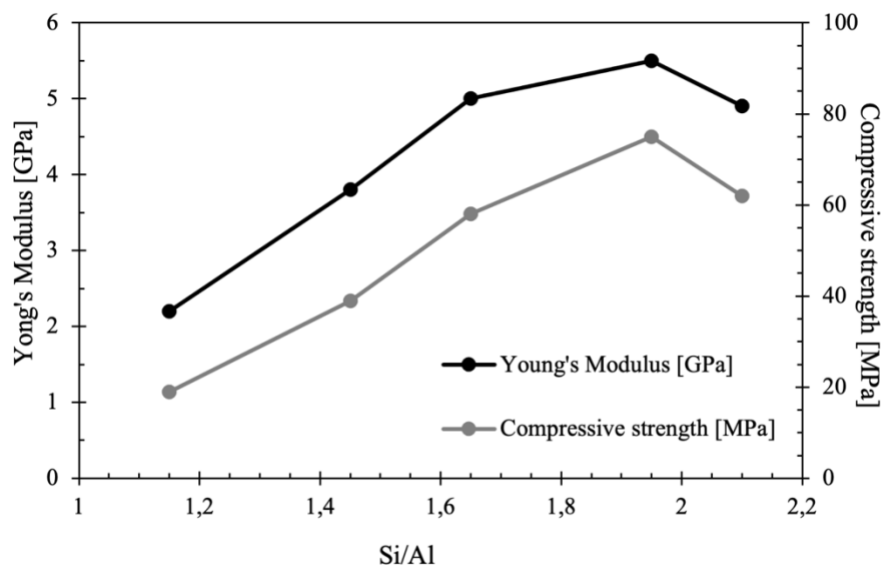


Figure 1-9. Young's moduli and ultimate compressive strength of alkali-activated Materials[55]

It is clear that more work is needed in this area to determine the interrelationship between binder structure evolution and elastic properties, and recent work using micromechanical modelling and nanoindentation may be providing some useful initial

steps in this direction, but the complete links between this work and macroscopic concrete performance remain to be drawn.

1.5 Curing conditions

The mechanical properties of alkali-activated slag are extremely influenced by curing conditions, as the proper curing is essential for high strength development. The experimental data shows that the ideal curing conditions for Portland cement, such as underwater curing, is not applicable, as it would lead to premature leaching and unavoidable loss of strength [60]. A more appropriate option is curing in a humid chamber ($RH > 90\%$) at $T=20^{\circ}\text{C}$ [61]. Only if the reaction at room temperature is relatively slow then heat or steam curing would be required. However, the heat curing might lead to strength loss, if the water present in the system and required for the alkali reaction continuance is irreversibly lost. Furthermore, the heat treatment promotes high early-strength and reduces shrinkage; nevertheless, it causes inhomogeneity of the microstructure and coarse pore structure, and therefore there is a lowering of the long-term compressive strength compared to AASC cured at room temperature. Finally, it is almost universally agreed that an extended period of sealed curing is important in the development of a dense and durable matrix [62].

1.6 Applications of alkali-activated slag

Since the 1970s, masonry blocks, workshops, retail buildings, storehouses and drainage systems have been built in Russia, China, Belgium, Finland, etc [8]. Particularly, in Russia, several over 20 floors' residential buildings have been constructed. The exterior walls of buildings were cast in situ, and floor slabs, stairways and other structural components were pre-cast. All the concrete was made using alkali carbonate-activated GGBFS with w/b equal to 0.35 [8]. In 2000 these buildings were inspected, revealed that the alkali-activated slag based structures were in good condition, showing no deterioration or cracks on the surface.

In 1965 to prevent soil erosion, 40 alkali-carbonate activated slag concrete pipes were fabricated and used to build a 33 km long underground drainage collector along the sea bank in Odessa, Ukraine. After 34 years in service the results of an examination confirmed that the alkali-activated slag concrete pipes exhibited good durability. Moreover, the compressive strength of the material had increased from 40 MPa to 62 MPa, the pH remained above 11.5, water absorption was less than 5%, and there was no visual indication of corrosion of embedded steel reinforcement, although the cover depth was only 3 mm [62].

In 1974 a storehouse was built in Krakow using pre-cast AAS concrete for the slabs and wall panels. More than 25 years after its construction, cylindrical core samples were taken from the outside wall panels, and used to determine the compressive strength, carbonation depth and microstructures. A significant increase in compressive strength was found from 28 days to 27 years in all cases and an average rate of carbonation of less than 0.5 mm/years in all samples. Electron microscopy did not evidence micro-cracking, alkali-silica problems, or steel corrosion after 25 years of service [63].

In 1984 in Russia, a 6 km long test section was built using GGBFS activated with sodium carbonate. After 15 years in service, the trial section exhibited very good working conditions, while those built using OPC concrete deteriorated seriously.

In Ukraine in 1999 the Ilych Iron and Steel Integrated Works started the production of ready-mixed alkali-activated slag concrete. Its pre-mixed concrete is mainly used for cast-in-situ or precast slabs driveways for heavy vehicles, as well as commercial production for load-bearing structures [62]. In 4 years more than 20,000 m³ of concrete have been produced, in various strength class, and economic calculations show very significant cost savings (up to 50%) for sodium carbonate-activated slag concretes compared to OPC concrete, at equal compressive strength.

1.6.1 AAM for repair of existing masonry buildings and concrete structures

In Italy, almost 59 billion € were spent on residential construction in 2020, of which 74% for the extraordinary repair of the structures alone [64]. Delatte reported the “Law of Fives”: \$1 spent on design and construction is equivalent to \$5 spent as damage initiates and before it propagates, \$25 once deterioration has begun to propagate, and \$125 after extensive damage has occurred [65]. Furthermore, the use of low-durability

materials involves the need for frequent repair, consuming large quantities of raw materials and energy.

Zhang et al. [66] proposed novel alkali-activated materials with the aim of protecting the concrete structures exposed to marine environment. The systematical experiments from laboratory and field application have demonstrated that the innovative materials possess suitable setting time, high bonding strength and excellent anti-corrosion properties. Also, the chemical stability under marine conditions enables them to provide a sustainable protection to concrete structures.

1.7 CO₂ emissions

There is an area in which alkali-activated binders have certainly higher performances if compared with their OPC counterparts: the reduction of the carbon footprint and the energy saving [67]. Definitively, one of the most advantages of AAS is the easier availability of their aluminosilicate raw materials with respect to Portland cement. In a planet where the consumption of traditional cement is, in relation to the quantity, second only to water consumption [68], the considerable emissions of CO₂ required to manufacture and transport the cement itself can do no other than be in the long term hardly sustainable. This reality has long been the engine that drives the development of international engineering research on the development of alkali-activated materials in numerous applications thanks to their lower pollutant load. The production of Portland cement emits this large amount of CO₂ (0.98 kg_{CO2}/kg) due to the calcination of calcium carbonate involved in the production of the clinker of Portland cement. On the contrary, alkali-activated materials are not produced by limestone calcination and the production of CO₂ during the production process is very limited, with an estimated reduction of greenhouse emissions up to 90% compared to conventional cements depending [68]. In fact, it is obvious that the use of an industrial by-product do not need any additional treatment, therefore no emission. It should be underlined that the processes necessary for the production of alkaline activators involve a significant amount of researches. Nevertheless, some studies [69] show a general energy savings in the production of alkali activated slag compared to that of OPC mortars, at equal compressive strength.

CHAPTER 2.

SUSTAINABILITY

2.1 Climate change, population growth and concrete industry

Recent decades have seen increasing climate changes, many of which science is now able to attribute to anthropogenic greenhouse gases emissions and consequent global warming [70,71]. In the last five years, the warmest on record [72], the risks related to the climate changes were striking harder and increased more rapidly than expected [73]. Natural climate-change related disasters such as droughts, extreme rainfalls, wildfires and hurricanes are becoming more severe and more frequent, reportedly today more than a disaster a week on average [74]. The World Economic Forum (WEF) Global Risk Report 2020 [73] indicated that the number one long-term risk is the failure of climate-change mitigation, underlining several near-term consequences that could lead to a planetary emergency. Firstly, the loss of life and destruction of ecosystems. In fact, the increasing number and severity of disasters is responsible for huge economic damages and human losses (casualties), especially in tropical regions [75]. In particular, it was reported that the worldwide economic stress from natural disasters in 2018 was US\$ 165 billion [74] while USA National Climate Assessment estimated that climate-related economic losses could reach, in the United States alone, 10% of gross domestic product by 2100 [76]. Moreover, several ecosystems are under such stress that, in addition to the extinction of animal and plant species, there will be harsh troubles also for human life. One of the best-known risks is the rise in sea level related to the melting of polar glaciers that is estimated to reach about 30 cm by 2050 and, in the worst scenario, up to 2 m by the end of the century [77–79]. This means that, under high emissions, not only over one billion people living in land less than 10 m above current sea level are in danger [80] but also that the ice-cap melting could modify the gulf stream causing further ecosystem

disorders and major changes in the pattern of severe weather perils [81]. Another significant little-known risk connected with the melting of ice caps is the release of carbon dioxide due to the de-icing of permafrost soil around the poles. Recent researches [82,83] estimated that about 50 – 150 Gt of the soil organic carbon stored in permafrost soils could be emitted as greenhouse gases by 2100 due to sunlight oxidation, enhancing the global warming.

On 2020, global temperatures are over about 1°C above pre-industrial levels [72]. The current trend figures that global temperatures are likely to reach 1.5 °C between 2030 and 2052 [84] while United Nations Environment Programme (UNEP) Emission Gap Report 2019 estimates that temperature will rise to at least 3°C by the end of the century [85]. To avoid the catastrophic economic, social and environmental consequences, climate scientists advise that the temperature rise must be limited to 1.5°C [84]. This implies a remaining carbon budget of less than 10 more years of emissions at their current level, approximately equal to 420 Gt of CO₂ [86]. In 2019 the CO₂ emissions from the building sector are the highest ever recorded at about 10 Gt of CO₂ per year (38% of total global energy-related carbon dioxide emissions with the inclusion of emissions from the building construction industry) as well as buildings decarbonization commitments are growing in view of 2050 when all new buildings, infrastructures and renovations will have net zero embodied carbon [87].

In this scenario, the United Nations state that the world's population reached 7.7 billion in mid-2019 with a growth rate close to 1% per year, having added one billion people since 2007 and two billion since 1994 [88]. The global population is expected to reach 8.5 billion in 2030 and 9.7 billion in 2050 with Sub-Saharan Africa as a driving force for world's population growth and several other regions (such as Asia, Latin America, Europe and North America) that will experience decreasing or stationary population numbers (Figure 2-1). At the same times, the World Urbanization Prospect [89] evidences that the more developed regions were already highly urbanized by 2018 (about 79% of their population live in cities or towns) and the projected proportion urban in 2050 is expected to reach 87%. On the contrary, the less developed regions will be characterized by a strong rate of urbanization, rising from 50% to 65% over the next three decades. Just in India, for example, about 20 million houses were or will be realized in the urban regions in the 2019-2022.

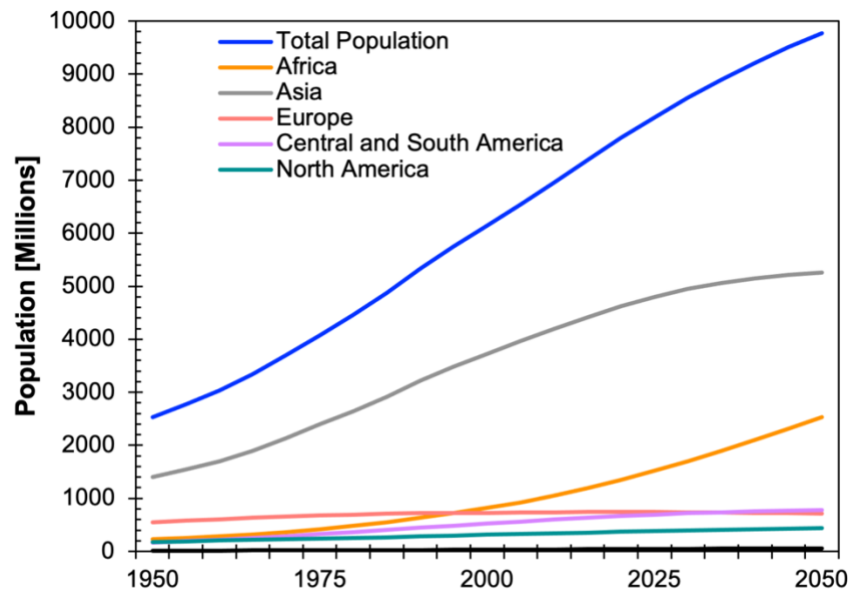


Figure 2-1 Population evolution and estimation from 1950 to 2050. Data re-elaborated from [88]

The construction industry will therefore be called upon to respond to two apparently incompatible needs of humans, to preserve the environment and support the growth by providing housing and infrastructures to the increasing population. Concrete, although more sustainable per kilo with respect to other construction materials such as steel, glass, timber and brick (Figure 2.2), has a very high impact due to its huge volume of use, estimated at over 10 billion cubic meters per years (in 2019, the cement production was 4.1 Gt [90]).

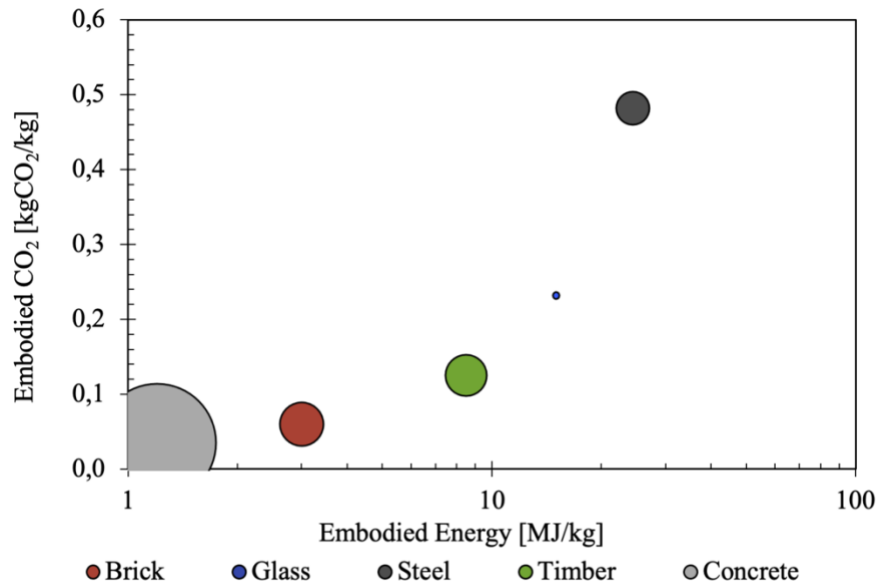


Figure 2-2 - Embodied CO₂ and energy for construction materials. The radius of bubbles represents the worldwide production per year. Data re-elaborated from [90–92]

Actually, it is estimated that concrete production is responsible for 9% of total greenhouse gas emissions [92], of which 7-8% from only from cement plants [93]. In other words, if the concrete industry were a country, it would be the third largest CO₂ emitter in the world with up to 2.8 Gt per year, surpassed only by China (10.18 Gt) and United States (5.29 Gt) [94]. Even if the energy requirements for cement production only have continued to decline gradually due to important technological innovations (i.e. new grinding equipment, dry-process kiln instead of wet-process kiln, etc), the global thermal energy for clinker production in modern cement plant (with dry-process kiln and multi-stage preheater) is close to 3.4 GJ/t [95]. Taking into account an average clinker-to-cement ratio of 0.70, it is possible to estimate an energy consumption for cement industry only of about $1.4 \cdot 10^{10}$ GJ/year, about 2-3% of energy use worldwide [96] and more than the energy consumed for residential sector in USA in 2019 [97]. Another important issue related to the concrete production is the raw materials consumption. Not only the binder manufacture requires huge amount of natural materials (on average, 1.22 ton of limestone and 0.31 ton of clay are required to produce 1 ton of clinker [98]) but also the production of aggregates has a strong environmental impact due to the consumption of non-renewable resources. In USA, about 0.45 Gt of natural sand and gravel (46% of total sand and gravel mined in USA) are used every year as concrete aggregates [90].

Improving the sustainability of concrete and cementitious materials is therefore an essential and complex challenge for both academic and industrial researchers in order to meet the future demands of building materials while protecting the environment.

2.2 Strategies to sustainable concrete

When it comes to improving the sustainability of concrete, the focus is often only on decreasing the environmental impact resulting from its production [99–101]. The reduction of the amount of CO₂ generated, energy used and natural raw materials consumed is an efficient strategy with a view to sustainability but it could be totally ineffective if durability and performance are not also evaluated. In fact, it is quite simple to reduce the environmental impact of concrete by 50% but this could easily lead to a halving of its service life or to a strong performance decline. In this way, no improvement in sustainability is achieved but simply an extension of the environmental impact over time or the spreading on a large volume of materials is realized. It is for this reason that the most effective way to improve sustainability of concrete structures is by making them last longer through design for durability. Durability design includes more than the selection of concrete materials and mix proportions. Furthermore, by analyzing only the data reported in Figure 2.2, it could be stated that concrete is more sustainable than other building materials, which is a wrong conclusion caused by the lack of evaluation of the huge differences between the construction materials' properties.

Several developments towards sustainable concrete were attained in the last years and they vary from alternative constituent (binders, aggregates and water) to innovative “smart materials”, admixtures and techniques able to improve the performance, prolong the service life and/or reduce the environmental impact of cementitious mixtures [102].

2.2.1 *Alternative binders to OPC-replacement*

One of the main methods to reduce the impact of Portland cement is to replace this binder with other more eco-friendly materials. In previous chapter, alkali-activated slag were described. Such technology may shortly reach a stage of development in which it will serve as a link in the necessary transition from Portland cement to the cements of the future. Above all, working with solid activators instead of alkaline solutions would afford

an enormous technological advantage, for the former would emulate one of the most estimable properties of Portland cement: its conversion from a dehydrated solid state into an effective binder by mere mixing with water. Furthermore, the use of “one-part” (solid precursor +solid activator) would solve the problems related to handling large amount of corrosive and hazardous alkaline solutions that would limit the use of AAM. Obviously, if recycling raw materials (especially activators) or low embodied carbon alkaline activators are not used or if transport distances of precursors and activators are considerable, the reduction of CO₂ emission is questionable.

2.2.2 Smart and multifunctional concrete

Smart and multifunctional concrete represent a building material that is associated with modern technology and the typical concrete construction in an effort to improve its structural properties. In other words, the smart and multifunctional concrete is an intelligent system [103–105]. It has properties different from those of conventional concrete, such as self-sensing [106,107], self-cleaning [108,109], self-healing [110–112], or has the ability to react upon external stimulus. These materials can be used for different applications, for example monitoring, damage assessment, structural control, structural repair and maintenance, integrity assessment and recently also for asset management, preservation and operation of infrastructures. The potential benefits of this technology include improved functionality, safety, reliability, durability and reduction of the life cycle cost of the infrastructure. For this reason, it can be said that smart concretes provide a new approach for the sustainable development of the construction and building sector. There are several ways to obtain smart concretes and structures: the design of the composition, special processing, the introduction of other functional components or the modification of the microstructure [105]. The field of smart concretes and structures is interdisciplinary between science and technology and combines the knowledge of physics, mathematics, chemistry, computer science, and material, electrical and civil engineering. The attribute of smart and multifunctional concrete is typically represented by the adaptability to environments. Its characterizing parameters mainly include accuracy, sensitivity, persistence, stability and effectiveness of responses, which reflect the “smartness and multifunction” degree or “intelligence quotient” [103]. Various types of smart concrete are used to improve the properties of infrastructures, thus increasing its

sustainability. In fact, by ensuring durability for a long period of time, the life of cementitious materials and service life of structures can be extended, thereby reducing the environmental load. In fact, the most basic strategy for obtaining a durable concrete is the appropriate choice of its constituents according to the environmental exposure (“the right concrete for the right application”).

Concretes made by adding titanium dioxide nanoparticles to the mixture has self-cleaning properties and other benefits that can help to keep the environment clean. Similarly, it has the ability to allow for the photocatalytic degradation of pollutants produced [113]. Cement-based composites reinforced by CNTs have self-sensing abilities for detection of health hazards or damages. Additionally, graphene oxide (GO) and graphene can be added to cement-based materials to improve durability and mechanical strength [114]. Self-healing concrete, also called self-repairing concrete, is mostly defined as the ability of concrete to repair its cracks autogenously or autonomously. Cracks inevitably exist in concrete due to chemical shrinkage, dry shrinkage, autogenous shrinkage, the relatively low tensile strength, and so on [115]. Self-healing of cracks in concrete contributes to a longer service life of concrete structures and makes the material not only more durable but also more sustainable. Self-heating concrete refers to concrete material using electrical resistance heating based on Joule effect, when a voltage is applied, thermal energy is radiated from it in the same fashion as a metallic wire conductor. This concrete has excellent potential for deicing and snow-melting of parking garage, sidewalks, highway bridges and airport runways. It would eliminate or dramatically reduce the need for using salt, thus providing an effective and environmentally friendly alternative [105,116]. These are just some of the concretes ones defined as smart or multifunctional, in fact, more than 20 types of smart concrete with different behaviors have been developed

2.3 Education and standard

In the last century, although innovations as blended cements and admixtures were already available, concrete was seen as the simple mixture of cement, water, sand and gravel. Today this perception is slowly changing as a greater knowledge of cement

chemistry combined with high-technology admixtures and additives allows to obtain improved and tailored performances of concrete. Despite the current advances in cements, aggregates, fillers and chemical admixtures, design standards in force mainly refers on traditional concrete without taking into account new constituent such as fibers and alternative aggregates or recent techniques such as self-compacting concretes and ultra-high-performance concretes. In particular, the regulations on aggregates very often strongly limit the use of materials other than natural sand and gravel, also giving the wrong perception of producing “poor quality” concrete when using artificial aggregates. In this context, the achievements of high substitution rates face strong legal and political barriers. At the same times, innovative admixtures (i.e. self-healing crystalline admixtures), even if not expressly prohibited, are not accompanied by a regulation that establishes their minimum performance and related test methods. Also for alternative binders (both non-Portland clinkers and alkali activated materials), beyond the technical-economic issues mentioned in the previous paragraphs, the main hinderance that limits their use is the prescriptive nature of specifications for building materials that precludes the use of non-Portland cements. In Europe, EN 197-1:2011 (cement) and EN 206:2013+A1:2016 (concrete) standards do not allow, except through European Technical Approval (ETA), the use of binders other than OPC. In the United States, ASTM C150-20 contains the specifications for Portland cement (prescriptive) while ASTM C1157-20 and ASTM C1600-19 cover performance requirements for hydraulic cements for general and special applications without restriction on the composition of binders (performance-based standard); however, the last two standards are not yet fully accepted by state authorities. The only exception is the Ukrainian building code DSTUB B V.2.7-181 that regulates the use of alkali activated materials as binders for structural concrete. Probably, as Juenger et al. [18] claim, the greatest challenge for developers of performance-based standards is to indicate test methods able to properly evaluate the performances of a wide range of binder systems, often characterized by distorted results if studied with traditional techniques developed for OPC. Also the education of engineers, architects, employers and final users must be able to support the sustainable development of innovative building materials [117]. The skills and knowledge of designers on new eco-materials will be the driving force for their large-scale implementation but today, in civil engineering curricula, topic as materials performance and chemistry often plays a

minor role with respect to basic science subject (i.e. chemistry, physic, mathematic) and management. At the same time, education of final users is also relevant, since wrong applications of sustainable cementitious materials could compromise their environmental benefits, especially in developing countries where the employers' skills cannot be compensated by process automations. Finally, governments and lawmakers must guide the transition towards an appropriate use of sustainable construction materials both with updated standards and codes open to new materials and with incentives/taxes.

CHAPTER 3.

DURABILITY OF AAS

3.1 Introduction

Durability is one of the most important desired properties of concrete. The durability of alkali-activated materials is strongly affected by nano- and micro-structure of the reaction products forming in these systems, as a function of the characteristics of precursor and the nature and the concentration of the activators. Slag-based systems have a structure mainly dominated by a C-S-H gel that is one of the main factors controlling the transport properties of AAS.

3.1.1 Resistance to freeze-thaw

One of the major problems in cold climates is the frost action in the form of freezing and thawing cycles, that can lead to damage of concrete materials. The freezing and thawing resistance of concretes depends mainly on the microstructure of hardened binder matrix (e.g. its porosity, pore size, capillaries, distribution and type of pores). Proper pore distribution can cause pressure diffusion and improvement in resistance against freezing-thawing cycles. The durability problems related to cold weather conditions can take two principal forms:

- Internal cracking due to freezing and thawing cycles, which generally causes a loss of concrete strength and stiffness. It is often evaluated from the variation of strength or dynamic modulus of elasticity with freeze-thaw cycles.
- Surface scaling due to freezing in the presence of de-icing salts, which leads to a loss of concrete cover. The mass of scaling debris is usually the parameter measured to characterize this degradation.

The deterioration of concrete structures in cold regions can be more pronounced in alkali-activated slag-based materials respect to Portland cement-based mixtures (OPC)

due to the porous nature of AAS [118]. According to Pachego-Torgal et al. [119] alkali-activated slag composites exposed to freeze and thaw only showed some scaling after 40 cycles, but other mixtures not having air entrainer did not show any scaling at the same number of cycles. Furthermore, the high resistance of AAS to freezing and thawing was observed in samples without air entrainers, compared to OPC samples, which passed less than 300 cycles before deteriorating [120]. Tan et al. [121] reported that no deterioration or weight loss occur in alkali-activated slag samples with high compressive strength when exposed to freeze and thaw cycles. Shahrajabian et al. [122] found that adding 1% to 3% nano-silica to alkali-activated slag mixtures improve resistance to freeze-thaw damage. Furthermore, Fu et al. [123] demonstrated that the percentage of mass loss of AAS concrete is very small, less than 1% after 300 cycles, so this material can meet the frost-resisting requirements in cold areas with frost-resisting grade of F300 at lowest (Figure 3-1).

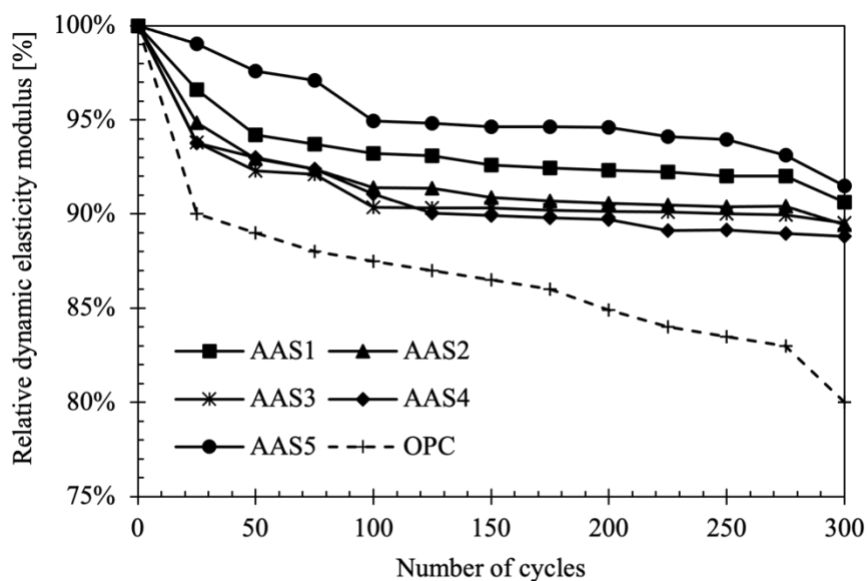


Figure 3-1 Elastic modulus loss of mortars as a function of number of freezing/thawing cycles [123]

Cai et al. [124] highlighted that the decisive factor influencing the freeze-thaw resistance is the air bubble spacing coefficient. However, the resistance to freeze and thaw could be increased by using air entraining agents, similarly to what is already done for OPC-based concretes.

3.1.2 Chloride penetration

Penetration of chloride ions into the concrete is mainly responsible for the corrosion of reinforcements [125]. Chloride ions get in contact with concrete from sources such as sea water and de-icing salts used in winter season. In AAS concrete, chloride transport is influenced by: the type of precursor and its physical and chemical properties, the chemistry of the alkali activating solution and curing regime. There are limited number of papers focused specifically on the chloride permeability of alkali-activated slag conglomerates, nevertheless Awoyera et al. [126] found that AAS conglomerates have lower chloride diffusion coefficient compared to OPC concrete due to the increased tortuosity, lower total porosity and water absorption properties (Figure 3-2). Moreover, the type of activator influences the resistance to chloride: slag activated with $\text{Ca}(\text{OH})_2$ presented higher corrosion resistance than AAS mortars activated with KOH and NaOH activators, which was attributed to the formation of $\text{Ca}(\text{OCl})_2$ to remove free chloride from the pore solution, and thus to mitigate the corrosion risk [127]. Furthermore, increased alkali concentration in the activator, and the use of sodium silicate activator with a molar ratio $\text{SiO}_2/\text{Na}_2\text{O}$ of 1.5, gave a desirable microstructure which improved the resistance to chloride transport and corrosion [128].

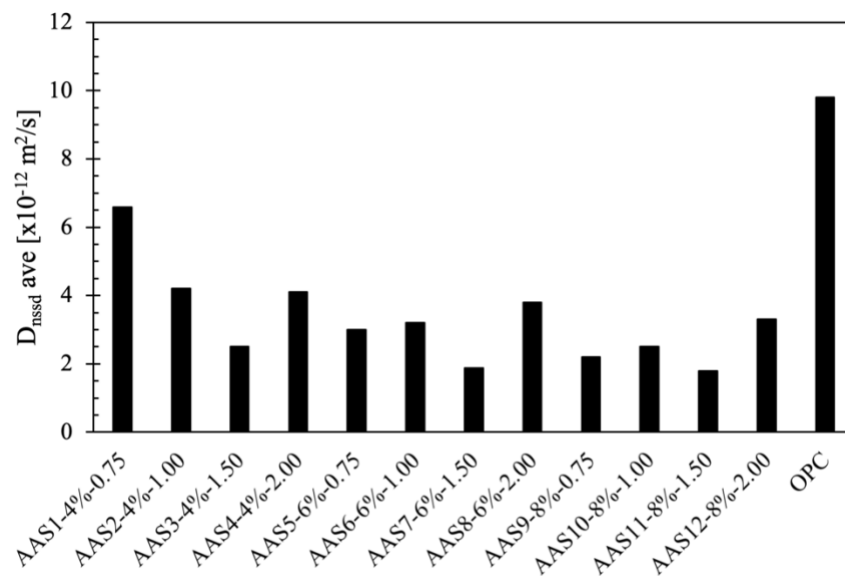


Figure 3-2 Chloride diffusion coefficient (D_{nssd}) values measured for AAS concrete mixes (the first number indicated the percentage of Na_2O and the second the M_s ratio) [129].

Finally, there is not yet an extensive database of chloride diffusion coefficients available for AAS concretes and mortars. Recently, Ismail et al. [130] have demonstrated that the nature of the binder gel strongly influences the chloride permeability in AAS systems. C-S-H gels have the capacity to physically adsorb chloride ions without changing mineralogical structure, while in high-Ca mixtures, chloride ions can not only be physically adsorb onto C-S-H products in the layers and interlayers spaces but can also be chemically bound to the C-S-H.

3.1.3 Sulphate attack

External sulphate attack refers to the deterioration of a binder material resulting from chemical reactions occurring when a binder is exposed to a solution containing a high concentration of dissolved sulphates. Foundations and/or parts of structures in contact with groundwater and soils in arid regions or concrete in contact with wastewaters may be subjected to sulphate attack [10]. There is a limited knowledge on resistance of alkali-activated slag to sulphate attack. Immersion of two-parts alkali-activated slag binders in sodium sulphate solutions, according to traditional method for Portland cement-based (OPC) concretes, does not promote expansion and cracking binder paste [61,131]. On the contrary, OPC-based samples show significant expansion and cracking associated with the formation of secondary ettringite and gypsum [132]. Recent results [133] revealed that the key factor controlling the degradation mechanism of AAS is not the sulphate itself, as tends to be the case in Portland cement mixtures, but rather it is the nature of cation accompanying the sulphate anions. Exposure to sodium sulphate seems to favor the structural evolution of the binding phases and densification of the system, and therefore cause a lower loss of strength. Conversely, the presence of magnesium leads to decalcification of the Ca-rich gel phases in alkali-activated materials, promoting the decay of the main binding phases and leading to formation of low-strength M-S-H type phases (Figure 3-4).

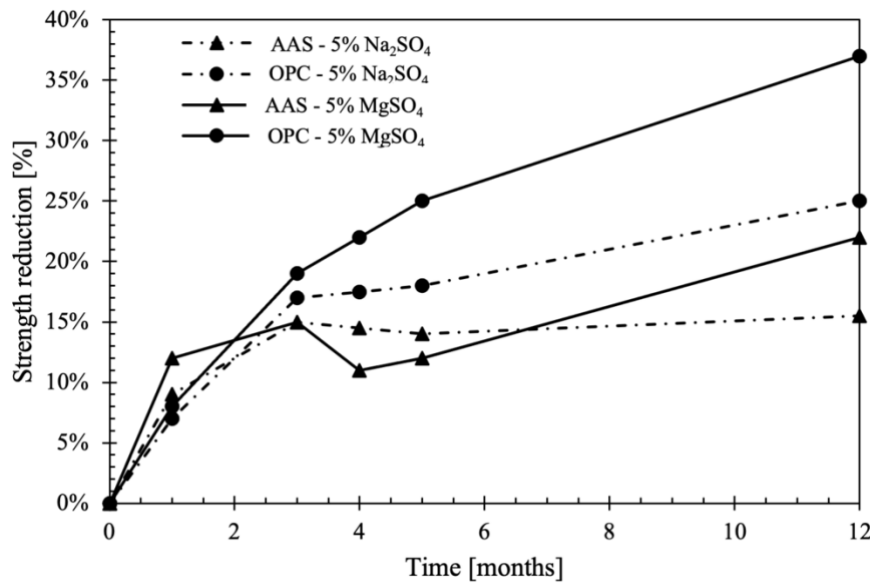


Figure 3-3 Compressive strength reduction of AAS and OPC samples subjected to sulfate attack in 5% MgSO₄ or in 5% Na₂SO₄

3.1.4 Carbonation resistance

The chemical reaction between a cement-based material and carbon dioxide (CO₂) is referred to as carbonation, and is one of the most harmful degradation processes that can drastically affect the long-term durability of civil infrastructure [10]. A truly sustainable material must be durable, and therefore efforts have been focused in the past decade to understand the changes induced by carbonation in the microstructure of alkali-activated slag, and its consequent effect on permeability and mechanical strength, in order to predict service life performance. In alkali-activated materials, the mechanism of carbonation is not yet completely understood, but it has been demonstrated that it is fundamentally a chemically controlled mechanism that occurs in two steps: 1) carbonation of the pore solution leading a reduction in pH and the eventual precipitation of Na-rich carbonates, 2) decalcification of Ca-rich phases (mainly C-S-H, as portlandite usually does not form in these systems) and carbonation of secondary reaction products present in the system [134]. He et al. [135] observed that the strength of the AAS is related to its resistance to carbonation. In particular, a concrete with compressive strength less than 30 MPa undergo rapid carbonation, which might lead to slight reduction in strength. However, AAS with compressive strength between 30 MPa and 50 MPa undergo less carbonation, and there's no significant strength loss. Also, concrete with compressive

strength higher than 50 MPa was found to undergo no carbonation. Furthermore, increasing the slag content can be used to reduce the rate of carbon dioxide penetration into AAS, as a result of a more densified microstructure (Figure 3-4). Also the type of activator influences the carbonation of these materials. Puertas et al. [136] observed higher accelerated carbonation depths in slag-based mortars activated with sodium silicate than in sodium hydroxide activated specimens. This was mainly attributed to the differences in the composition and structure of the C-S-H product forming in each system. As reported by Ye et al. [137] a high alkali dosage tends to increase the carbonation resistance of AAS due to higher level of alkalinity than can absorb more CO₂. However, controversial results are documented in the literature regarding the effect of silica modulus. In particular, the increase of this modulus reduces the Ca/Si ratio of C-S-H and potentially enlarges carbonation susceptibility and strength loss; while it may reduce carbonation depth through advancing slag reaction and refining the pore structure of alkali-activated slag.

Bakharev et al. [138] found that, when both binders were evaluated with the accelerated carbonation test, the rate of carbonation of alkali-activated slag is faster than that of Ordinary Portland Cement. However, the rate of carbonation of AAS, when evaluated with natural carbonation, is only slightly faster than that of OPC.

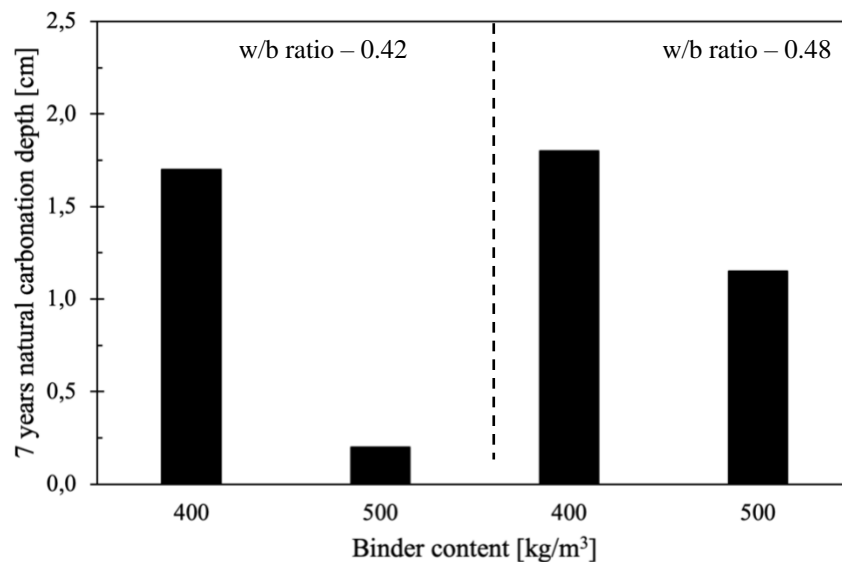


Figure 3-4 Natural carbonation depths of aged silicate-activated slag concretes, as a function of mix design [139]

3.1.5 Acid attack

The spectrum of aggressive acid media to which concrete can be exposed is broad. Sources usually originate from industrial or agricultural processes, but can also be due to urban activity. Acids can be more or less aggressive towards hydrated compounds: particularly and among others, nitric (HNO_3), hydrochloric (HCl), sulfuric (H_2SO_4) acids are strong acids and can be very damaging to concrete. A practical consequence of chemical degradation caused by an acid attack is the gradual weakening of the mechanical strength and solid cohesiveness of concrete, resulting in crushing and dropping of material, and continues its destructive progression into the interior portions [10]. Alkali-activated slag show higher acid corrosion resistance compared to Portland cement, due to the absence of portlandite and low Ca/Si ratio in the binder. In particular, after acid corrosion hardened alkali-activated slag and OPC binders formed a surface layer whose composition is mainly $\text{SiO}_2 \cdot n\text{H}_2\text{O}$ gel. This layer provides a barrier which prevents further corrosion of the internal, non-corroded cores. However, there is a noticeable difference between the layers formed by AAS and OPC. The first one produce a protective dense silica gel layer, but hardened OPC leads to a porous layer. Differing calcium content (greater in OPC than in alkali-activated slag) could be responsible for this effect [140].

AAS cements corroded faster in acetic than in nitric acid. Bernal et al. [141] investigates acid resistance of AAS sample in comparison to OPC, the mortar samples were exposed to pH 3 hydrochloric, nitric and sulfuric acid solutions, as well as to pH 4.5 acetic solution. Negligible changes in compressive strength were identified both in Portland cement and alkali-activated slag mortar during exposure to mineral acids. On the other hand, exposure to acetic acid caused significant reduction in strength both in Portland cement and AAS mortars, indicating that acetic acid was more aggressive than the mineral acids. Although exposure to acetic caused strength loss and a substantial increment in porosity in both OPC and AAS, the alkali-activated slag performed better than Portland cement, retaining 75% of their original strength after 150 days of exposure to acetic acid. Higher stability of AAS under acetic acid attack is attributed to lower initial permeability, higher alkalinity of the pore solution and low CaO/SiO₂ ratio in the alkali-activated slag system. Moreover, Davidovits et al. [142] reported mass losses of 6% and 7% for AAS immersed in 5% concentration hydrochloric and sulfuric acids during 4

weeks. For the same conditions they also reported that Portland cement-based concretes suffered mass losses between 78% and 95% (Figure 3-5).

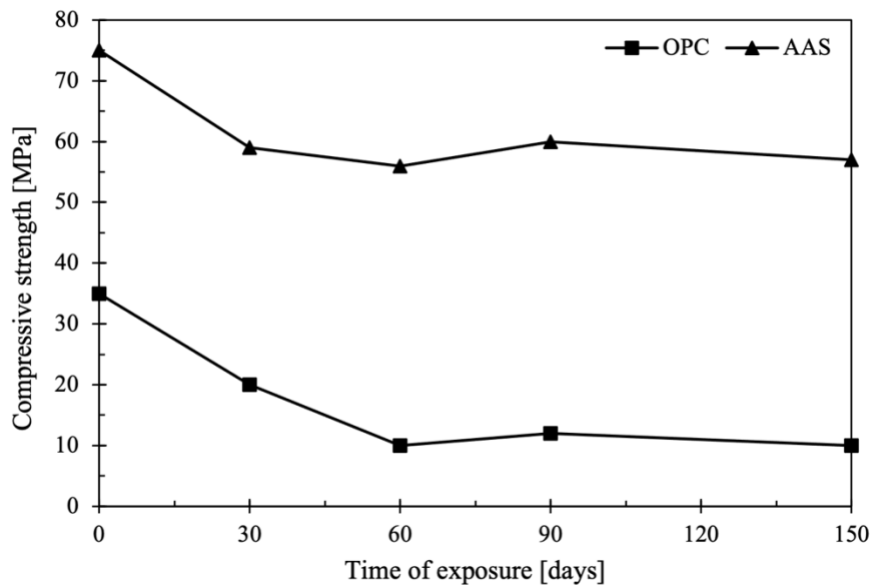


Figure 3-5 Compressive strength of OPC and AAS mortars as a function of the time of exposure to pH 4.5 acetic acid [141]

3.1.6 Permeability

Permeability of conglomerates is one of the major factors that determines its durability. During design, adequate measures are mostly taken to ensure that the concrete is less permeable as much as possible. Several studies [143,144] have shown that AAS has a lower permeability compared to OPC concrete. However, some other studies [145,146] also found that alkali-activated slag is more permeable compared to OPC. Zhang et al. [66] studied the effects of liquid/solid ratio on permeability of AAS, as expected, the permeability coefficient k increased along with the increase in liquid/solid ratio from 0.55 to 0.65 (Figure 3-6). It suggested that more connected pores were formed in the slag cement matrix prepared at higher liquid/solid ratios. Furthermore, when the liquid/solid ratio was higher than 0.65, it seemed the water permeability remained constant. This behavior is probably due to the decreased elastic modulus of the samples at such high liquid/solid ratios. Moreover, the dense structure and much smaller pore structure of AAS mixtures respect to OPC, cause a much lower permeability, only 1/100 to 1/10 of that of cement conglomerates. Different admixtures or micro filling nano materials may be dosed with the AAS mixture to possibly enhance its pore structures. A

replacement of 10% slag with micro-silica has been found to improve the impermeability of AAS, which was attributed to the effect of additional reaction product and particle of the system, leading to a more densified microstructure [147]. Bernal et al. [146] found that increasing the slag content in AAS could lead to significant decrease in the capillary sorptivity. Similar results were reached by Rodriguez et al. [148], where they outlined that permeability and total porosity were reduced when the slag content was increased from 300 kg/m^3 to 400 kg/m^3 in AAS cement. However, when the binder content was increased to 500 kg/m^3 , there was no significant change in the permeability value.

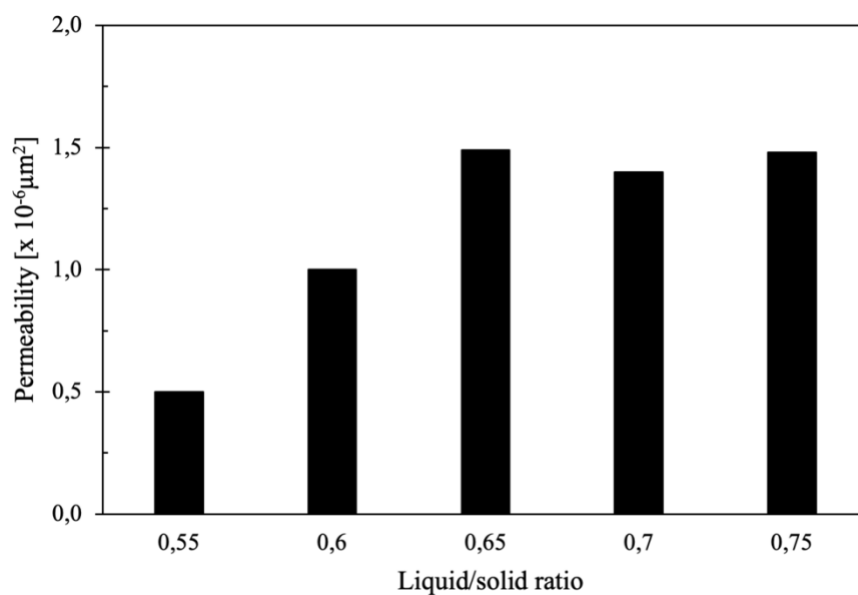


Figure 3-6 Effect of liquid/solid ratio on permeability of AAS binders [66]

3.1.7 Resistance to high temperature and fire

OPC-based concretes show a weak performance when subjected to a thermal treatment and when the temperature rises above 400°C they begin to disintegrate. In particular, the mechanical properties deteriorate due to chemical and physical changes in the hydrated phases of the binder. The thermal transformations lead to dehydration and loss of chemically bound water, mainly from the dehydroxylation of the portlandite, which induces a reduction in chemical bonding and strength [132]. In addition to strength loss, Portland cement-based mixtures are prone to fire induced spalling which can reduce the section thickness and expose the steel bars to fire. Shoaie et al. [149] showed that AAS concrete manifested a higher fire resistance compared to that of the equivalent

Portland cement concrete for temperatures beyond 300°C. The remarkable high temperature resistance of AAS may be partially attributed to the absence of portlandite. On the other hand, the physicochemical alterations of AAS binders at high temperatures are the causes of thermal degradation, including strength loss, matrix cracking and volumetric disintegration [150]. De Gutierrez et al. [151] concluded that the residual strength of alkali-activated slag materials up to 1000°C were similar to the control OPC mixtures. Similar results were obtained by Guerrieri et al. [152] that detected that AAS mortars had a rapid strength loss of approximately 60% between 100 and 200°C and a further strength loss in the order of 30% at 800°C (Figure 3-7). Furthermore, the addition of fibers to the cementitious matrix has been shown to enhance the fire resistance since fibers can mitigate cracking due to thermal loading. Shoaie et al. [149] reported that the AAS mortar with the addition of glass fiber has a higher residual strength than OPC mortars after exposure to 500°C, with the same initial compressive strength. Mastali et al. [153] investigated the fire resistance of AAS mortar reinforced with different types of fibers up to a temperature of 600°C. They reported that the minimum compressive strength and flexural strengths reduction were recorded for the steel fiber-reinforced mix and basalt fiber(BF)-reinforced mix showed the lowest strength loss among the nonmetallic fibers.

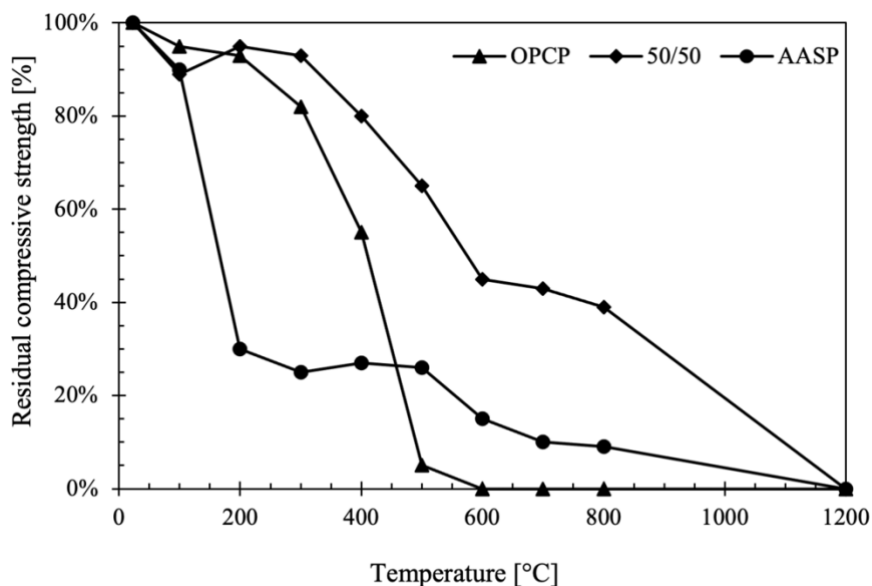


Figure 3-7 Residual compressive strength [152].

(OPCP = ordinary Portland cement paste, 50/50 =blended 50% OPC/50% slag paste, AASP=alkali activated slag paste).

3.1.8 Alkali-silica reaction

The alkali-silica reaction (ASR) occurs when the amorphous or poorly crystallized silica phase in an aggregate is attacked and dissolved by the alkali hydroxides in the concrete pore solution. The formation of an alkali-silica gel leads to concrete swelling and cracking. ASR will develop only if there is a sufficient amount of alkalis in the concrete pore solution and a sufficient moisture level in the concrete and reactive aggregate.

Though slag is used in Portland cement concrete to curb the expansions due to ASR, the scientific literature does not yet have an answer about the resistance of AAS made with ASR reactive aggregates. With the high slag and directly calcium content in AAS, it is expected that AAS should be resistant to alkali ASR. However, Awoyera et al. [126] found out the resistance of Alkali-Activated Slag to ASR is lower to that of OPC composites. In particular, the expansions observed in AAS samples were attributed to the formation of sodium calcium silicate hydrate. Shi et al. [154] reviewed the effect of alkali dosage and/or silica modulus on ASR. Some studies [155,156] reported that ASR expansion increased with the increase of alkali dosage, and others reported that ASR expansion decreased with the increase of alkali dosage (Figure 3-8).

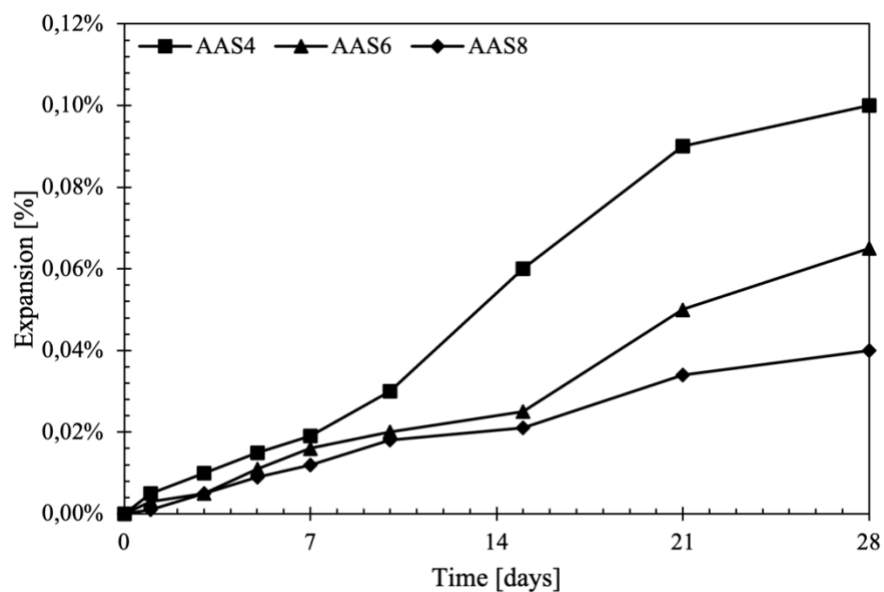


Figure 3-8 ASR expansion of the AAS mortars containing different alkali dosages, the numbers represents the weight percentage of activators [157]

3.2 Experimental research on AAS mortars

3.2.1 Materials

The one-part alkali activated slag-based mortars were prepared by using a ground granulated blast furnace slag (GGBFS) with 28-day pozzolanic activity index equal to 0.76 (according to EN 196-5) as precursor and an alkaline powder as activator. In particular, a blend of sodium silicate, potassium hydroxide and sodium carbonate (all technical grade) with relative mass ratio of 7:3:1 was used as activator in accordance with previous studies [69,158]. Moreover, two different cement-based mortars were manufactured as reference by using a Type I Portland cement CEM I 42.5R (PC) and a CEM III/B 42.5N blast furnace cement with high slag content (BFC). The physical properties and the chemical composition of binders (Table 3.1) were investigated by means of laser granulometry (Mastersizer 3000 Malven Instruments Ltd) and SEM-EDS measurements (Inspect, FEI company).

Table 3-1 Chemical composition and physical properties of binders

	Component wt%									Spec. mass [kg/dm ³]	Spec. surface [m ² /kg]
	CaO	Al ₂ O ₃	SiO ₂	Fe ₂ O ₃	SO ₃	TiO ₂	K ₂ O	MgO	Others		
PC	63.7	5.2	19.1	3.5	2.9	0.3	0.6	1.1	3.6	3.0	350
BFC	47.7	6.3	32.9	2.5	3.1	1.8	0.4	4.8	0.5	3.0	410
GGBFS	45.8	10.0	32.8	1.5	0.2	2.0	0.5	6.4	0.8	3.1	345

The XRD pattern (Rigaku Miniflex 60, X-ray source Cu K-alpha 0.15418 nm, 40 kV, 15 mA, theta step 0.02, rate 1°/min) of GGBFS shows the typical amorphous hump around $2\theta = 25^\circ - 35^\circ$ that reflects the short range order of CaO-Al₂O₃-MgO-SiO₂ glass structure in accordance with [26] (Figure 3-9). Furthermore, the basicity coefficient K_b and the quality coefficient K_q , calculated according to Wang et al. [15] starting from the chemical composition of GGBFS, were equal to 1.20 and 1.77, respectively.

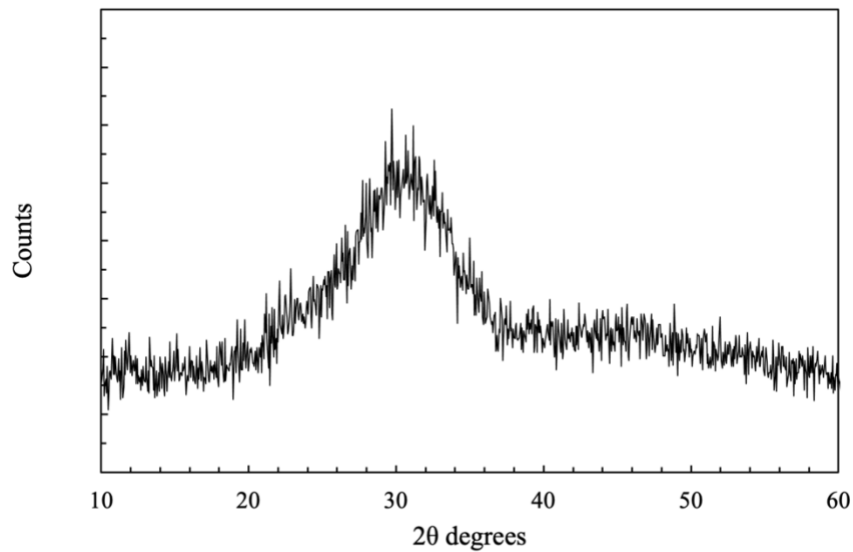


Figure 3-9 XRD pattern of GGBFS

Five different natural siliceous sands (Table 3.2) with maximum size of 2.5 mm were used as aggregates. Finally, a superplasticizer based on ester of methacrylic acid monomer (PCE) having 1000 g/mol side chain length and an acid/ester ratio equal to 3.5 and an air-entraining agent (AEA) based on cocamide diethanolamine (according to EN 934-2 and EN 480-2) were used.

Table 3-2 Physical properties of aggregates

Aggregate size [mm]	Specific mass [kg/dm ³]	Water absorption s.s.d. [wt%]	Dosage [wt% vs total aggregates]
0.00/0.25	2.41	1.20	25
0.25/0.50	2.70	0.76	30
0.50/1.00	2.58	0.77	25
1.00/1.50	2.63	0.93	10
1.50/2.50	2.62	1.02	10

3.2.2 Mixtures, preparation and samples curing

Three one-part alkali activated slag-based mortars were prepared at equal silica modulus ($M_s = 0.48$) by varying the alkali content (A_c) between 0.038 and 0.075 [159]. In addition, two cementitious mortars manufactured with Portland cement (PC) or blast furnace cement (BFC) were used as control mixtures. In all mixes, the water/binder (w/b) and the sand/binder (s/b) of mortars were fixed at 0.55 and 3.00, respectively. Furthermore, in order to ensure a thixotropic consistency of cement-based mortars, a superplasticizer was used at 0.5 wt% vs cement mass. Finally, a second set of mortars was prepared by using the air-entraining agent in order to achieve an air content equal to

10 ± 1% in order to evaluate the effectiveness of AEA to enhance the freeze/thaw resistance of one-part AAS. Details on the mix composition are listed in Table 3.3.

Cement based mortars were manufactured according to EN 196-1 while AAS mixtures were prepared in accordance with the “Dry mixing method” reported in [160] and already used in previous studies [69,161]. In particular, the procedure is composed by five phases:

- i) GGBFS, alkali activator in solid form and tap water are placed into the steel bowl;
- ii) The mixer starts at low speed (140 rpm for the revolving action, 62 rpm for the planetary action) for 30 seconds;
- iii) The mixing proceeds at high speed (285 rpm for the revolving action, 125 rpm for the planetary action) for 60 seconds;
- iv) The mixture rests for 90 seconds;
- v) The mixer completes the procedure with further 60 seconds at high speed.

Prismatic specimens were cast and kept in laboratory conditions for 24 hours (20 ± 2°C). Then, the specimens were removed from the steel mold, rinsed in water and cured in a climatic chamber (20 ± 2°C, 60 ± 5% R.H.) till the time of experiment.

Table 3-3 Composition of mortars. PC: Portland cement-based mortars; BFC: Blast furnace cement-based mortars; AAS: Alkali activated slag-based mortars (the number indicates the activator to slag ratio by mass); AE: mortars containing AEA

Composition [g]	PC <i>PC_AE</i>	BFC <i>BFC_AE</i>	AAS8 <i>AAS8_AE</i>	AAS12 <i>AAS12_AE</i>	AAS16 <i>AAS16_AE</i>
PC	450				
BFC		450			
GGBFS			450	450	450
Activators			36	54	72
Aggregates	1350	1350	1350	1350	1350
Water	225	225	225	225	225
Superplasticizer	2.25	2.25			
Air entraining agent	0 <i>0.140</i>	0 <i>0.125</i>	0 <i>0.225</i>	0 <i>0.200</i>	0 <i>0.160</i>
Water/binder	0.55	0.55	0.55	0.55	0.55
Aggregates/binder	3.00	3.00	3.00	3.00	3.00

3.2.3 Experimental methods

3.2.3.1 Fresh state and elasto-mechanical properties

After the mixing, the workability was measured on mortars by means of a flow table (EN 1015-3), the specific mass was evaluated at fresh state according to EN 1015-6 and the air content was detected in accordance with EN 1015-7. Specific mass at hardened

state, flexural and compressive strength were determined at 1, 7, 28, 56 and 84 days from casting (EN 1015-11). Furthermore, dynamic modulus of elasticity of mortars was estimated by means of Ultrasonic Digital Indicator Tester at 28 days in accordance with EN 12504-4.

3.2.3.2 *Freezing and thawing resistance*

The freeze-thaw cycles resistance of AAS manufactured with and without AEA was evaluated according to the Italian Standard UNI 7087 (minimum temperature -20°C , maximum temperature $+5^{\circ}\text{C}$, cooling speed $-4,5^{\circ}\text{C/h}$, cycle time of 12 hours) measuring the mass change, the compressive strength loss and the elastic modulus variations every 25 cycles up to 150 cycles. The experimental test was performed on mortar samples cured for 28 days at 20°C and relative humidity R.H. equal to 60%.

3.2.3.3 *Calcium chloride resistance*

The aptitude to the formation of the expansive compound (calcium oxychloride) of AAS in CaCl_2 -based deicing salts-rich solutions was investigated. Mortar specimens were cured for 28 days in a climatic chamber at 20°C and 60% R.H., subsequently were stored for 28 days in a 30 wt% CaCl_2 solution at 38°C to promote the calcium chloride ingress in the matrix and finally were cooled at 4°C in order to enhance the expansive compound formation as a consequence of reaction between calcium chloride, lime and water [162]. The durability was evaluated as mass change and strength loss compared with mortars stored in deionized water following the same thermal cycle (20°C for 28 days, 38°C for 28 days and then cooled at 4°C).

3.2.3.4 *Magnesium sulphate attack resistance*

After 28-day curing at 20°C and R.H. 60%, the prismatic specimens were partially immersed in 10 wt% MgSO_4 solution. The efflorescence formation was monitored every 7 days up to 130 days, then the degradation of cementitious matrix was determined by measuring both the mass of efflorescence and the strength loss of specimens in different areas (totally immersed in the solution, exposed to air and close to the free surface of solution) as reported in Figure 3-10.

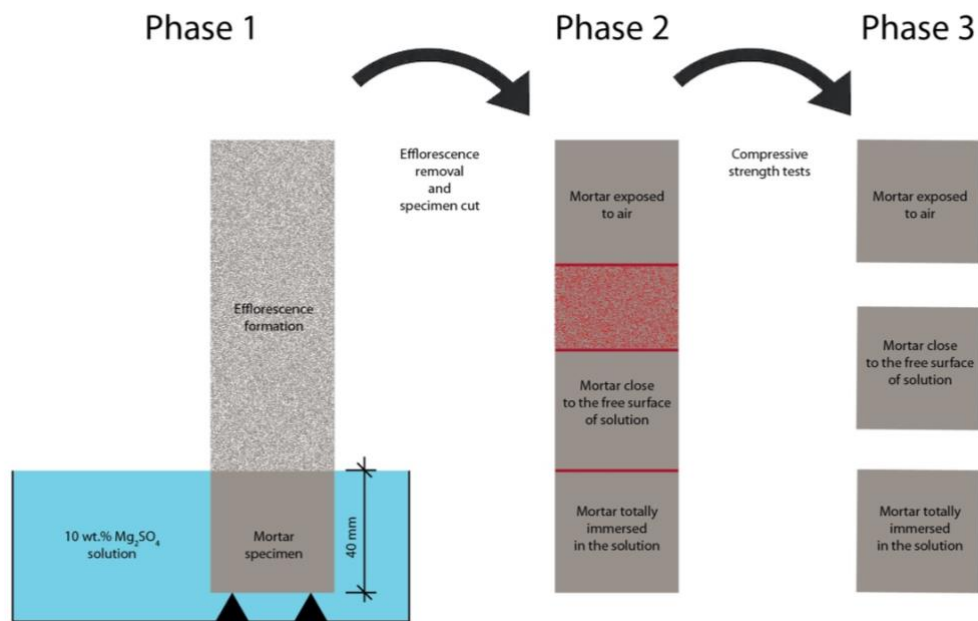


Figure 3-10 Schematic procedure for evaluating the durability of mortars in sulphate-rich aqueous solution

3.2.3.5 Carbonation resistance

After 28-day curing at 20°C and R.H. 95%, the specimens were removed from the humidity chamber, and then the lateral surface of the specimens were covered using an epoxydic resin, applying a minimum of 2 layers, to direct the ingress of CO₂ through the top and bottom of the specimens during the testing. Samples were then transferred to the carbonation chamber for CO₂ exposure, without application of an intermediate drying or conditioning step. A CO₂ concentration of $3.0 \pm 0.5\%$ was used, at a temperature of $20 \pm 2^\circ\text{C}$, and R.H. values of $57 \pm 3\%$, values in according to EN 12390-12:2020. Carbonation depths were measured after 1, 4, 7, 14, 28 and 56 days of CO₂ exposure. Mortars were split into two halves and the fresh surface was immediately sprayed with 1 wt% phenolphthalein in ethanol. The carbonation depths were measured on the mortars after the color had stabilized. Also, the compressive strength test uncarbonated and carbonated samples (40 x 40 x 40 mm³) were tested and an average of results from at least three samples was reported.

3.2.3.6 Sulfuric acid resistance

After 28-day curing at 20°C and R.H. 60%, the specimens (40 x 40 x 40 mm³) were removed from the climatic chamber, and then the lateral surface and the bottom of the specimens were covered using an epoxydic resin, applying a minimum of 2 layers, to

direct the ingress of sulfuric acid through the top of the specimens during the testing. The cubes were weighted before immersion in an acid solution. Two different tests were carried out: a traditional one, where the pH of sulfuric acid was equal to 4, 4.5 and 5.5 (values in accordance to UNI 11104) and an accelerated test, where the pH of sulfuric acid is equal to 1 (5% of sulfuric acid). The pH of the solution was measured at regular intervals to ensure its value established during the test. The mass loss, the compressive strength and the depth of the area lost alkalinity of specimens were measured at 5 h, 1, 3, 7, 9, 11, 14, 16, 18, 21, 23, 25 and 28 days of exposure.

3.2.3.7 Permeability

After 28-day curing at 20°C and R.H. 60%, the prismatic mortars samples with the dimensions (40 x 40 x 160 mm³) were used to evaluate the capillary water absorption, according to UNI EN 13057, and the total water absorption, according to ASTM C642. Moreover, water impermeability test and determination of the water penetration depth was carried out according to UNI EN 12390-8. In line with this standard, the specimens were placed in a specially designed cell and its lower surface was subjected to a water pressure of 5 bars for 72 h. Sample was then split open from the middle and the maximum water penetration depth was measured by a caliper. Finally, the Karsten tube penetration, according to UNI EN 16302:2013 were used. Karsten tubes are calibrated glass tubes with volume graduation. The tubes were applied onto the surface of the specimens using plasticine and the tubes were filled with water. The duration of the test was 60 minutes, while the drop in the water level was recorder at regular intervals of 5 minutes.

Table 3-4 Summary of tested properties and sample details

Property type	Tested property	Sample details	Testing procedure
Physical	Flexural and compressive strength, specific mass	40x40x160 mm ³ mortars beam (three samples for each mix)	Test procedure according to UNI EN 1015-11. Three samples were tested at the age of 1, 7, 28, 56 and 84 days
	Modulus of elasticity	40x40x160 mm ³ mortars beam (three samples for each mix)	Test procedure according to UNI EN 12504-4. Three samples were tested at the age of 28 days
Freeze-thaw resistance	Visual appearance	40x40x160 mm ³ mortars beam	Three samples were assessed after every 25 freeze-thaw cycles up to 150 cycles
	Mass change	40x40x160 mm ³ mortars beam	Three samples were assessed after every 25 freeze-thaw cycles up to 150 cycles

	Compressive strength loss	40x40x160 mm ³ mortars beam	Three samples were assessed after every 25 freeze-thaw cycles up to 150 cycles
	Elastic modulus variations	40x40x160 mm ³ mortars beam	Three samples were assessed after every 25 freeze-thaw cycles up to 150 cycles
Calcium chloride resistance	Visual appearance	40x40x160 mm ³ mortars beam	Three samples were assessed after every 2 days
	Mass change	40x40x160 mm ³ mortars beam	Three samples were assessed after every 7 days
	Compressive strength loss	40x40x160 mm ³ mortars beam	Three samples were assessed after every 7 days
Magnesium sulphate resistance	Visual appearance	40x40x160 mm ³ mortars beam	Three samples were assessed after every 7 days up to 130 days
	Mass of efflorescence	40x40x160 mm ³ mortars beam	Three samples were tested at the age of 130 days
	Compressive strength loss	40 mm mortars cubes	Three samples were tested at the age of 130 days
Carbonation resistance	Carbonation depth	40x40x160 mm ³ mortars beam	Three samples were tested at the age of 1,4,7,14,28 and 56 days
	Compressive strength	40 mm mortars cubes	Three samples were tested at the age of 1,4,7,14,28 and 56 days
Sulfuric acid resistance	Visual appearance	40 mm mortars cubes	Three samples were tested at the age of 5 h, 1, 3, 7, 9, 11, 14, 16, 18, 21, 23, 25 and 28 days
	Mass loss	40 mm mortars cubes	Three samples were tested at the age of 5 h, 1, 3, 7, 9, 11, 14, 16, 18, 21, 23, 25 and 28 days
	Strength loss	40 mm mortars cubes	Three samples were tested at the age of 5 h, 1, 3, 7, 9, 11, 14, 16, 18, 21, 23, 25 and 28 days
	Depth of the area lost alkalinity	40 mm mortars cubes	Three samples were tested at the age of 5 h, 1, 3, 7, 9, 11, 14, 16, 18, 21, 23, 25 and 28 days
Permeability	Capillary water absorption	40x40x160 mm ³ mortars beam	Test procedure according to UNI EN 13057. Three samples were tested at the age of 28 and 90 days
	Total water absorption	40x40x160 mm ³ mortars beam	Test procedure according to ASTM C642. Three samples were tested at the age of 28 and 90 days
	Water impermeability test	150 mm mortars cubes	Test procedure according to UNI EN 12390-8. Three samples were tested at the age of 28 and 90 days
	Karsten tube penetration	150 mm mortars cubes	Test procedure according to UNI EN 16302. Three samples were tested at the age of 7 and 28 days

3.2.4 Results and discussion

3.2.4.1 Fresh state and elasto-mechanical properties

The mortars manufactured without AEA present a thixotropic consistency with a workability determined by the flow table ranging from 150 and 190 mm (Table 3-5).

Moreover, as expected, the workability of AAS mortars increases by increasing the alkali content due to the deflocculating and plasticizing effect promoted by the use of sodium silicate as activator that reduces the yield stress at early ages [29,163].

Table 3-5 Fresh and hardened properties of mortars manufactured without AEA

	PC	BFC	AAS8	AAS12	AAS16	
Workability [mm]	150	160	165	180	190	
Entrapped air [%]	5.0	5.2	4.7	4.5	4.0	
Specific mass at fresh state [kg/m ³]	2140 ± 5	2140 ± 4	2150 ± 3	2150 ± 4	2165 ± 5	
Specific mass at hardened state [kg/m ³]	2110 ± 4	2100 ± 6	2010 ± 5	2090 ± 4	2120 ± 4	
Flexural strength [MPa]	1 day	4.9 ± 1.2	3.0 ± 0.4	0.3 ± 0.1	2.5 ± 0.3	2.7 ± 0.6
	7 days	6.8 ± 0.3	4.3 ± 1.5	2.1 ± 0.6	2.7 ± 0.6	3.0 ± 0.5
	28 days	9.1 ± 0.7	6.7 ± 1.6	2.7 ± 1.2	3.1 ± 0.9	3.4 ± 0.4
	56 days	9.2 ± 1.1	6.8 ± 1.8	2.7 ± 1.1	3.2 ± 0.4	3.4 ± 0.6
	84 days	9.3 ± 1.3	7.0 ± 0.9	2.9 ± 0.8	3.8 ± 1.1	3.5 ± 0.7
Compressive strength [MPa]	1 day	27.8 ± 2.3	12.4 ± 1.6	1.1 ± 0.3	9.4 ± 1.1	10.9 ± 1.7
	7 days	46.5 ± 3.1	31.5 ± 2.1	15.4 ± 0.7	25.5 ± 1.6	30.2 ± 2.6
	28 days	47.7 ± 3.5	43.1 ± 3.4	18.1 ± 1.2	34.0 ± 2.6	39.1 ± 3.1
	56 days	48.1 ± 3.8	44.2 ± 3.8	19.0 ± 1.1	35.0 ± 3.1	40.2 ± 3.3
84 days	48.3 ± 3.4	44.7 ± 3.9	19.4 ± 0.9	35.8 ± 3.8	41.3 ± 2.9	
28-day elastic modulus [GPa]	32.8 ± 2.8	30.2 ± 2.4	20.9 ± 1.5	24.9 ± 2.4	27.9 ± 2.7	

The addition of the AEA determines an increase of workability of about 50% both in cementitious and alkali activated mortars (Table 3-6) due to the spherical air bubbles that act as a fine aggregate of very low surface friction. The air content and the specific mass at fresh state of mortars without AEA are similar, generally close to 5% and 2150 kg/m³, respectively. On the contrary, the 28-day specific mass of AAS8 is 110 kg/m³ lower than that of AAS16, probably due to the smaller degree of reaction of slag and higher free water content as reported by Coffetti [164]. As reported in Table 3-3, the effectiveness of AEA in the air-entrained mortars varies depending on the nature of the binder (PC and BFC require less admixture respect to AAS mortars) and the Ac of alkali activated mortars (by increasing the Ac, the dosage of AEA to obtain an air content close to 10% decreases down to 40%).

Table 3-6 Fresh and hardened properties of mortars manufactured with AEA

	PC_AE	BFC_AE	AAS8_AE	AAS12_AE	AAS16_AE	
Workability [mm]	180	185	210	220	220	
Entrapped air [%]	11.0	11.0	10.5	10.0	11.0	
Specific mass at fresh state [kg/m ³]	2000 ± 5	2010 ± 6	2020 ± 5	2020 ± 4	2010 ± 5	
Specific mass at hardened state [kg/m ³]	1950 ± 4	1950 ± 4	1970 ± 3	1980 ± 3	1980 ± 3	
Flexural strength [MPa]	1 day	3.2 ± 0.4	1.9 ± 0.4	0.2 ± 0.1	1.8 ± 0.5	1.9 ± 0.3
	7 days	5.7 ± 1.2	3.1 ± 0.7	1.2 ± 0.2	2.1 ± 0.3	2.5 ± 0.7
	28 days	7.8 ± 1.8	5.0 ± 1.1	1.8 ± 0.4	2.5 ± 0.7	2.9 ± 0.4
	56 days	8.0 ± 1.3	5.2 ± 0.8	2.0 ± 0.6	2.9 ± 0.4	3.0 ± 0.6
	84 days	8.0 ± 1.7	5.8 ± 1.2	2.1 ± 0.2	3.0 ± 0.6	3.2 ± 0.3
Compressive strength [MPa]	1 day	19.4 ± 2.4	8.0 ± 1.6	0.8 ± 0.2	5.6 ± 1.3	7.2 ± 1.3
	7 days	39.1 ± 3.7	26.3 ± 2.4	12.5 ± 1.4	19.3 ± 2.5	25.4 ± 2.4
	28 days	41.2 ± 3.6	36.3 ± 3.3	13.4 ± 0.9	22.6 ± 2.8	30.2 ± 3.3
	56 days	42.1 ± 4.4	37.0 ± 3.6	14.1 ± 1.5	25.1 ± 3.1	32.1 ± 3.7
	84 days	42.5 ± 3.8	37.9 ± 3.9	15.0 ± 1.7	27.0 ± 3.3	33.5 ± 3.9
28-day elastic modulus [GPa]	28.1 ± 3.1	27.0 ± 2.4	17.9 ± 1.6	21.6 ± 1.8	25.9 ± 2.6	

Concerning the compressive strength measured on prismatic specimens (Table 3-5 and 3-6), it is possible to note that by growing the alkali content, the strength increases regardless of age due to the higher pH of activating solution that promotes the dissolution of silica and alumina of GGBFS [13] and the formation of a denser microstructure [164]. In particular, after 28 days, AAS8 reaches a strength class of 20 MPa, AAS12 of 35 MPa and AAS 16 of 40 MPa while PC shows strength close to 48 MPa and BFC is characterized by a compressive strength of 43 MPa. Furthermore, it is evident that the flexural strength and the dynamic elastic modulus of elasticity of cement-based mixtures are generally higher than those of AAS mortars, mainly due to the micro-cracks formation related to the high shrinkage of alkali activated materials [165,166]. The influence of AEA addition on the compressive strength of mortars was evaluated by means of coefficient η at different ages calculated as the ratio between the strength of air-entrained mortar and the mixture manufactured without AEA. Results reported in Figure 3-11 evidence a delay in the strength development at 24 hours (η is in the range 60% - 70% for all mixes) while the strength of the air-entrained mixtures at late ages is about 75% for alkali activated mortars and 85% for cementitious mortars with respect to the mixtures manufactured without AEA.

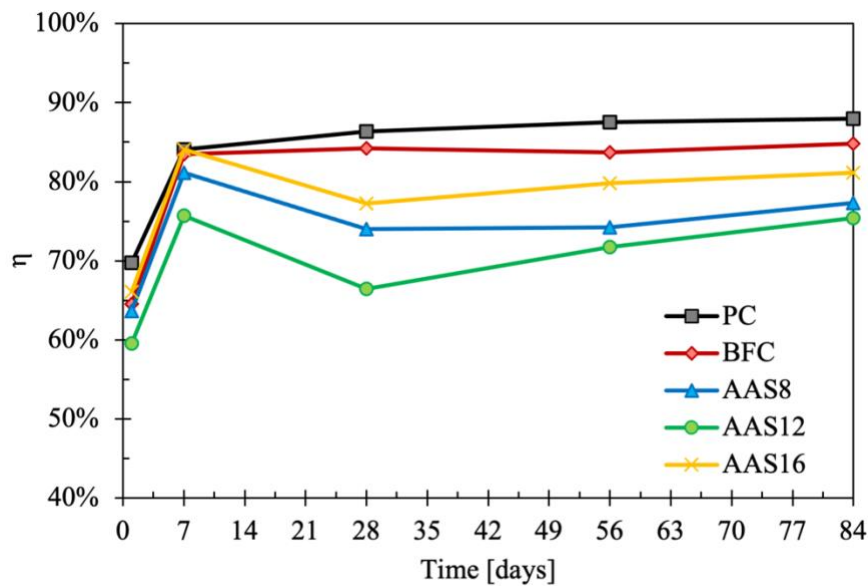


Figure 3-11 Ratio η between the compressive strengths of air-entrained mortars and mixtures produced without AEA at different ages

3.2.4.2 Freezing and thawing resistance

The visual observation of specimens subjected to freeze and thaw cycles highlights a strong superficial deterioration of AAS8 and AAS8_AE mortars already after 50 cycles while the other alkali activated mortars (AAS12 and AAS16) and the cement-based mortars (PC and BFC) are characterized by minor damages or appear intact at the end of 150 cycles, regardless of the addition of AEA (Figure 3-12).

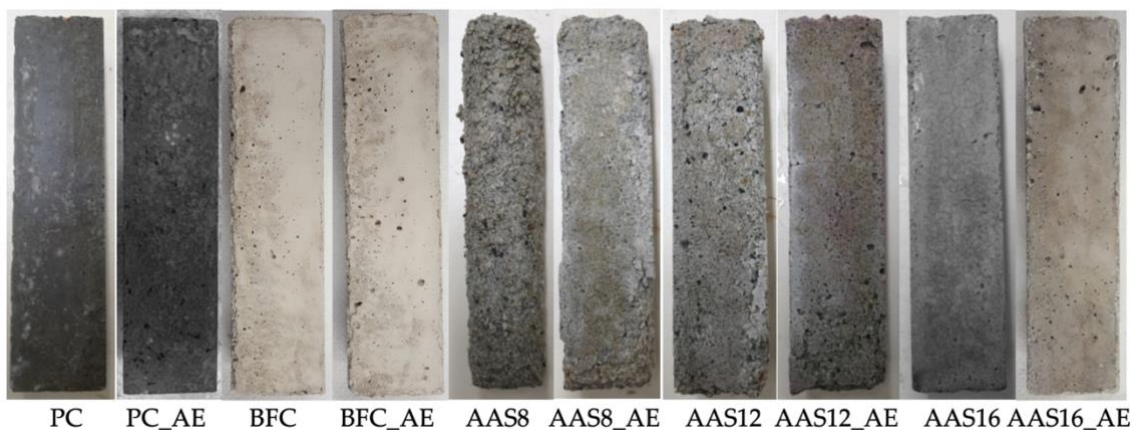


Figure 3-12 Superficial deterioration of specimens after 150 cycles

The superficial deterioration of AAS8 is combined with a pronounced mass loss that reaches 2% after 75 cycles and achieves 12% at the end of test that corresponds to a reduction in the specimen size of about 3 - 4 mm. On the contrary, the mass change after

150 cycles is close to zero for all the other non-admixed samples (Figure 3-13). The addition of the AEA promotes a strong enhancement in the freezing and thawing resistance of AAS8_AE with a reduction of the mass loss at the end of the freeze/thaw cycles approximately by half. However, the mass loss of this mixture, despite the addition of the AEA, is very high due to its poor mechanical properties.

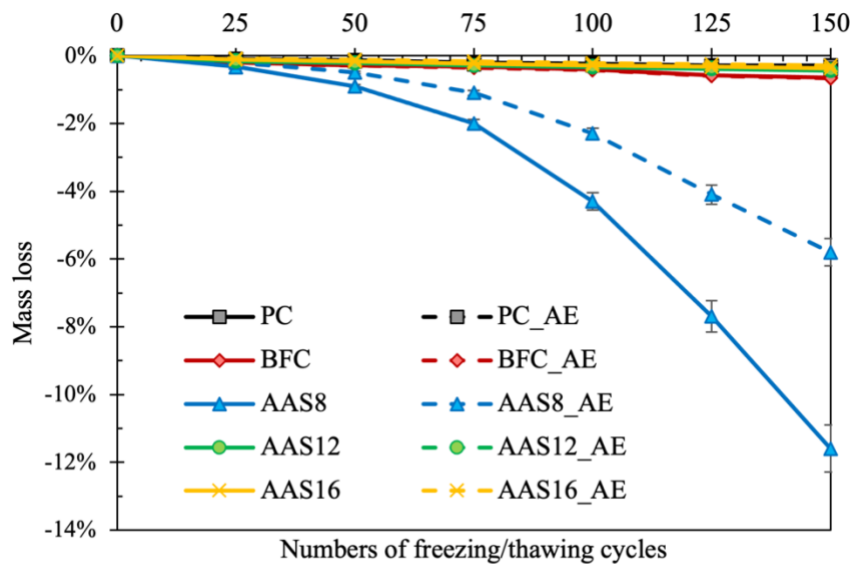


Figure 3-13 Mass loss of mortars as a function of numbers of freezing/thawing cycles

In Figure 3-14 the strength loss of mortars is reported over time with respect to specimens cured at 20°C. Results indicate that PC samples are not affected by compressive strength variation, BFC, AAS12 and AAS16 worsen their mechanical performances by about 25-30% while alkali activated mortar AAS8 shows strength loss of 70% after 150 cycles. The mortars manufactured with the addition of AEA show a greater resistance to freezing and thawing cycles, with strength loss strongly reduced respect to the non-admixed mortars. In particular, by the addition of the AEA, the AAS8_AE reduces the compressive strength loss from 67% to 45%, the AAS12_AE from 30% to 22%, the AAS16_AE from 25% to 18% and the BFC_AE from 26% to 14%. No significant variations were detected in Portland cement-based mortars.

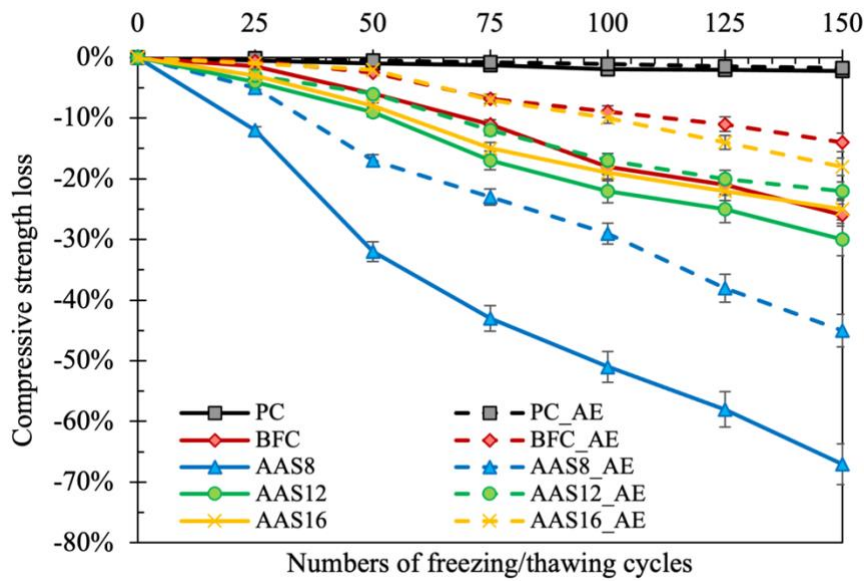


Figure 3-14 Strength loss of mortars as a function of numbers of freezing/thawing cycles

Nevertheless, Fu et al. [123] claim that it is improper to set the mass change and the strength loss of alkali activated materials as index of freeze and thaw damage, suggesting to evaluate the dynamic modulus of elasticity to estimate the freeze and thaw resistance of AAS. Experimental results reported in Figure 3-15 show that with increase of freeze and thaw cycling times, elastic modulus of PC decrease extremely slowly (less than 10% after 150 cycles), evidence of excellent durability, while BFC and AAS lose approximately 25-30% of dynamic modulus of elasticity at the end of test. Alkali activated mortar AAS8 is an exception because it shows an extremely marked stiffness loss (60% after 150 cycles), consistently with the mass change and the strength loss reported in previous figures. The use of AEA determines a reduction of stiffness loss for all mixes up to 50%, in accordance with the other results reported in the paragraph. Moreover, by measuring the dynamic modulus of elasticity it is possible to appreciate the role of the air entraining admixture in the improvement in the freeze/thaw resistance of Portland cement-based mortar, with a reduction in stiffness loss from 7% (PC) to 2.2% (PC_AE).

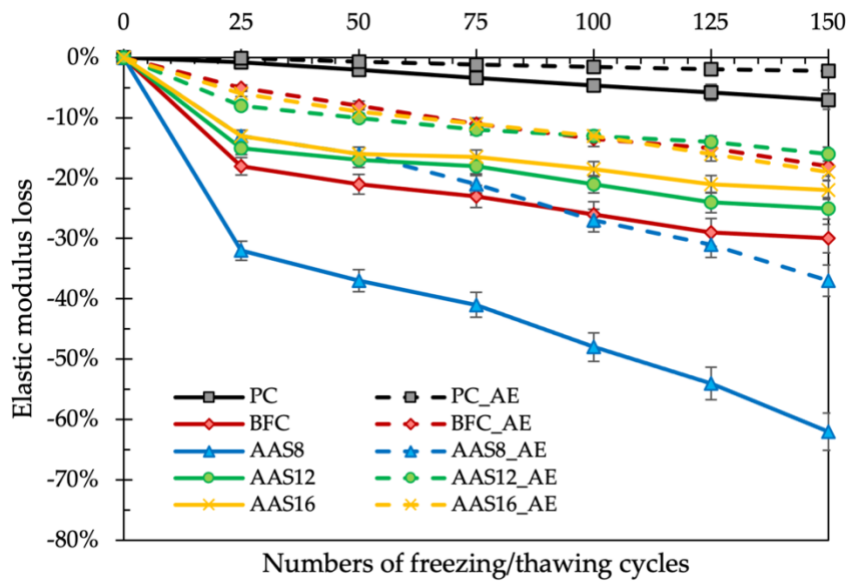


Figure 3-15 Elastic modulus loss of mortars as a function of numbers of freezing/thawing cycles

The different behavior between the non-admixed mortars is primarily attributable to the compactness of matrix. In fact, according to Shahrajabian and Behfarnia [120], low compactness of the mortars promotes the water penetration, freezing and saturation, thereby reducing the durability against freeze and thaw cycles. This is confirmed by optical microscopy observation on AAS8 sample (before the freeze and thaw cycles) that highlights a low-density structure with micro-cracks and air void ranging from 20 and 200 μm (Figure 3-16).

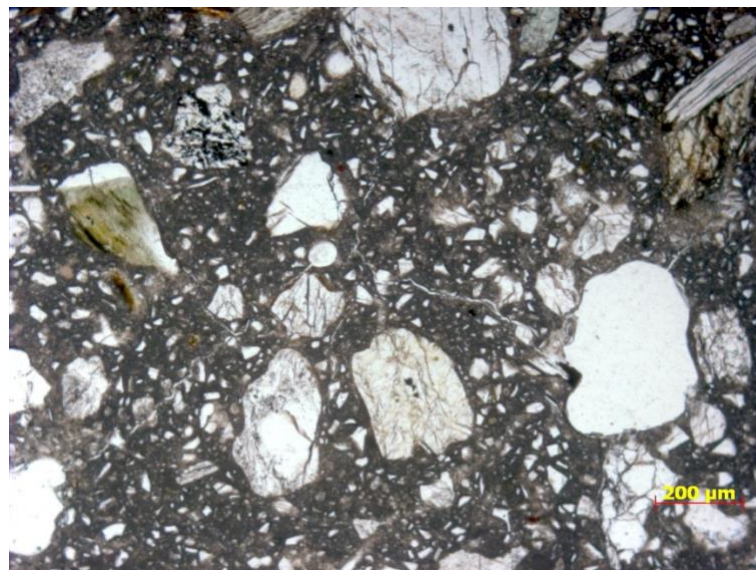


Figure 3-16 Optical microscopy observation of AAS8 before freeze/thaw cycles

3.2.4.3 Calcium chloride resistance

The visual examination was regularly made (every 2 days) to assess the conditions of the specimens. Micro-cracks along the edges and separation of the surface layer from the core of the specimens are the main damages detected on PC mortars (Figure 3-17). Also, the mass loss and the strength loss are very pronounced (Figure 3-18 and 3-19), reaching values close to 2% and 40%, respectively, already after 7 days at 4°C. On the contrary, BFC and AAS samples appear unaltered without significant mass changes and strength loss lower than 8%.



Figure 3-17 PC specimen after 42 days in CaCl_2 -rich solution

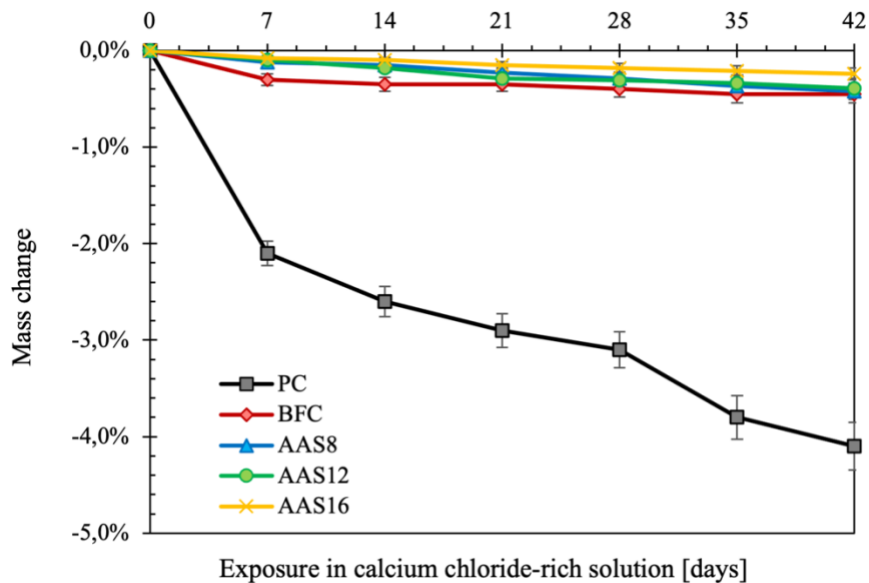


Figure 3-18 Mass change of specimens exposed to CaCl_2 -rich solution

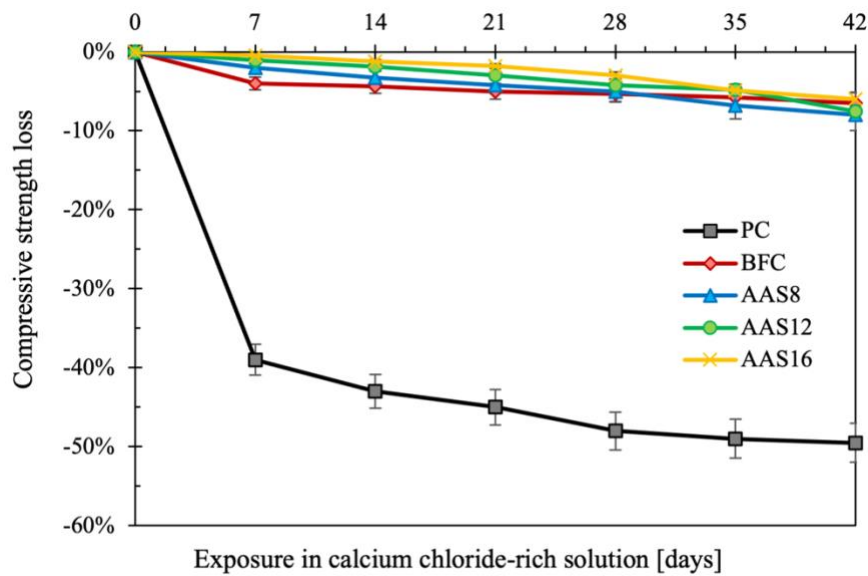
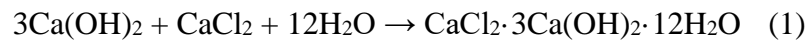


Figure 3-19 Compressive strength loss of specimens exposed to CaCl₂-rich solution

This behavior could be related to the calcium hydroxide content of alkali activated mixtures and cement mortars. In fact, the reaction can occur between the calcium hydroxide in the matrix, the calcium chloride in the deicing salt and the water as reported in equation 1:



The higher the amount of Ca(OH)₂, the greater the calcium oxychloride formation [167]. As well known, in the Portland cement-based mixtures, one of the main hydration products is the calcium hydroxide which is therefore widely available for the reaction with calcium chloride. On the other hand, the pozzolanic reaction involving the blast furnace cements promotes the transformation of calcium hydroxide into calcium silicate hydrate (C-S-H) and calcium aluminate hydrate (C-A-H), severely limiting the oxychloride formation due to the reagent shortage. Myers et al. [168,169] highlighted that the calcium hydroxide in the reaction products of AAS produced with high calcium GGBFS are totally missing or very limited. For this reason, the use of alkali activated slag-based binders instead of Portland cement could strongly enhance the durability of mortars and concretes exposed to calcium chloride-based deicing salts.

3.2.4.4 Magnesium sulphate attack resistance

The partial immersion of specimens in magnesium sulphate-rich solution promotes the development of whitish efflorescence combined with an intense deterioration of AAS mortars close to the free surface of solution (Figure 3-20).

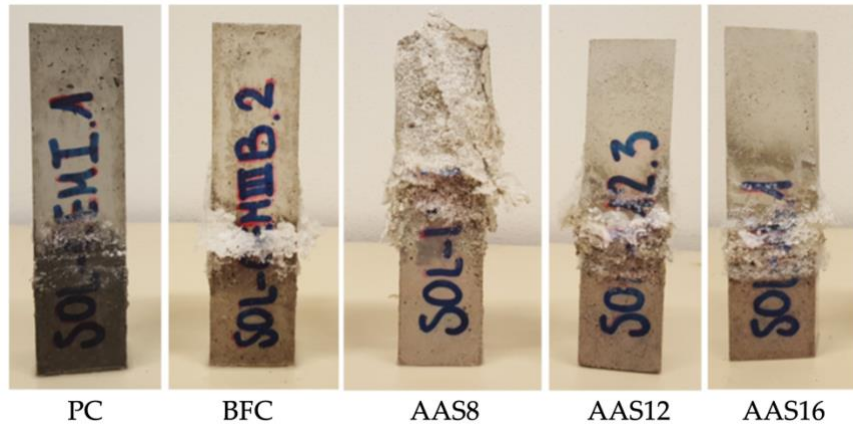


Figure 3-20 Efflorescence formation after 130 days in sulphate-rich solution

Moreover, the amount of efflorescence is strictly related to the compactness of matrix and is inversely proportional to the alkali content of mortars: the higher the alkali content, the lower the efflorescence volume (Figure 3-21). On the contrary, PC samples are almost efflorescence-free while BFC specimens are characterized by an efflorescence formation similar to that of AAS16.

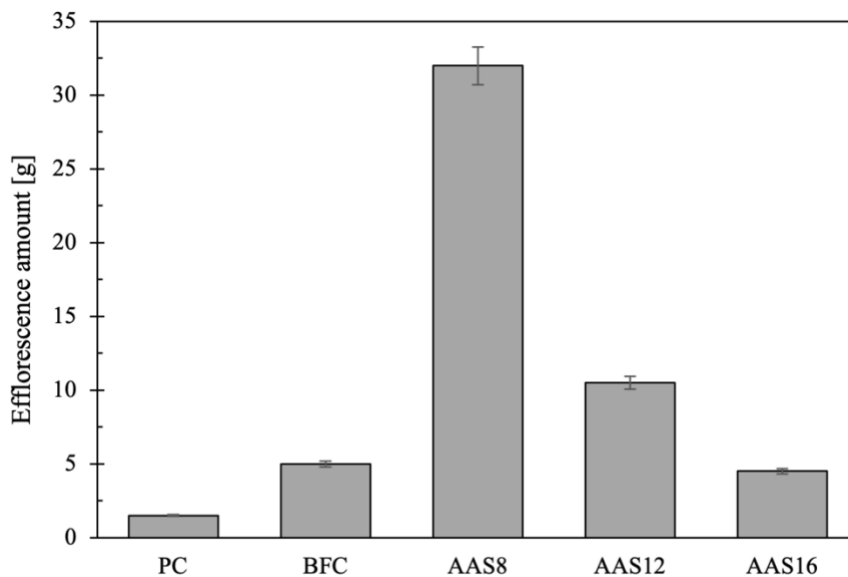


Figure 3-21 Efflorescence amount after 130 days in sulphate-rich solution

The evaluation of compressive strength after the sulphate attack evidences the vulnerability of activated alkali systems. As reported in Figure 3-22, negligible deterioration (PC, BFC and AAS16 show compressive strength unaltered) or very limited damages (AAS8 and AAS12 reduce their strength of about 5-10%) were detected in the areas totally immersed in the $MgSO_4$ solution while areas subjected to the efflorescence formation show strength losses that reach values up to 60% for AAS mortars while cement-based mixtures reduce their strength of about 15-25% after sulphate exposure. The degradation in these areas could be ascribed to the effect of the sulphate attack (formation of expansive products such as ettringite and gypsum) in combination with the deteriorating effect of the recrystallization of the sulphate salts in the mortar pores as a consequence of the evaporation of the water absorbed by the specimens by capillary. In particular, as reported by Bakharev et al. [131] and Ismail et al. [133], the mechanisms of ettringite and gypsum formation are important in sulphate attack on Portland cement-based mortars while the deterioration of AAS under sulphate attack is associated with decalcification of C-S-H gel, responsible for the precipitation of gypsum and the reduction of the binding capacity of the pastes. Moreover, the porosity of mortars and the calcium hydroxide (CH) content influences also the sulphate resistance of alkali activated mixtures and cementitious mortars. In fact, high CH contents promote the formation of gypsum as a consequence of reaction with sulphate ions. Blast furnace cements and alkali activated materials present limited or negligible calcium hydroxide content [132,164] and they are potentially very resistant to sulphates. On the other hand, the lower mechanical strengths of the AAS8 respect to Portland cement-based mortars are strictly correlated with high porosity of mortars and thus with a high permeability that limited resistance in SO_4 -rich environments.

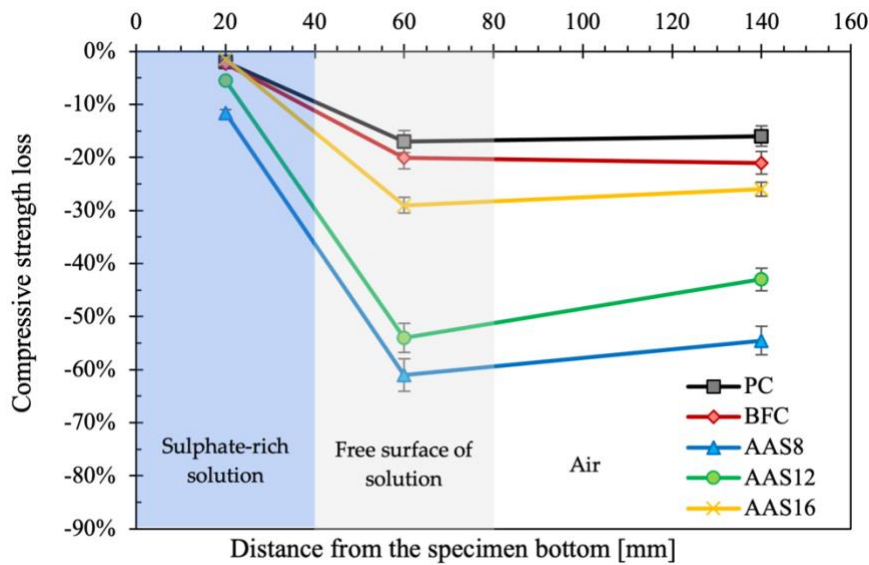


Figure 3-22 Compressive strength loss after 130 days in sulphate-rich solution

3.2.4.5 Carbonation resistance

The carbonation depths of the AAS mortars together with Portland cement mortars measured by the phenolphthalein spray method are shown in Figure 3-23 as a function of square root of time. The 56-day data for AAS8 mortars indicates that the whole mortar has been carbonated. On the other hand, complete carbonation has not been achieved for all the other mixtures investigated up to 56 days of CO₂ exposure. The results indicated that the alkali-activated slag mortars with too low activator/precursor ratio (a/p ratio) are more susceptible to carbonation compared to the Portland cement or alkali activated slag with high percentage of activators under the accelerated carbonation condition, which is in agreement with the observations from several studies [136,148,170]. AAS16 mortars exhibit carbonation resistance similar to blast furnace cement mortars, although slag-based mixtures have a lower strength than BFC mortars, 40 MPa and 45 MPa, respectively. Therefore, it can be deduced that 3% CO₂ seems to be already too aggressive to evaluate the carbonation resistance of the AAS8 mortars. The accelerated carbonation testing method used for Portland cement system may not be suitable for the evaluation of carbonation resistance of all alkali-activated cements and concretes. Also, the results in Figure 3-23 show that the carbonation depth of AAS12, AAS16, PC and BFC has a linear dependency of square root of time over the period of CO₂ exposure. This can be simply explained by a diffusion controlled mechanism [171], where carbonation reaction is

relatively instantaneous compared to the diffusion of CO₂. However, similar linear relationship is not observed in AAS8, an acceleration of carbonation is observed for these mortars after 28 days of CO₂ exposure, which might be attributed to different drying mechanism of AAS8, since the change of moisture profiles will have a significant impact on diffusion of carbon dioxide [172].

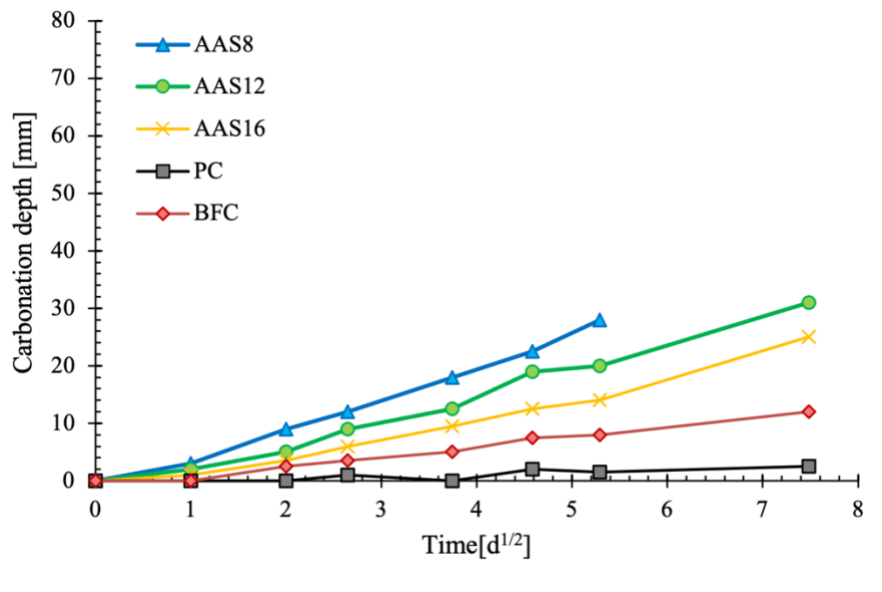


Figure 3-23 Carbonation depths of the alkali-activated mortars and Portland cement mortars

	Carbonation rate [mm/days ^{1/2}]	R ²
CEM I	0.29	0.84
BFC	1.52	0.99
AAS8	4.95	0.99
AAS12	3.87	0.99
AAS16	2.88	0.98

The effect of carbonation on the evolution of the compressive strength of the AAS mortars over the time of CO₂ exposure is shown in Figure 3-24. First of all, it is possible to observe that the carbonation increased the compressive strength of Portland cement mortars by up to 14.5%. The results are consistent with studies reported in the literature [173–175]. Carbonation of Portland cement was mainly related to the chemical reaction of Ca(OH)₂ and C-S-H with CO₂ and formation of CaCO₃ particles. CaCO₃ particles are generally micro-sized crystals which can fill pores in the matrix, reduce the porosity; and hence improve the compressive strength [173]. Also, the results show that the compressive strength of the other mortars decreased over the period of CO₂ exposure.

Similar observation in carbonation-induced strength reduction for alkali-activated slag mortars has also been reported in literature [136,148,172]. Bernal et al. [176] reported that the compressive strength decreased by approximately 60% upon complete carbonation compared to the initial compressive strength, and the fully-carbonated samples did not appear to be further degraded by longer-term exposure to CO₂. Li et al. [177] proposed two hypothetical mechanisms to explain the strength loss. One related the strength loss to a lower rate of CaCO₃ crystallization during carbonation process to fill the pore structure. Availability of trace amounts of CH and ettringite as source of Ca²⁺ for CaCO₃ formation was regarded as one main reason [178]. Besides, CaCO₃ formation rate can be suppressed by low Ca/Si of C-S-H in hardened alkali-activated slag. The other mechanism stated that, in spite of a low Ca/Si of C-S-H gel with high durability, once the decalcification occurred, the C-S-H gel damaged more quickly and cohesion of gel decreased [136].

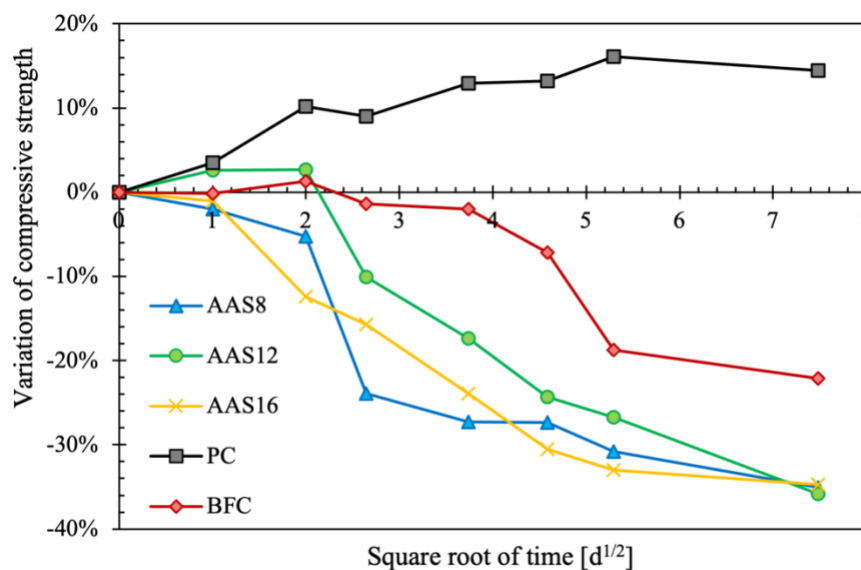


Figure 3-24 Effect of carbonation on variation of compressive strength

3.2.4.6 Sulfuric acid resistance

Figure 3-25 shows the time in minutes, depending on the volumetric ratio between solution and specimens, necessary for a sulfuric acid solution at pH = 4 to reach a pH value equal to 7. It can be observed that it is not possible to guarantee a pH below 7 for more than 160 minutes, regardless of the type of the binder and the volumetric ratio. For this reason it was decided not to continue with the traditional tests (pH of solution equal

to 4, 4.5 and 5.5), but to continue exclusively with the accelerated tests (pH approximately equal to 1, 5% of sulfuric acid). In fact, with this pH value it was found that with a volumetric ratio equal to 4, after 28 days, the sulfuric acid solution has a pH close to 2 (Figure 3-26). In particular, it was decided to monitor the pH of the acid solutions containing the AAS16 and PC mixtures as they are the conglomerates that most rapidly change the pH of the acid solution.

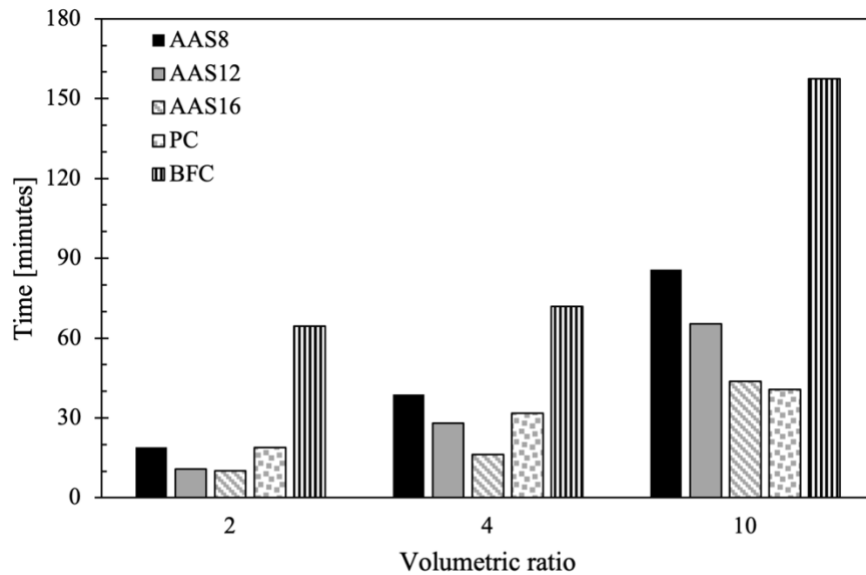


Figure 3-25 Minutes necessary for a sulfuric acid solution at pH=4 to reach a pH value equal to 7, as a function of volumetric ratio

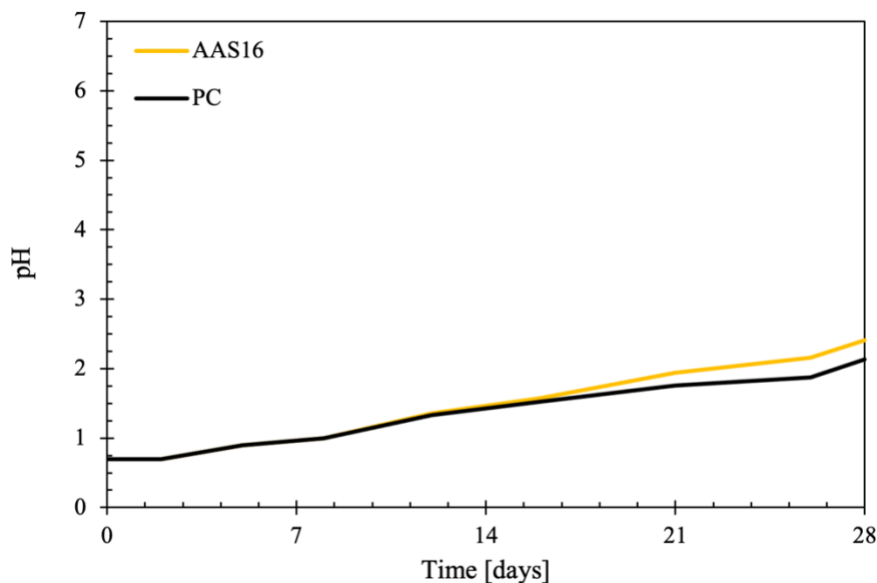


Figure 3-26 pH variation of the 5% of sulfuric acid solution as a function of time

Figure 3-27 compares the visual appearances of mortar specimens prepared with Portland cement, blast furnace cement and with alkali-activated slag after immersion in 5% sulfuric acid solution for 28 days. PC specimens exhibited some surface roughening, pointing out the surface attack of matrix by sulfuric acid. On the other hand, the specimens BFC, AAS8, AAS12 and AAS16 displayed less visible surface deterioration to 28 days of exposure.

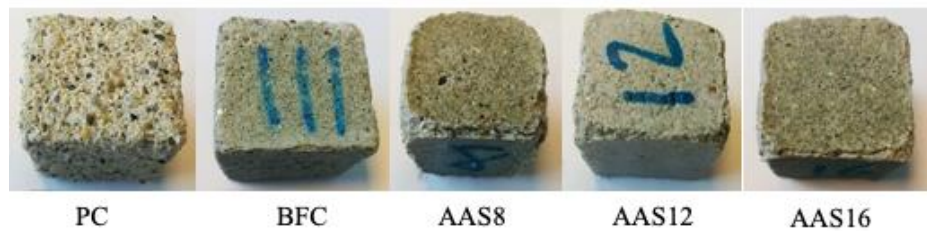


Figure 3-27 Superficial deterioration of specimens after 28 days in 5% of sulfuric acid

The mass change of the mortars over time due to sulfuric acid attack is shown in Figure 3-28. In the case of PC mortar, the mass decreased significantly, after 28 days of exposure the mass loss is equal to 23%. On the other hand, in the case of the AAS and BFC mortars the mass remained practically constant over time. This finding confirms that the AAS provides high resistance to acid attack when compared with Portland cement-based binder. In fact, the low concentration of calcium hydroxide, and low Ca/Si ratio in the alkali binder provide improved acid resistance [179].

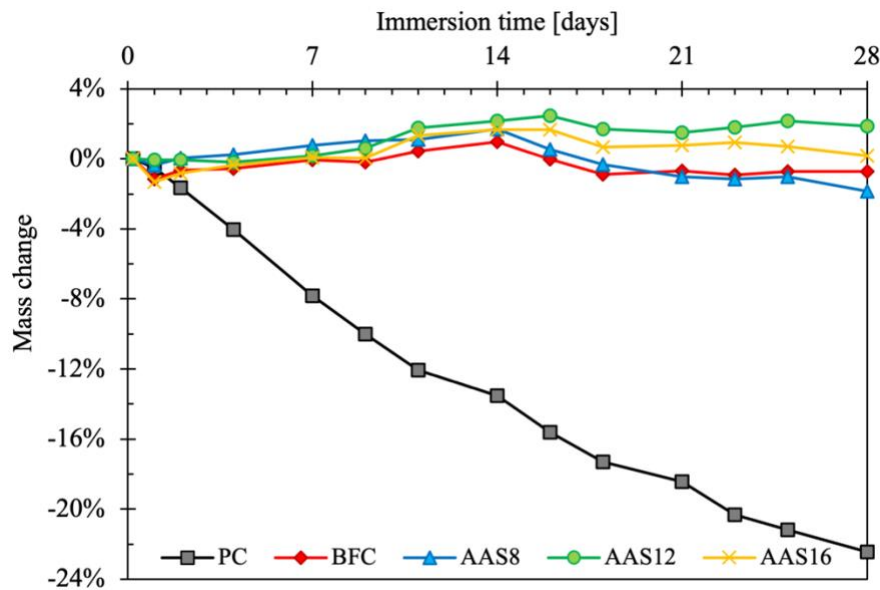


Figure 3-28 Mass change of specimens exposed to 5% sulfuric acid solution

In Figure 3-29 the strength loss of mortars is reported over time with respect to specimens cured at 20°C. Results indicate that PC shows strength loss of 75%, AAS8 and AAS12 worsen their mechanical performances by about 35% while alkali activated mortar AAS16 and BFC show strength loss of 25% after 28 days of exposure in 5% sulfuric acid solution. The action of acids on cement mortars consists in an attack on the components of the hardened cement mortars. Bakharev et al. [180] believed that this action leads to a conversion of all the calcium compounds, unreacted residue of C₃S and C₂S in cement grains, calcium hydroxide, calcium silicate hydrate, and calcium aluminate hydrate to the salt of the attacking acid. As a result of the conversation, the binding capacity of the hardened cement is destroyed. It is accepted that the rate of attack would depend on quality of the concrete and also on the solubility of the resulting salt and the permeability of precipitates. Also, it is possible that PC mortar is more vulnerable than slag mortar to acid attack due to difference in chemical and phase composition. In AAS mortars there are two causes of the deterioration due to a sulfuric acid attack [181]. The first is corrosion by means of SO₄²⁻ penetration through surface of the binder, which is associated with permeable voids and a rate of water absorption. An attack of sulfuric acid ion can take place easily in a more porous structure. The second is corrosion of the reaction products present in the AAS binder. When sulfuric acid ion penetrates into mortar, it reacts with C-S-H gel, resulting in the decalcification of the gels and the

formation of calcium sulfate. Due to the decalcification, the C-S-H gel is disintegrated, and the compressive strength of AAS mortars decreases. This explains the difference in variation of compressive strength between the AAS mixtures: by increasing the percentage of activation, the permeability decreases and therefore also the loss of resistance caused by the attack of sulfuric acid.

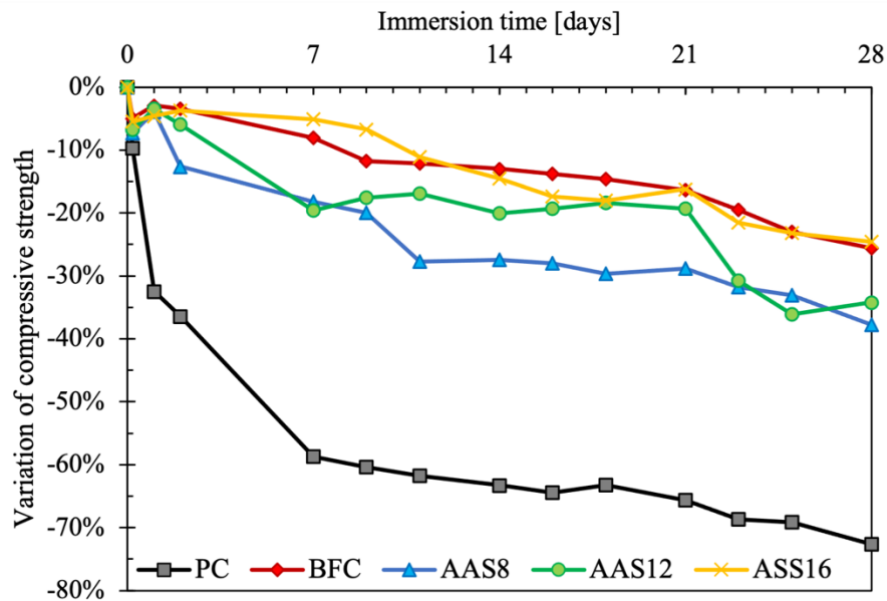


Figure 3-29 Variation of compressive strength of specimens exposed to 5% sulfuric acid solution

Using phenolphthalein, the depth into the specimens at which the pH of the mortars has reduced was measured from the average of nine measurements on a sample. This provides an indication of how far the acid has penetrated or how far into each mix significant ion exchange with the acid solutions has taken place. The results from three unique samples, for mortars type, are shown in Figure 3-30 at each exposure time. The depth of lost alkalinity indicates very similar acid penetration depths for AAS mortars and BFC mortars. However, outliers values are observed for PC mortars, in fact there is a depth of area lost alkalinity close to zero. It is possible that the concentration of sulfuric acid affects the development of gypsum crystals and the development of a protective barrier. This protective barrier could be chemical through a local reduction in pH [182] or physical in the form of blocking the pore space [183]. In contrast, the depth of penetration in AAS and BFC continues to increase with time suggesting that the reaction product in AAS and BFC have a much smaller effect in creating an impediment to diffusion. This was also observed in numerous studies of acid resistance of AAS pastes

and mortars [184,185]. Furthermore, as found by [185] the majority of the region which was considered to have lost alkalinity was removed due to the acid attack in the PC mixes. On the other hand, the majority of the region of the AAS and BFC mixes which had lost alkalinity remained attached to the undamaged core. This suggests that AAS mixes are able to withstand sulfuric acid penetration better than PC mixes.

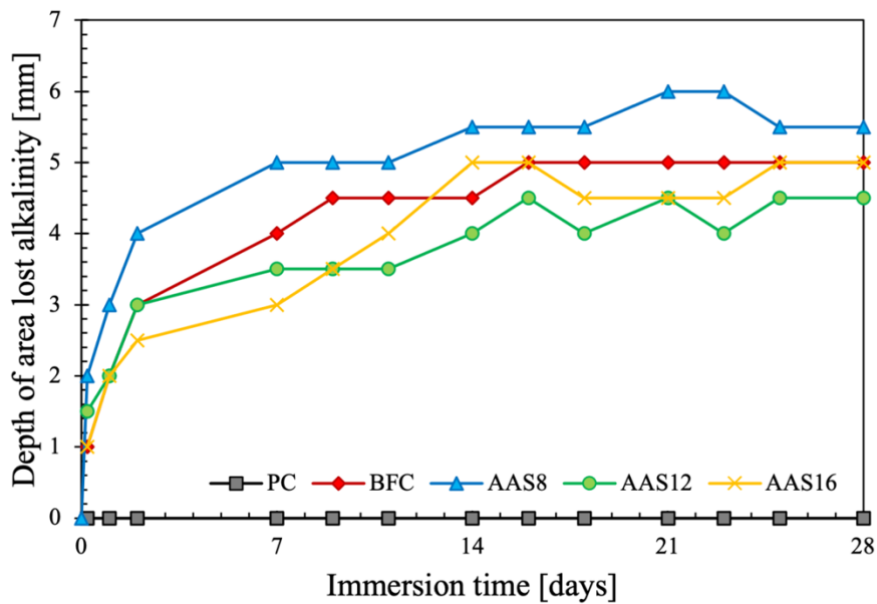


Figure 3-30 Depth of lost alkalinity of specimens under 5% sulfuric acid attack

3.2.4.7 Permeability

Sorptivity is a measurement of one-dimensional capillary absorption rate as a function of time, and provides a reasonable indication of the pore structure and its connectivity. The capillary penetration of a liquid into pore space that have become dried after being initially filled with liquid is a spontaneous process driven by interfacial pressure differences. Sorptivity curves of the mortars are shown in Figure 3-31. Alkali-activated slag mortars exhibit higher water absorption compared to Portland cement-based mortars. Furthermore, AAS8 and AAS12 did not reach saturation after 1 days of testing, consistent with a minor compressive strength [186]. Conversely, mortars AAS16, PC and BFC reached saturation after 1 days of testing. Considering that the water/binder ratio used in these samples is constant, it is clear that the reaction products obtained at different percentage of activator are the main factor determining the water absorption properties of alkali-activated slag [187]. After 90 days of curing, the alkali-activated slag

mortars show an increase in absorbed water, indicating that the nature of the binding gel is the main factor controlling the water uptake. This behavior is in agreement with the increased formation of reaction products at this age, which leads to binding gel collapse due to drying [188].

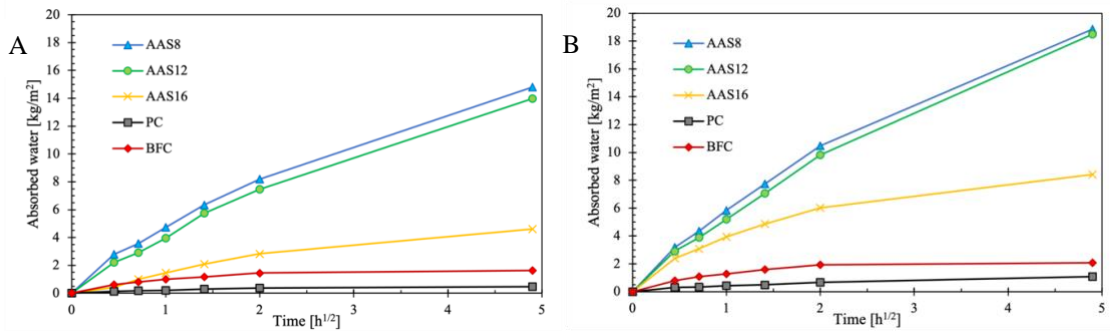


Figure 3-31 Capillary sorptivity curves of mortars as a function of time of curing. A) after 28 days of curing, B) after 90 days of curing

The kinetic of the capillary sorption of water into mortars can be described by the capillary absorption coefficient (k , the initial slope of the sorptivity curves up to the saturation limit). In Table 3-7 it can be observed that AAS mortars have k value higher than Portland cement-based mixtures. In particular the mortars AAS8, AAS12 and AAS16 possess a k value equal to 2.86, 2.76 and 0.93 $\text{kg/m}^2\text{h}^{1/2}$, respectively, while the PC and BFC possess a k value equal to 0.09 and 0.27, respectively. The results were in line with those for water absorption by immersion. Alkali-activated slag mortars exhibit superior absorption for total immersion compared to Portland cement-based materials. It is worth stating that AAS mortars have a lower compressive strength than those of PC and BFC mixtures. Furthermore, it can be observed that increasing the activation percentage decreases both capillary and total water absorption. This is because increasing the a/p ratio increases the mechanical properties and therefore also the compactness of the cement matrix and this leads to a less porous matrix [189].

Table 3-7 Capillary absorption coefficient k and total porosity at 28 and 90 days

	k [$\text{kg/m}^2\text{h}^{1/2}$]		Total porosity [%]	
	28 days	90 days	28 days	90 days
PC	0.09	0.20	7.4	7.4
BFC	0.27	0.35	7.2	7.4
AAS8	2.86	3.69	9.2	9.6
AAS12	2.76	3.65	9.5	9.7
AAS16	0.93	1.52	8.8	9.0

Mortars permeability plays a crucial role in long-term performance of concrete structures, as it controls both the seepage flow and degradation in freezing conditions and the penetration depth of chemical agents. The water penetration depth of mortars are reported in Figure 3-32. The data obtained from this test also confirm what was deduced from the previous ones: alkali-activated slag mortars improve their permeability as the activation percentage increases. Furthermore, it can be observed that the AAS16 mortar has a depth of water penetration equal to or less than the Portland cement-based mixtures.

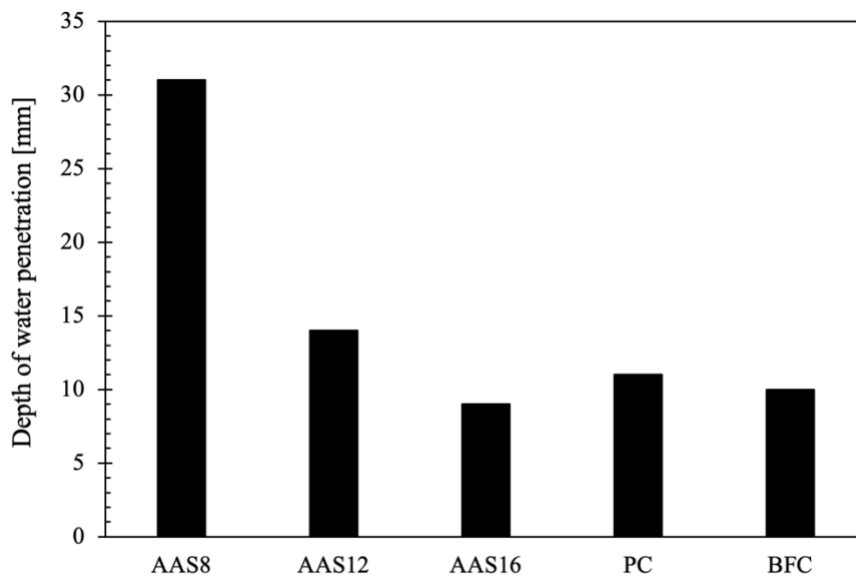


Figure 3-32 Water penetration depth

As far as the water absorption through Karsten tubes is concerned, the results indicated a high absorption of AAS8 mortars. After 28 days a slight increase in value is detected for all the mortars, meaning that they absorb water faster compared to 7 days. This is related to microstructural changes and pores creation during curing [190].

Table 3-8 Karsten tube results

	Water penetration [ml/min]	
	7 days	28 days
PC	0.001	0.002
BFC	0.001	0.002
AAS8	0.044	0.049
AAS12	0.007	0.014
AAS16	0.004	0.009

3.2.5 Conclusions

In this chapter, the durability of one-part alkali activated slag-based mortars in different severe environments in comparison with traditional cementitious mortars were evaluated. Experimental results indicated that:

- The alkali content plays a crucial role both in elasto-mechanical properties and in durability performances of alkali activated materials. In general, the higher the alkali content, the higher the strength and the resistance in severe conditions;
- High-alkali content AAS mortars evidenced a freeze-thaw resistance similar to that of BFC mortars but lower than that of PC probably due to the different compactness of AAS matrix respect to Portland cement mortars at equal water content. On the contrary, AAS manufactured with low dosages of activators are characterized by a very limited resistance in cold environments;
- The use of AEA enhances the freezing and thawing resistance of alkali activated slag-based mortars without any strong reduction in compressive strength;
- Similarly to BFC, alkali activated mixtures are quasi-immune to expansive calcium oxychloride formation in presence of CaCl_2 -based deicing salts due to the negligible calcium hydroxide content;
- Alkali activated slag-based mortars suffer from severe damages and high strength loss as a consequence of semi-immersion in 10 wt% Mg_2SO_4 solution due to decalcification of C-S-H gel and gypsum formation;
- The compressive strength of the AAS mortars decrease over the period of CO_2 exposure and the alkali-activated slag mortars with too low a/p ratio (AAS8) are more susceptible to carbonation compared to the Portland cement or alkali activated slag with high percentage of activators under the accelerated carbonation condition;
- Alkali-activated slag mortars exhibit better performance than PC specimens exposed to 5% of sulfuric acid solution: PC shows strength loss of 75%, AAS8 and AAS12 worsen their mechanical performances by about 35% while alkali activated mortar AAS16 and BFC show strength loss of 25% after 28 days;
- The alkali content plays a crucial role in permeability of alkali activated materials: the higher the alkali content, the lower the water permeability.

CHAPTER 4.

CEMENT-FREE ALKALI-ACTIVATED SLAG PLASTER

4.1 Introduction

The growing attention to the preservation of the historical heritage has remarkably boosted research in the field of the structural rehabilitation, drawing the scientific community toward the investigation of the conservation state and the mechanical properties of materials [191–193], the modelling and the analysis of the structural response of unreinforced and reinforced masonry constructions [194–197], as well as toward the conceptual design of effective and targeted strengthening techniques [198–201]. Interestingly, the assessment of the quality of the masonry was shown to stand as a prerequisite to any other in-depth study on the existing construction. Quality of the masonry is the result of the quality of the constitutive materials, the effectiveness of the bonding between the elements, the accuracy of the arrangement of the stonework and structural details, level and extension of material decay [158]. Different technical solutions have been proposed to consolidate poor quality masonry walls, such as random rubble stonework or three-leaf stone masonry walls. To date, the upgrade of their static and seismic performances can be pursued by repointing or deep repointing, grout injections, jacketing and transversal tying of the external leaves, or by partial replacement of masonry wall portions [158]. However, none of these techniques secures the wall with respect to possible disassembly induced by the vertical acceleration typical of superficial earthquakes. For this reason, jacketing with structural plaster and transversal tying of the external leaves is often proposed to improve the in-place capacity of the stone walls against seismic actions [202]. The existing plaster is removed and the exposed masonry is finished with a new plaster layer. Two different layouts can be adopted: single-side or double-side strengthening. The latter represents the best option as it maintains symmetry

along the wall. The technique remarkably increases the in-plane resistance to shear sliding, diagonal tensile cracking, and flexure, depending on the material properties and thickness of the coating layer, as well as on the height-to-thickness ratio of the masonry wall. The beneficial effects are triggered by the additional layers, which can withstand large in-plane actions. Tying rods avoid instability or detachment of the coating layer from the support. The same technique can also be adopted to increase the load bearing capacity with respect to both vertical and horizontal actions of random rubble and concrete-like stone masonry, whose capacity depends on the internal cohesion, the aggregate interlocking between the elements, and residual tensile strength after cracking, as well as on the possible confinement stress level [203]. In this application, the thin coating, together with the tying steel rods, provides a beneficial restraining confinement action to the masonry cross section, introducing a triaxial stress state, improving ductility and resistance of the existing stonework against both vertical and horizontal actions. Cement based plaster should be discarded for incompatibility in the case of existing masonry with building lime mortars. In fact, use of Portland cement mixtures on masonry structures can cause damages due to the presence of sodium and potassium ions that can promote alkali-aggregate reaction or, in presence of wet environments and sulfuric-rich natural stones, they could determine development of thaumasite and secondary ettringite, with expansion and cracking phenomena. Furthermore, another inconvenient of cement-based mortars are the low porosity and the high elastic modulus that are very different from lime mortars ones and make them incompatible to repair historical buildings. To this end, natural hydraulic lime (NHL) represents the only binder that can be used in these contexts due to their high compatibility with the substrates [204]. However, due to their low mechanical strength, NHL-based mortars often do not meet the elasto-mechanical requirements and, for this reason, are very often mixed with Portland cement.

The experiences in the restoration of structures in the past led to the awareness that repair materials should be compatible with the old ones they would be in contact with, meaning they should not interfere in the global behavior of the original system and of the building as a whole. Compatibility is defined as using materials that do not have negative consequences on the authentic materials. For repair mortars, the applied materials and techniques thus have to, under the given circumstances fit with the original. As such, attention should go to physical, mechanical, chemical compatibility in between the repair

and original mortars [205]. However, the knowledge on how to apply the concept of compatibility in practice soon revealed to be lacking. It was only in the last four decades that the most revealed achievements regarding this subject were attained, namely the establishment of methodologies for the development of repair materials and the definition of technical terms and requirements that help its application [206]. The concept of compatibility is nowadays given a broader sense, where the similarity between the repair materials and the original ones is not enough. It is also necessary to take into account the time to perform the conservations actions, such as the techniques of application and the time of the materials, the availability of skilled workmanship and the socio-cultural conditions [207]. The management of the conservation process should depend on all these variables and should be made by a multidisciplinary team [208]. The reversibility of the interventions is another issue that has often been experienced as unreachable, with compatibility and reversibility offering more realistic results. The minimum intervention principle should be applied to maximize the preservation of the original materials, but whenever its substitution is inevitable, the durability of the intervention should be prioritized [209].

In this scenario, a new material based on alkali-activated slag is conceived to serve as structural plaster to improve the structural performance of poor quality masonry typologies, particularly random rubble stone masonry walls. The use of alkali-activated materials in restoration and conservation of existing structures seems to be very promising due to outstanding properties at fresh and hardened state [210,211] as well as the durability in severe environments [212] and very low environmental impact [98]. In particular, these materials have properties and characteristic that can be modulated as the activator/precursor ratio varies, which makes them more versatile materials. On the other hand, shrinkage values for AAS are significantly higher compared to that of a cement-based mortars with the same compressive strength. However, the use of combination of expansive agent with shrinkage reducing admixture, methylcellulose and starch strongly reduce the shrinkage of one-part alkali-activated slag-based plaster. Furthermore, it has been observed that the elastic modulus is significantly lower than that of Portland cement mortar, consequently the tensile strength induced by restrained shrinkage could still be low, preventing the Alkali-Activated Slag from cracks and detachments.

The aim of this research is to develop an alkali-activated slag-based plaster for seismic retrofitting of stone masonry buildings. In particular, the following target have been identified: a) 28-day compressive strength not lower than 10 MPa, b) cost effectiveness of plasters less than 60€/ton, to be competitive on the marketplace.

4.2 Experimental program

The experimental campaign to characterize the best plaster for the outlined application was planned in three phases. The purpose of the first one was to evaluate the essential characteristics of the mortars at different aggregate content and to identify the ideal mix proportioning that has 28-day compressive strength up to 10 MPa. In the second stage, choice of the type/dosage of additive intended to improve the rheological, physical and elasto-mechanical properties of the mortars. In the last stage, the optimization of the mix design of plaster was carried out and the elasto-mechanical properties were investigated.

4.2.1 *Materials*

The one-part alkali activated slag-based plasters were prepared by using a ground granulated blast furnace slag (GGBFS) with 28-day pozzolanic activity index equal to 0.76 (according to EN 196-5) as precursor and an alkaline powder as activator. In particular, a blend of activator in powder form (sodium silicate : potassium hydroxide : sodium carbonate = 7 : 3 :1) was used as activator in accordance with previous studies [69,158]. The physical properties of binder and the laser granulometry were reported in the previous chapters. The water was adjusted in order to attain the same workability at the end of mixing, equal to 170 mm \pm 10 mm by means of a flow table.

Four different natural calcareous sands (Table 4-1) with maximum size of 1.4 mm were used as aggregates.

Table 4-1 Physical properties of aggregates

Aggregate size [mm]	Specific mass [kg/dm ³]	Water absorption s.s.d. [wt%]	Dosage [wt% vs total aggregates]
0.00/0.25	2.64	0.20	10
0.25/0.40	2.42	0.76	40
0.40/0.80	2.61	0.77	20
0.80/1.40	2.64	0.89	30

On the second stage, an air-entraining agent (AEA) based on ethylene oxide and propylene was added to the mix at different dosage to lighten the mortars, reducing, at the same time, the tendency to bleeding and segregation. Also, due to improve the rheological properties of plaster, methylcellulose (MC), modified starch (MS) and polypropylene fibers (length 6 mm) were added to the mortar in order to minimize the risk of cracking and detachments of plaster (Table 4-2).

Table 4-2 Properties of admixtures

Admixtures	Composition	Specific mass [g/cm ³]
Methylcellulose (MC)	Methylhydroxyethyl cellulose	1.39
Air-Entraining Agent (AEA)	Ethylene oxide and propylene	0.99
Modified Starch (MS)	Hydroxy propylated starch	1.30
Fibers	Polypropylene	0.91

4.2.2 Experimental methods

4.2.2.1 Screening test

One series of alkali-activated slag plaster was manufactured by varying the aggregate/binder ratio according to the composition reported in Table 4-3. Workability was measured by means of flow table according to EN 1015-3, the test was conducted at 0, 30, 60 and 90 min after mixing in order to determine the rate at which the workability is lost. Specific mass at fresh state was detected in accordance with EN 1015-6. Specimens 40 x 40 x 160 mm³ were produced, cured for 24 hours in mold and stored in a climatic chamber at 20°C and R.H. 60%. Specific mass at hardened state, compressive and flexural strength were also determined on three specimens for each age and composition (EN 1015-11). Finally, the cost effectiveness of plasters were calculated. Table 4-4 shows the costs of the materials used, that were considered generally representative of the trends in the Italian market.

Table 4-3 Composition of mortars (nomenclature: S8: Alkali-Activated Slag plaster with alkaline reagents/binder ratio in mass equal to 8, the following number represents the aggregates/binder ratio) (GGBFS:ground granulated blast furnace slag)

Composition [kg/m ³]	S8 3:1	S8 4:1	S8 5:1	S8 6:1	S8 7:1	S8 9:1
GGBFS	460	365	305	260	225	180
Activators	37	29	24	21	19	14
Aggregates	1385	1465	1525	1565	1590	1625
Water	258	256	253	252	251	253
%water vs dry weight	13.7%	13.7%	13.6%	13.6%	13.6%	13.6%

Table 4-4 Costs of the materials used

Materials	Costs
GGBFS	85 €/ton
Aggregates	6 €/ton
Sodium silicate	1.76 €/ton
Potassium hydroxide	2.20 €/ton
Sodium carbonate	1.76 €/ton
MC	4.30 €/kg
MS	2.05 €/kg
AEA	3.20 €/kg
Fibers	2.30 €/ton

4.2.2.2 Improvement of rheological properties

During the second stage, several tests were carried out on mortars that reached the “target” performance (S8 4:1, S8 5:1 and S8 6:1) and on the same mixture manufacturing by adding MC, AEA, MS and fibers (Table 4-5). In addition to the tests conducted on the first phase, entrapped air was detected in accordance with EN 1015-7. Furthermore, dynamic modulus of elasticity of mortars was estimated by means of Ultrasonic Digital Indicator Tester at 28 days in accordance with EN 12504-4 (direct transmission). A thin layer of glycerol paste was interposed between the mortar surface and the transducers of the ultrasonic digital indicator tester (UDIT) in order to ensure an adequate acoustical coupling between the specimen and the transducers. The UDIT measures the transmission time of ultrasonic pulse, allowing to calculate the velocity of ultrasonic pulse, know the length of the specimen (160 mm). E_d can be calculated through the equation:

$$E_d = \frac{v^2 \rho [(1 - 2\gamma) \cdot (1 + \gamma)]}{(1 - \gamma)}$$

With v : velocity of the ultrasonic pulse [m/s], ρ : specific mass at hardened state [kg/m³] and γ : Poisson's modulus (assumed equal to 0.20) [213]. Moreover, the best plaster was applied with different thicknesses (30 and 45 mm) on a brick wall to evaluate the ability of the mixture to be applied on a vertical wall.

Table 4-5 Composition of mortars (M: methylcellulose + Modified starch, E: Air-entraining agent, F: fibers)

Composition [kg/m ³]	S8 4:1 MF	S8 4:1 MEF	S8 5:1 MF	S8 5:1 MEF	S8 6:1 MF	S8 6:1 MEF
GGBFS	345	315	280	245	235	205
Activators	28	25	22	20	18.8	16.5
Aggregates	1380	1260	1400	1225	1410	1230
MC	0.53	0.47	0.51	0.45	0.50	0.43
MS	0.18	0.16	0.17	0.15	0.17	0.14
AEA	--	0.63	--	0.60	--	0.57
Fibers	3.5	3.15	3.40	2.95	3.33	2.87
Water	280	240	265	220	260	215
%water vs dry weighth	15.9%	15.2%	15.6%	15.0%	15.6%	15.0%

4.2.2.3 Development of the plaster

After the application test, the mix design of the plaster was slightly changed, modifying the content of the additives, to improve its rheology. In addition to the tests conducted on the second phase, drying shrinkage was also measured over time on prismatic specimens stored 24 hours after the mixing in a climatic chamber at a controlled temperature and humidity ($T = 20^{\circ}\text{C}$, R.H. = 60%). Moreover, capillary water absorption coefficient of plaster was investigated according to EN 13057. Finally, the conservation conditions were evaluated. In particular, 8 dry bags containing the same mixture were packaged and stored for 2 months in different environmental conditions to study the effect of environment of the mixture. Four pre-packed bags (2 paper bag and 2 plastic bag) were stored at $T = 20^{\circ}\text{C}$ and R.H. = 60%, the other 4 bags (2 paper bag and 2 plastic bag) were stored outdoors, but weather protected. The pre-packed plasters were mixed after 1 and 2 months of storage, using the same amount of water used to carry out the laboratory tests, and both the fresh and hardened properties were studied.

Table 4-6 Composition of mortars (M:methylcellulose + Modified starch, E: Air-entraining agent, F: fibers)

Composition [kg/m ³]	S8 4:1_def
GGBFS	315
Activators	25
Aggregates	1260
MC	0.12
MS	0.16
AEA	0.63
Fibers	0.98
Water	240
%water vs dry weight	14.8%

Table 4-7 Mortar's specimens manufactured for each test

Test	Ages	Format	Number
Specific mass, flexural and compressive strength	1-7-28-84 d	Beam 40x40x160 mm ³	12
Ed	28 d	Beam 40x40x160 mm ³	3
Free shrinkage	Up to 126 d	Beam 40x40x160 mm ³	3
Water absorption	28 d	Beam 40x40x160 mm ³	3

4.2.3 Results and discussion

4.2.3.1 Screening test

The Table 4-8 shows the properties at fresh state of plasters. It is possible to observe that the specific mass at fresh state decreases as the aggregate/binder ratio increases, due to a lower specific gravity of aggregates ($\approx 2.60 \text{ g/cm}^3$) respect to GGBFS (3.13 g/cm^3). Moreover, the workability over time is not affected by the aggregates/binder ratio, and also the water demand did not change with the aggregates/binder ratio.

Table 4-8 Properties of mortars at fresh state

	S8 3:1	S8 4:1	S8 5:1	S8 6:1	S8 7:1	S8 9:1
Specific mass at fresh state [kg/m ³]	2140	2115	2105	2100	2085	2070
Workability [mm]						
0'	170	170	170	170	170	170
30'	160	165	165	160	155	170
60'	145	150	160	160	155	155
90'	130	145	150	155	150	150

Table 4-9 shows compressive strength and specific mass at 1,7, 28 and 84 days. After 24 h plasters with aggregate/binder ratio greater than 6 were not enough hardened to measure mechanical properties. The compressive strength of the plasters decreases

with increasing the aggregate:binder ratio. It has been reported that the addition of aggregate or granular fillers in some cases may strengthen the alkali-activated matrix [214]. However, in most cases [215,216] fine-grained fillers typically reduce the mechanical properties of the mixtures, in agreement with our results. Moreover, Chen et al. [216] found that excessive aggregate content in AAS mixtures results in insufficient binder for coating and binding aggregate together. Nonetheless, the 28-day compressive strength of S8 4:1, S8 5:1 and S8 6:1 may be considered as promising for plasters without additive. This is important because the reduction in the amount of binder (increasing that of aggregate) could be reflected in lower costs. The consumption of GGBFS for the plasters with ratio 4:1, 5:1 and 6:1 were about 460, 365 and 305 kg/m³ of plaster, respectively.

*Table 4-9 Properties of mortars at hardened state (** the mixture is not hardened enough to be demolded)*

	S8 3:1	S8 4:1	S8 5:1	S8 6:1	S8 7:1	S8 9:1
Specific mass at 1d [kg/m ³]	2170 ± 4	2120 ± 5	2090 ± 3	2070 ± 6	**	**
Compressive strength at 1 d [MPa]	10.8 ± 1.1	4.9 ± 1.2	1.4 ± 0.2	0.9 ± 0.3	**	**
Specific mass at 7 d [kg/m ³]	2160 ± 3	2100 ± 5	2070 ± 3	2050 ± 4	2030 ± 4	2010 ± 5
Compressive strength at 7 d [MPa]	25.4± 2.8	17.6± 2.4	15.3± 1.8	14.0± 1.7	10.9± 0.7	9.0 ± 0.6
Specific mass at 28 d [kg/m ³]	2120 ± 2	2095 ± 3	2050 ± 6	2030 ± 2	2020 ± 4	1960 ± 3
Compressive strength at 28 d [MPa]	31.5± 3.1	24.0± 2.7	18.9 ± 1.5	17.3± 1.9	12.5± 0.8	10.1± 0.7
Specific mass at 84 d [kg/m ³]	2080 ± 1	2075 ± 4	2000 ± 4	1980 ± 6	1970 ± 3	1950 ± 2
Compressive strength at 84 d [MPa]	31.7± 3.5	24.8± 2.7	20.6 ± 1.9	17.9± 1.6	13.3± 0.9	9.2± 0.7

Table 4-10 shows the costs of the plasters. It can be observed how the choice of the aggregate/binder ratio affects the cost of the mixtures: the lower the aggregate/binder ratio, the higher the cost of the conglomerates, as a greater quantity of binder and activators is used. All the mixtures manufactured, except for the mixture made with aggregates/binder ratio equal to 3, have a cost of less than 60 €/ton, the maximum price of the plaster on the marketplace. The cost over 60 €/ton leads to discard this plaster, it would have an excessive final cost.

Table 4-10 Costs of plasters

	S8 3:1	S8 4:1	S8 5:1	S8 6:1	S8 7:1	S8 9:1
Costs €/ton	63.4	51.3	44.2	38.7	34.7	28.9

4.2.3.2 Improvement of rheological properties

In this stage, the results of the tests carried out on the mortars that reached the “target” performance and costs will be presented. In particular, the properties of plasters manufactured with the addition of MC, MS, AEA and fibers were analyzed.

Rheological properties

The workability of the AAS mixtures is strongly influenced by the addition of admixtures as reported in Table 4-11. The addition of MC, MS and fibers increases the amount of water at equal workability. However, Coppola et al. [161] found that the addition of the MC and MS admixtures does not affect the consistence of mixtures. For this reason, it is possible that the increases in water demand are caused by the addition of fibers in the mixtures. Furthermore, loss of flow upon the inclusion of different fibers in one-part alkali activated materials is also reported by various researchers [217,218]. The loss in workability is experienced due to uneasy flow of mortars as a result of added fibers in the AAMs composite [219]. Moreover, it is possible to note that the addition of AEA decreases the amount of water at equal workability. Bakharev et al. [220] found that the AEA considerably improved workability of AAS mortars due to the spherical air bubbles that act as fine aggregates of very low surface friction. Furthermore, the reduction of specific mass at fresh state caused by AEA varies slightly as the dosage of the aggregate/binder ratio changes. There is a reduction of 185 kg/m³ for the S8 4:1 mixtures, 260 kg/m³ for the mixtures with an aggregate/binder ratio equal to 5 and a reduction of 250 kg/m³ for the S8 6:1 conglomerates.

Table 4-11 Properties of mortars at fresh state

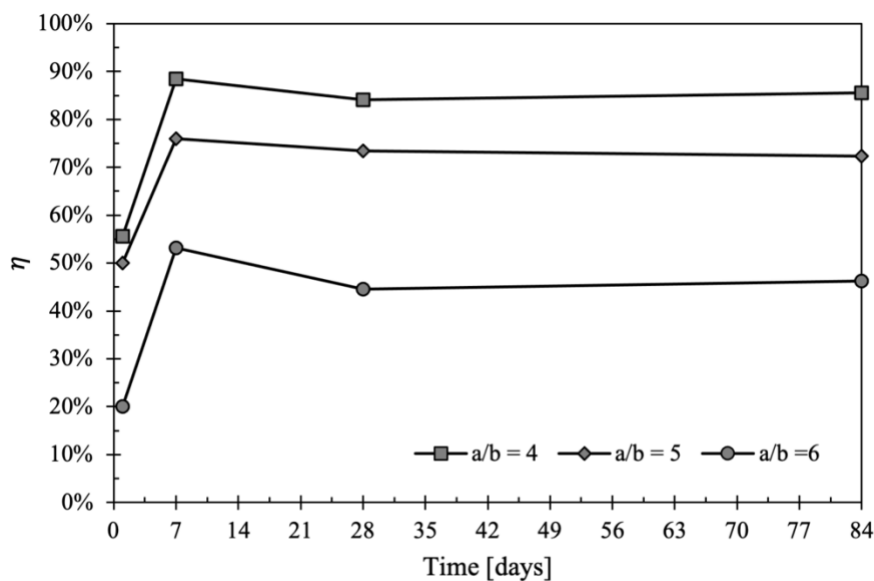
	S8 4:1 MF	S8 4:1 MEF	S8 5:1 MF	S8 5:1 MEF	S8 6:1 MF	S8 6:1 MEF
Specific mass at fresh state [kg/m ³]	2035	1850	1970	1710	1930	1680
Air content [%]	--	15	--	13	--	15
% water vs dry weight	15.9%	15.2%	15.6%	15.0%	15.6%	15.0%
Workability [mm]						
0'	170	170	170	175	170	170
30'	165	170	170	170	170	165
60'	160	165	170	165	165	165
90'	155	150	165	160	165	160

Elasto-mechanical properties

The use of admixtures restricts the development of the mechanical strength of alkali-activated plasters as reported in Table 4-12. The addition of MC, MS and fibers reduced the compressive strength by approximately 25%. Wang et al. [221] found that the presence of MC made pores and flexible polymers increase in mortar and so the compressive strength be decreased. Furthermore, the influence of AEA addition on compressive strength of mortars was evaluated by means of coefficient η at different ages calculated as the ratio between the strength of air-entrained mortar and the mixture manufactured without AEA. Results reported in Figure 4-1 evidence a delay in the strength development at 24 h (η is in the range 50% - 55% for a/b = 4 and a/b =5, η is in the range 20% for a/b = 6) while the strength of air-entrained mixtures at late ages is about 80% for plaster with aggregate/binder ratio equal to 4 and 5, and 50% for plaster with aggregate/binder ratio equal to 6 with respect to the mixtures manufactured without AEA.

Table 4-12 Properties of mortars at hardened state

	S8 4:1 MF	S8 4:1 MEF	S8 5:1 MF	S8 5:1 MEF	S8 6:1 MF	S8 6:1 MEF
Specific mass at 1d [kg/m ³]	2010 ± 5	1825 ± 3	1945 ± 5	1690 ± 2	1895 ± 6	1670 ± 5
Compressive strength at 1 d [MPa]	0.9 ± 0.3	0.5 ± 0.2	0.8 ± 0.3	0.4 ± 0.2	0.5 ± 0.2	0.3 ± 0.1
Specific mass at 7 d [kg/m ³]	1895 ± 4	1795 ± 4	1865 ± 3	1660 ± 3	1840 ± 5	1600 ± 4
Compressive strength at 7 d [MPa]	14.8 ± 1.1	13.1 ± 2.3	12.1 ± 2.2	9.2 ± 1.7	9.6 ± 2.1	5.1 ± 0.9
Specific mass at 28 d [kg/m ³]	1785 ± 5	1720 ± 4	1760 ± 1	1590 ± 3	1730 ± 3	1480 ± 2
Compressive strength at 28 d [MPa]	18.3 ± 3.1	15.4 ± 2.8	15.4 ± 2.1	11.3 ± 1.7	11.9 ± 1.6	5.3 ± 0.9
Specific mass at 84 d [kg/m ³]	1755 ± 2	1695 ± 3	1735 ± 2	1575 ± 4	1720 ± 3	1465 ± 3
Compressive strength at 84 d [MPa]	18.7 ± 1.9	16.0 ± 1.4	16.3 ± 2.1	11.8 ± 1.9	11.9 ± 2.3	5.5 ± 0.8

Figure 4-1 Ratio η between the compressive strength of air-entrained mortars and mixtures produced without AEA at different ages

The dynamic elastic modulus of plaster is very low, close to 4 GPa (Table 4-13). The Young's modulus of the mortars is so low because this property depends strongly on the characteristics of the binder paste [132]. The mixtures have poor elasto-mechanical properties that minimize the stiffness of the mortar. Moreover, at the same strength class, Thomas et al. [222] have shown that alkali-activated slag mortars are characterized by

lower elastic modulus than Portland cement mortars. The reduction of E_d in AAS plaster respect to traditional plaster is a consequence of the high shrinkage of AAM mortars which caused microcracks formation.

Table 4-13 Elastic modulus of plasters

	S8 4:1 MF	S8 4:1 MEF	S8 5:1 MF	S8 5:1 MEF	S8 6:1 MF	S8 6:1 MEF
ρ [kg/m ³]	1785	1720	1760	1590	1730	1480
ν [km/s]	1.73	1.65	1.64	1.57	1.42	1.47
τ [μ s]	92.49	96.97	97.56	101.91	112.68	108.84
E_d [GPa]	4.8	4.6	4.3	3.9	3.1	2.8

Application test

The best plaster in terms of elasto-mechanical properties (S8 4:1 MEF) was applied with different thicknesses (30 and 45 mm) on a brick wall to evaluate the ability of the mixture to be applied on a vertical wall. After application it was necessary to slightly modify the mix design of the plaster to try to improve the rheology of the product, in fact the plaster tended not to remain well bonded when trying to increase the application thickness. For this reason, it was decided to slightly reduce the quantity of MC and fibers. As a result, the water content decreased. Furthermore, the application test was carried out by simulating the job-site conditions: mixing a quantity of raw materials equal to 25 kg with a hand-held mixer. In this way, it is possible to better understand the difficulties related to the transition between the creation of a material in the laboratory and its actual use in the construction site.



Figure 4-2 Application test: Support (left), application of plaster S8 4:1 MEF (middle) and application of plaster S8 4:1_def

4.2.3.3 Development of the plaster

Rheological and elasto-mechanical properties

There are no important change in the fresh and hardened state between the plaster S8 4:1 MEF and S8 4:1_def (Table 4-14).

Table 4-14 Properties of plaster at fresh and hardened state

Composition [kg/m ³]	S8 4:1_def
Specific mass at fresh state [kg/m ³]	1895
Air content [%]	14
Workability [mm]	
0'	170
30'	165
60'	165
90'	160
Specific mass at 1d [kg/m ³]	1870 ± 3
Compressive strength at 1 d [MPa]	2.5 ± 0.4
Specific mass at 7 d [kg/m ³]	1725 ± 5
Compressive strength at 7 d [MPa]	10.8 ± 1.8
Specific mass at 28 d [kg/m ³]	1700 ± 4
Compressive strength at 28 d [MPa]	11.9 ± 2.1
Specific mass at 84 d [kg/m ³]	1690 ± 6
Compressive strength at 84 d [MPa]	11.9 ± 1.7

Shrinkage

Dry shrinkage of alkali-activated slag plaster S8 4:1 and S8 4:1_def is given in Figure 4-3 that shows high shrinkage of AAMs compared to mixtures manufactured with traditional binders, as widely reported in the scientific literature [166,223,224]. The addition of admixtures and fiber reduced shrinkage in alkali-activated slag plaster by up to 25%. This reduction in the drying shrinkage after the addition of fibers might be attributed to several phenomena: (i) the fiber-matrix interfacial friction may hinder part of shrinkage energy, consequently control the shrinkage of alkali-activated slag [225]. Moreover, (ii) fibers can bridge the cracks and reduce their propagation [226], (iii) the presence of fibers on specimens surface may slow down the evaporation rate, resulting in low drying shrinkage tendency [227]. Besides, (iv) the incorporation of fibers into the matrix may refine the micropores and produce more discontinuous pores, which has been recently reported to effectively block the moisture migration within the matrix and

resulting in less shrinkage [228]. Due to the low elastic modulus and the limited shrinkage of AAS plaster, tensile strength stress induced by restrained shrinkage is still low, preventing the mortars from cracks and detachments. This behavior was verified through the application of thin layers of plaster on brick stored in extra-dry conditions (R.H. < 30%) to emphasize the risk of cracking and detachment (Figure 4-4). A 2 cm-thick layer of S8 4:1 after a few weeks was totally detached from the support, while the plaster manufactured with the addition of admixtures and fiber showed no detachments or cracking up to 1 year. Moreover, no cracks were observed on the panels used for the application tests (Figure 4-2).

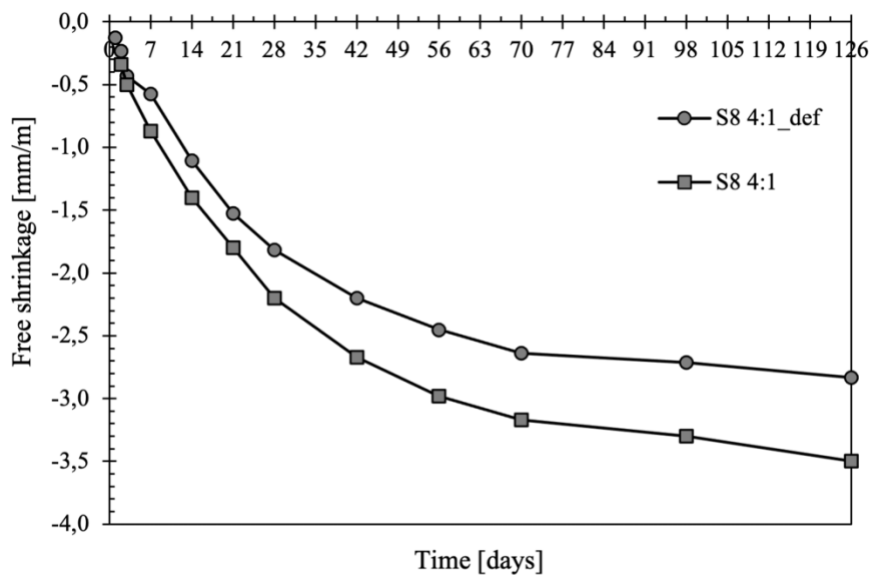


Figure 4-3 Free shrinkage of plaster up to 126 days



Figure 4-4 Test on a brick: S8 4:1 detached and S8 4:1_def adherent

Water absorption

The absorption coefficient of the alkali-activated plaster ($1.99 \text{ kg/m}^2\text{h}^{0.5}$) is slightly higher compared to a traditional mortar based on Portland cement and lime ($1.63 \text{ kg/m}^2\text{h}^{0.5}$) [132]. To reduce the water absorption of mortar it is possible to apply an alchilalcoxisilane-based coating that can reduce the absorption coefficient up to 80%, reducing the risk of saturation of the plaster [158].

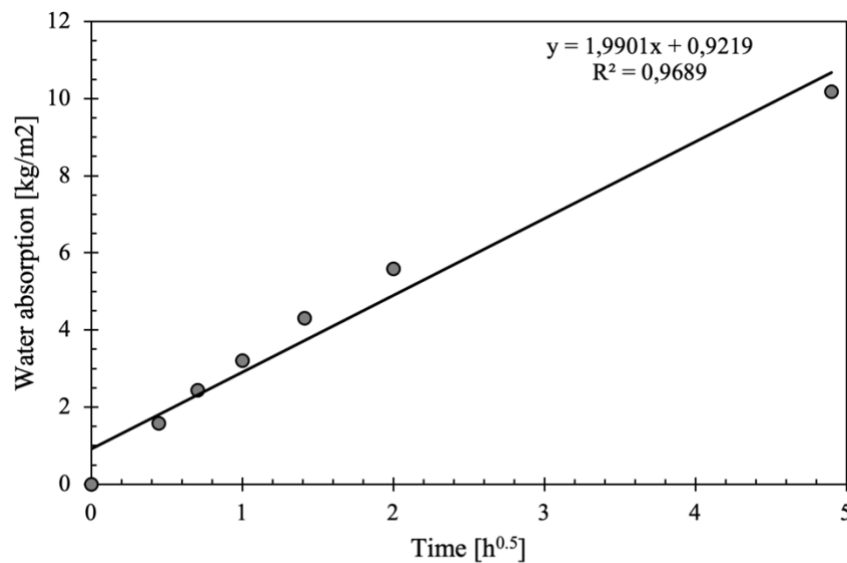


Figure 4-5 Capillary water absorption of plaster

Evaluation of storage conditions

Table 4-15 shows the properties of plasters at fresh and hardened state manufactured after 1 month of storage. It is noted that the setting time of compounds denominated P are dilated compared to the reference plasters, as the mixtures is not hardened enough to be demolded. This behavior was not found for the plasters manufactured with raw materials preserved for a month inside plastic bags. Moreover, the same trend has been observed when investigating the workability of mixtures: plasters denominated P have a significantly lower workability than the reference mortars, while whose denominated PL show a workability similar to that of reference. Furthermore, by analyzing the specific mass of the mixtures, it can be observed that plasters P have an extremely higher specific mass than mixtures PL. The value of IN_P and OUT_P are similar to that of the mixture manufactured without the addition of air-entraining agent

(S8 4:1 MF). Also, the mechanical properties were influenced by the different types of bags used: the mixtures P showed significantly lower performances than the reference ones, while the plasters PL, regardless the storage location, show compressive strength completely similar to those of the reference plaster. These behaviors can be caused by the hygroscopic nature of activators, as also found by Wang et al. [13] (Figure 4-6).

Table 4-15 Properties of mortars at fresh and hardened state after 1 month of storage (IN:store in laboratory, OUT:stored outdoors, P: paper bag, PL:plastic bag, ** the mixture is not hardened enough to be demolded)

Composition [kg/m ³]	S8 4:1_def	IN_P	IN_PL	OUT_P	OUT_PL
Specif at fresh state [kg/m ³]	1895 ± 5	2010 ± 6	1880 ± 3	2015 ± 6	1905 ± 6
Workability [mm]	170	130	170	125	170
Specific mass at 1d [kg/m ³]	1870 ± 6	**	1820 ± 2	**	1865
Compressive strength at 1 d [MPa]	2.5 ± 0.6	**	2.7 ± 1.3	**	2.8 ± 0.9
Specific mass at 7 d [kg/m ³]	1725 ± 4	1890 ± 7	1820 ± 4	1805 ± 5	1840 ± 5
Compressive strength at 7 d [MPa]	10.8 ± 1.5	6.5 ± 1.3	11.5 ± 0.9	5.3 ± 1.1	11.3 ± 1.0
Specific mass at 28 d [kg/m ³]	1700 ± 2	1825 ± 5	1750 ± 5	1805 ± 4	1785 ± 6
Compressive strength at 28 d [MPa]	11.9 ± 1.3	6.9 ± 0.9	12.3 ± 2.1	5.1 ± 1.1	12.4 ± 3.1
Specific mass at 84 d [kg/m ³]	1700 ± 3	1825 ± 4	1740 ± 4	1800 ± 5	1775 ± 3
Compressive strength at 84 d [MPa]	11.5 ± 2.7	5.6 ± 1.1	11.9 ± 2.6	4.4 ± 0.6	12.1 ± 2.9



Figure 4-6 Raw material stored for 1 month in the paper bags

Table 4-16 shows the properties of plasters at fresh and hardened state manufactured after 2 months of storage. As could be expected also the mixtures

manufactured with raw materials stored for 2 months inside bags and stored in different ways showed the same results as mixtures manufactured after 1 months of storage.

*Table 4-16 Properties of mortars at fresh and hardened state after 2 months of storage (IN:store in laboratory, OUT:stored outdoors, P: paper bag, PL:plastic bag, ** the mixture is not hardened enough to be demolded)*

Composition [kg/m ³]	S8 4:1_def	IN_P	IN_PL	OUT_P	OUT_PL
Specif at fresh state [kg/m ³]	1895 ± 5	2135 ± 7	1860 ± 4	2090 ± 6	1890 ± 5
Workability [mm]	170	130	170	130	170
Specific mass at 1d [kg/m ³]	1870 ± 4	**	1820	**	1815
Compressive strength at 1 d [MPa]	2.5 ± 0.1	**	2.4 ± 0.4	**	2.3 ± 0.7
Specific mass at 7 d [kg/m ³]	1725 ± 3	1980 ± 6	1775 ± 3	1910 ± 4	1790 ± 3
Compressive strength at 7 d [MPa]	10.8 ± 1.1	6.1 ± 0.9	11.1 ± 1.2	1.2 ± 0.4	12.1 ± 0.2.1
Specific mass at 28 d [kg/m ³]	1700 ± 3	1935 ± 4	1750 ± 4	1895 ± 3	1740 ± 6
Compressive strength at 28 d [MPa]	11.9 ± 3.1	6.9 ± 1.3	12.6 ± 11.9	1.1 ± 0.3	12.3 ± 2.7
Specific mass at 84 d [kg/m ³]	1700 ± 2	1930 ± 5	1730 ± 2	1915 ± 6	1725 ± 4
Compressive strength at 84 d [MPa]	11.5 ± 2.6	5.5 ± 0.7	11.7 ± 1.8	1.4 ± 0.6	11.6 ± 2.3

Costs of plaster

Table 4-17 shows the comparison of the costs of the plasters manufactured in the second and third phases. It can be observed that the addition of admixtures increased the costs of the plasters. The addition of AEA increased the costs of plasters of about 2.2% respect to the mixtures manufactured without the AEA. Finally, it is possible to underline that the S8 4:1_def is the mixture that possesses the best applicability properties and is also the cheapest compound manufactured with aggregates/binder ratio equal to 4, remaining well below the limit of price.

Table 4-17 Costs of plasters

	S8 4:1	S8 4:1	S8	S8 5:1	S8 5:1	S8 6:1	S8 6:1
	MF	MEF	4:1_def	MF	MEF	MF	MEF
Costs €/ton	58.0	59.3	50.4	55.2	56.4 €	53.1	54.4

4.2.4 Conclusions

In this chapter, a cement-free plaster for restoration and seismic retrofitting of stone masonry buildings was developed. Analyzing the experimental data, it is possible to conclude that:

- The compressive strength of the plasters decreases with increasing the aggregates:binder ratio;
- The plaster S8 4:1_def is able to provide a structural reinforcement (28-day compressive strength equal to 12 MPa) with a suitable rheology for a plaster;
- The high free-shrinkage of alkali-activated slag based-plaster was reduced by using blend of admixtures;
- The reduced shrinkage and the low elastic modulus ensure an excellent adhesion to the substrate and the absence of micro-cracks and detachments;
- The use of plastic bags for the storage of pre-packed plaster allows to solve the problems caused by the hygroscopic nature of the alkaline activators, guaranteeing the same properties of a plaster manufactured in the laboratory;
- The cost of the S8 4:1_def plaster is well below the cost limit imposed by the market.

CHAPTER 5.

SMART AND MULTIFUNCTIONAL MORTARS

5.1 Introduction

Concrete is the second most consumed material in the world after water, and the most used construction material. Yet, its benefits are masked with many ecological disadvantages through the way it is produced, transported or used. For example, it occurs in the brittle state owing to its low tensile strength, weak resistance to crack formation, and strain properties by integrating it with many fibers, admixtures, and supplementary cementitious components. In order to overcome these problems it is necessary that concrete has to be engineered at the nanoscale [104]. In fact, the addition of nano materials can improve the mechanical strength and the chemical composition of the resulting concrete. Examples of the recently manufactured and used nanomaterials include “nano-silica, nano titanium dioxide, nano iron oxide, carbon nanotubes, graphene oxide and graphene sheets” [229]. These addition allows to create a smart concrete, i.e. an intelligent system that has different structural properties as compared to the typical concrete made from cement and natural aggregates. The concept of “smartness” in concrete has been achieved using the four main methods, namely material design composition, special processing, introduction of other efficient components, and alteration of the microstructure. These methods have been tailored to achieve specific needs by improving the properties of the concrete, such as the durability, strength, serviceability, reliability, cost, among other properties [103].

5.2 Experimental research on self-sensing capability of alkali-activated slag mortars

Several studies have evaluated the self-sensing abilities of Portland cement-based concretes and mortars containing conductive fillers such as carbon nanotubes, carbon nanofibers, graphite powders and steel microfibers [26–29]. Research has demonstrated the monitoring capabilities of cement-based materials doped with conductive fillers and their promising application in structural health-monitoring [25,30–35], where issues related to the fillers' dispersion and to the electrical setup represented the main bottlenecks to solve [36,37]. Of the notable literature about smart cementitious materials, only a few studies focus on the use of conductive fillers on geopolymers [38,39] or alkali-activated slag cement-based mixtures [40–43]. Recently, Rovnanik et al. [41] showed that AAS mortars are characterized by enhanced electrical conductivity properties compared to OPC-based mixtures due to the presence of mobile hydrated alkali ions and metallic microparticles. The reduced electrical resistivity of alkali-activated slag cement-based materials allows us to observe just enough piezoresistivity and consequent self-sensing properties, even without the addition of conductive materials. In order to improve the electrical conductivity of AAS, Vilaplana et al. [43] used carbon fibers at different dosages, highlighting gage factors (GF) for compressive cycles equal to 52 and 661 for the 0.29 and 0.58 vol%, respectively. Rovnanik et al. [42] studied the effect of graphite addition (from 1 to 30 wt% respect to GGBFS) on the mechanical properties and self-sensing capability of AAS mortars, identifying an optimum filler content to maximize the smart properties equal to 10 wt%. However, the addition of an excessive amount of conductive fillers requires higher water dosages to ensure an adequate workability, strongly reducing the compressive strength of mortars.

The purpose of this research is the evaluation of the self-sensing capability of one-part alkali-activated slag cement-based mortars doped with different carbon-based nanofillers (carbon nanotubes, carbon nanofibers, carbon black and graphene nanoplatelets). Physical, mechanical and electromechanical tests have been carried out. The results show that all nano-modified materials exhibited enhanced properties, with the best sensitivity demonstrated by carbon black and carbon nanotubes.

5.2.1 Materials

Matrix

A ground granulated blast furnace slag (GGBFS, provided by Ecocem Ltd., Ireland) was used as a precursor to manufacture one-part alkali-activated slag-based mortars. The physical properties of binder and the laser granulometry were reported in the previous chapters. The solid alkaline activator was a blend of sodium silicate, potassium hydroxide and sodium carbonate (provided by Carlo Erba Spa, Italy, industrial grade) with a relative mass ratio equal to 7:3:1, as already used in previous studies by Coppola et al. [10,19]. As aggregates, five different natural siliceous sands (Table 5-1) with a maximum diameter of 2.5 mm were combined according to the ASTM C33 limits. Finally, 20 °C deionized water was used to manufacture mortars.

Table 5-1 Properties of aggregates

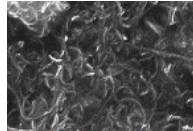
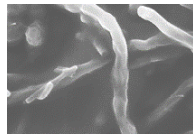
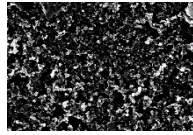
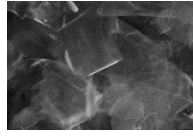
Min/Max Size [mm]	Specific Mass [g/cm ³]	Water Absorption s.s.d. [%]	Dosage [%]
<0.25	2.40	0.20	25
0.25/0.50	2.70	0.76	30
0.50/1.00	2.58	0.77	25
1.00/1.50	2.63	0.93	10
1.50/2.50	2.62	1.02	10

Fillers

The fillers chosen for the composites were all carbon-based, but with different structures and aspect ratios. The carbon nanotubes (CNT) were Multi Walled, type Graphistrength C100, from Arkema (Germany) [46]. They are 1-dimensional multiple concentric cylinders with an average external diameter of 10 nm and length up to 10 μm. They possess a specific surface area of the order of 200 m²/g and low apparent density, of the order of 100 kg/m³. The carbon nanofibers used in this research were type Pyrograf-III Carbon Nanofiber PE-19-XT-LHT (USA), considered 1-dimensional even if consisting of stacked cup linear structures. Their dimensions are greater than those of CNTs, with average diameters of 100 nm and lengths up to 200 μm. The Carbon black fillers adopted in this study were type Printex XE-2B produced by Orion (Luxemburg). They are 0-dimensional, as colloidal spherical particles of carbon. They were cheaper than the two previous fillers, and of the same typology of printer's powder. The fourth carbon-based fillers were graphene nanoplatelets (GNP), produced by Cheap Tubes Inc. (USA), consisting of stacks of graphene layers of a final thickness up to 10 nm. They

were 2-dimensional, with a visual appearance of grey powder, different from the other fillers which looked black. Table 5-2 summarizes the main characteristics declared by the producers of the four carbon-based fillers.

Table 5-2 Carbon fillers' characteristics (data provided by suppliers)

Carbon Filler	SEM Image	Property	
CNT		Apparent density	50–150 kg/m ³
		Length	0.1–10 μm
		Specific surface area	~210 m ² /g
NF		Density	1000 kg/m ³
		Diameter	150 nm
		Specific surface area	20–30 m ² /g
CB		Density	1800 kg/m ³
		Particle size	30 nm
		Specific surface area	~1000 m ² /g
GNP		Density	1800 kg/m ³
		Diameter	15 μm
		Specific surface area	100 m ² /g

5.2.2 Mixtures, preparation and samples curing

Five different one-part alkali-activated slag-based mortars were produced by varying the carbon filler type. The alkali content (A_c) and the silica modulus (M_s), calculated through Equations (1) and (2), were fixed at 0.0076 and 0.48, respectively, by using an activator to GGBFS ratio equal to 0.16.

$$A_c = \frac{Na_2O + K_2O}{GGBFS} = 0.0076 \quad (2)$$

$$M_s = \frac{SiO_2}{Na_2O + K_2O} = 0.48 \quad (3)$$

The carbon fillers used for manufacturing the AAS composites, as explained before, are at the amount of 1% by slag mass. Furthermore, the water to slag ratio was set at 0.65, while the sand to slag ratio was 3. The composition of mortars is reported in Table 5-3.

Table 5-3 Composition of mortars

Composition [g]	NEAT	CB	GNP	CNT	NF
GGBFS	1000	1000	1000	1000	1000
Activator	160	160	160	160	160
Sand s.s.d.	3000	3000	3000	3000	3000
Water	650	650	650	650	650
Carbon black (CB)		10			
Graphene nanoplatelets (GNP)			10		
Carbon nanotubes (CNT)				10	
Carbon nanofibers (NF)					10

The reference AAS mortar (NEAT) was manufactured in accordance with the “Dry mixing method” proposed by Bayuaji et al. [47], the procedure has been reported in the previous chapters. In alkali-activated-based mortars containing carbon fillers, an aqueous solution containing deionized water and fillers was used instead of pure water (Figure 5-1a). In particular, the fillers were uniformly dispersed in the aqueous solution by means of a Branson 1510 (Branson Ultrasuoni Srl, Italy) sonicator for 15 min (Figure 5-1b). Then, the sonicated suspension was added to the mixtures and the mortars were prepared in accordance with the “Dry mixing method” (Figure 5-1c and 5-1d). Finally, the mortars were poured into $40 \times 40 \times 160 \text{ mm}^3$ steel molds and protected from water evaporation with a plastic film (Figure 5-1e). After 24 h at $21 \pm 1 \text{ }^\circ\text{C}$, the specimens were demolded and cured in a climatic chamber at $21 \pm 1 \text{ }^\circ\text{C}$ and R.H. $60 \pm 5\%$ until the mechanical tests.

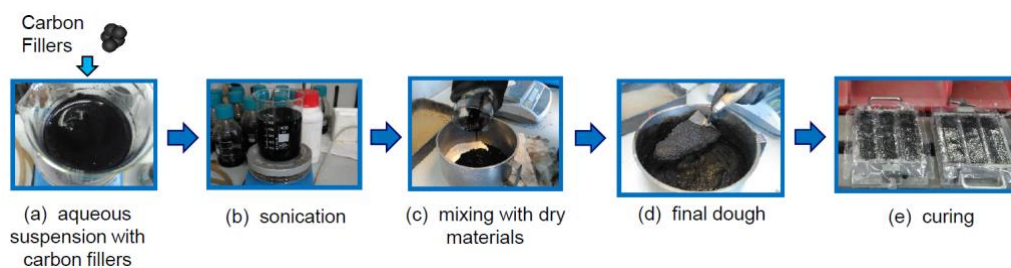


Figure 5-1 Nano-modified sample's preparation: dispersion of nano-fillers (a and b), mortar's preparation (c and d), curing (e)

5.2.3 Experimental methods

The workability of mortars was evaluated through a flow table according to EN 1015-3, and the specific mass at fresh state was measured in accordance with EN 1015-6. Moreover, the specific mass at hardened state, flexural and compressive strength were determined at 1, 7 and 28 days from casting (EN 1015-11). For the evaluation of the electrical properties of AAS-based composites, the samples were equipped with two

external electrodes made of 5 mm long ribs in copper, and applied in the perimeter of each sample at a distance of 80 mm by the use of a conductive epoxy resin with 0.75% of graphite. The samples were tested after the resin polymerization. Figure 5-2 shows the sketch of the instrumented specimens. The electrical tests were carried out by applying a voltage to the samples with a model RIGOL DG1022 generator (Italy), and measuring the current signal by using a DAQ NI PXIe-1073 (USA) equipped with a digital multimeter, model NI PXI-4071. The copper strips were directly connected to the function generator and the acquisition system (Figure 5-2a). The electromechanical tests consisted of compressive cycles of loading/unloading in the range of 1–3 kN, carried out in the longitudinal direction by the use of a Controls press with a maximum load of 15 kN. Three LVDTs were placed at 120° in order to evaluate the displacement (Figure 5-2b).

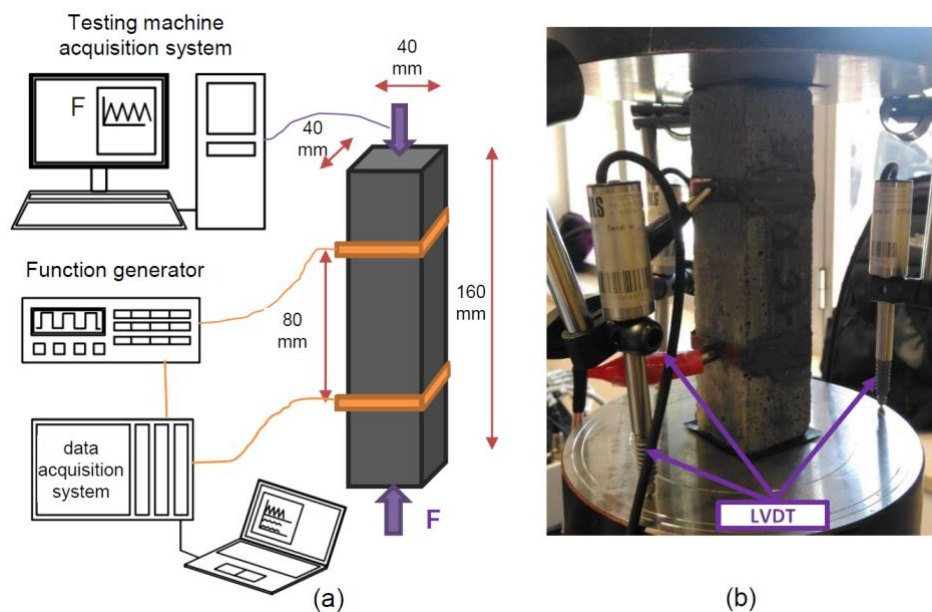


Figure 5-2 Setup of electromechanical tests: (a) Sketch and (b) detail of sample and LVDTs

The electrical and electromechanical tests were carried out by applying a square wave voltage signal with a duty cycle of 50% between the values of -10 V and $+10$ V, with a frequency of 1 Hz, and recording the electrical current with a sampling frequency of 10 Hz. Then, the outputs were sampled at 1 Hz, taking the point placed at about 80% of the positive part of each period of the square voltage signal [37]. The electrical resistance was computed using Ohm's law:

$$R(t) = \frac{V}{I(t)} \quad (4)$$

where V is the applied constant voltage in the positive part of the square wave, equal to +10 V, I is the current intensity, and t represents the instant of acquisition of the signal.

5.2.4 Results and Discussion

5.2.4.1 General characterization of mortars

The workability of mortars is in the range of 190–240 mm and it decreases when the carbon fillers are added to the mixture, as reported in Table 5-4. This is primarily due to the large surface area of nano-fillers, which demands a great amount of water to wet the surface, thereby reducing the free water content required for lubrication at a fixed water/binder ratio [48]. Moreover, mortars containing carbon fillers are characterized by a lower density, both at fresh and hardened states, in comparison to NEAT mortar. This result is probably due to voids forming within the matrix due to air entrapment associated with the addition of the fillers. The samples with CNT were too inhomogeneous and defective for electromechanical testing, and therefore not reliable enough to be considered for further investigation.

Table 5-4 General properties of mortars

	NEAT	CB	GNP	CNT	NF
Workability [mm]	240	210	220	200	190
Specific mass at fresh state [kg/m ³]	2200 ± 5	2095 ± 6	1925 ± 4	1770 ± 3	1770 ± 5
28-day specific mass [kg/m ³]	1980 ± 4	1920 ± 6	1840 ± 5	1690 ± 2	1670 ± 3
1-day compressive strength [MPa]	7.1 ± 2.1	9.3 ± 1.8	7.6 ± 1.6	4.8 ± 0.8	6.1 ± 1.7
7-day compressive strength [MPa]	14.8 ± 3.2	12.4 ± 2.5	11.3 ± 2.4	9.5 ± 1.4	9.8 ± 2.4
28-day compressive strength [MPa]	19.0 ± 2.7	17.4 ± 2.8	16.9 ± 1.9	15.3 ± 2.6	16.2 ± 3.1

Mortar manufactured without carbon fillers (NEAT) shows a compressive strength of about 7 MPa after 24 h, and 15 MPa and 19 MPa at 7 and 28 days, respectively (Figure 5-3). The addition of carbon fillers decreases the compressive strength of mixtures both at early and late ages up to 25%. The strength loss can be mainly ascribed to the reduction in specific mass (Figure 5-4) due to excessive air entrapment which occurred during the mixing of carbon fillers.

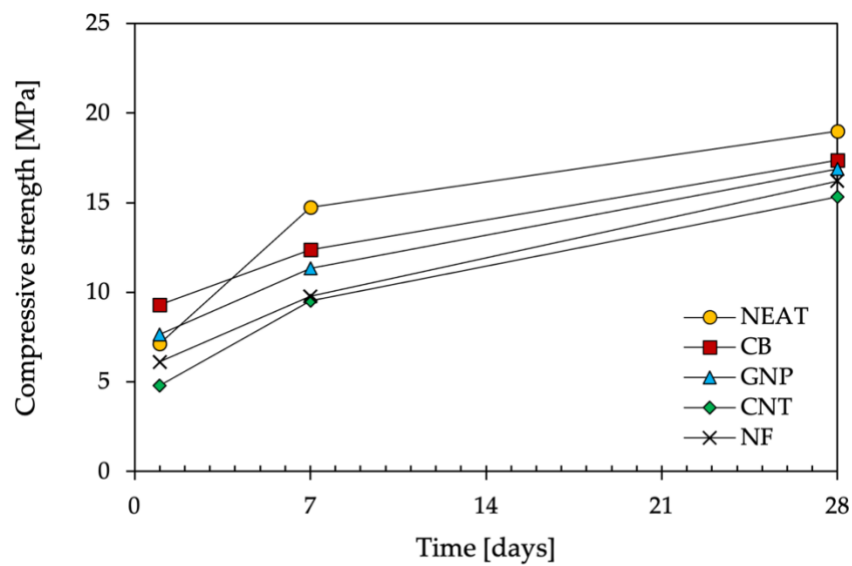


Figure 5-3 Compressive strength development of mortars

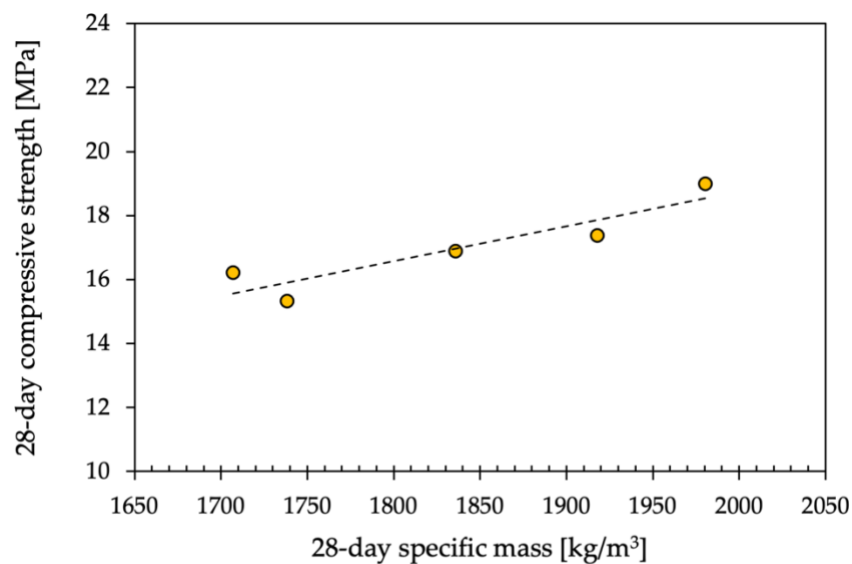


Figure 5-4 The 28-day compressive strength of mortars vs specific mass

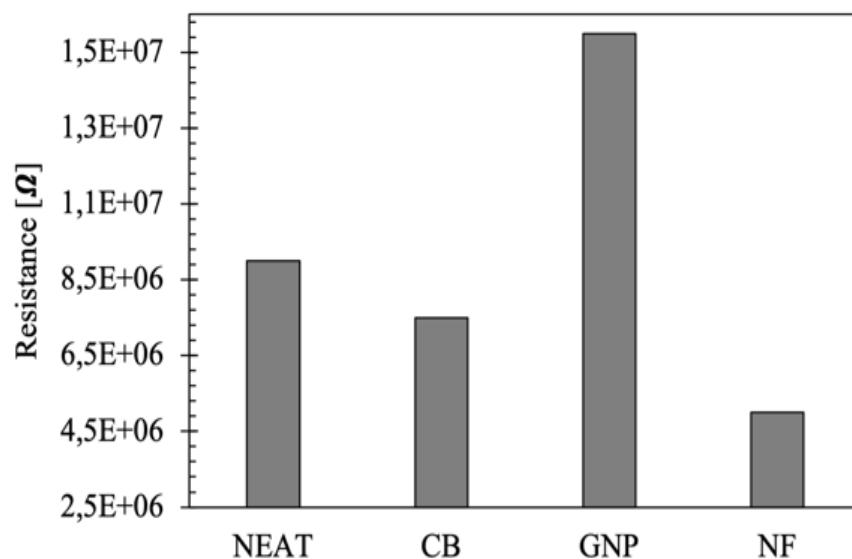
5.2.4.2 Electrical tests

Electrical tests were conducted on unloaded samples. Each element was simply resting on the worktable, while the voltage was applied at the two electrodes and recorded for 600 s (Figure 5-5a). The electrical resistance has been obtained using Equation (4), considering the current intensity measured at the end of the tests. Figure 5-5 shows the results of the electrical tests. The samples with CB and NF appear slightly more

conductive than the normal ones, while the samples with GNP exhibit a higher resistance, maybe due to the apparently higher porosity of the composite.



a)



b)

Figure 5-5 Electrical tests: (a) sample during the tests, (b) electrical resistance of mortars

5.2.4.3 Sensing tests

Electromechanical tests were conducted by applying triangular cyclical loads, as reported in Figure 5-6. Each sample was instrumented as in Figure 5-6a. Figure 5-6b reports the stress variation on the samples during the tests. Electrical tension was applied at the copper electrodes, and the current was measured through the 2-probe method. Loads and electrical signals were recorded separately through two different data acquisition

systems, with no perfect synchronization. The displacement was evaluated through the average value obtained from the LVDTs of the axial testing machine.

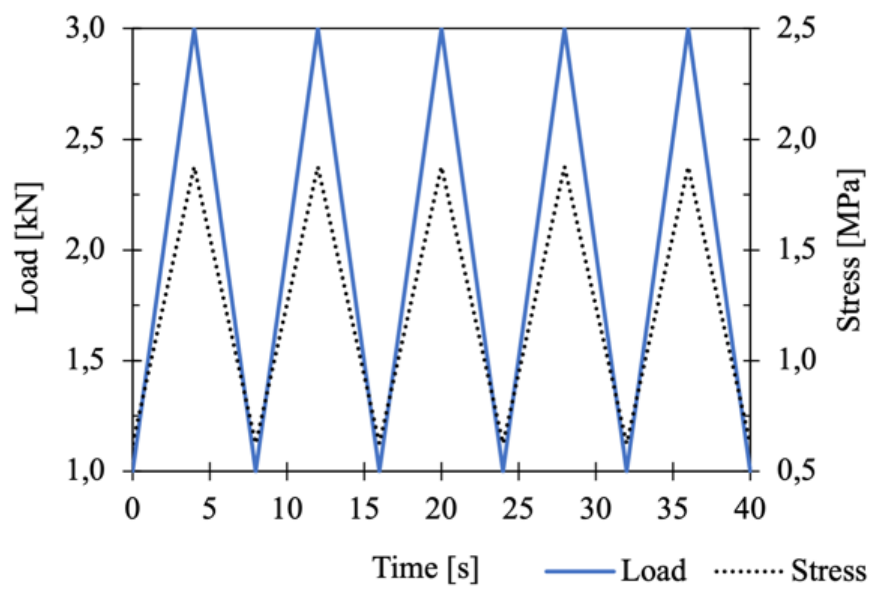


Figure 5-6 Electromechanical tests: (a) an instrumented sample during the tests; (b) load and stress history

Figure 5-7a shows the normalized variation of electrical resistance obtained from the electromechanical tests for the different composites. All the samples showed a certain sensitivity, even if the neat ones exhibited a slight drift of the signal. The sensitivity of the samples has been better analyzed through the computation of the gauge factor (GF),

reported in Figure 5-8. The figure shows that the neat samples and the samples with CB and NF appeared more sensitive than the samples with GNP. However, the results of the neat samples were less repeatable and exhibited a greater variability.

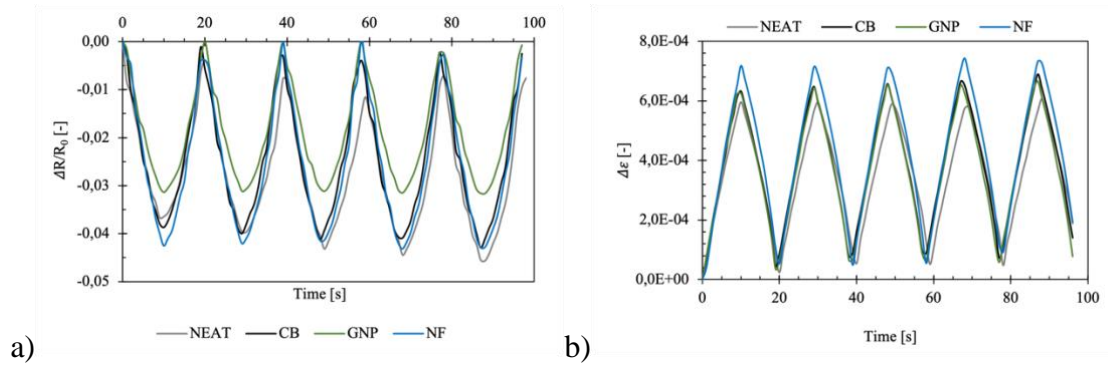


Figure 5-7 Results of the electromechanical tests on normal and nano-modified samples: outputs of normalized variation of electrical resistance (a); strain variation (b)

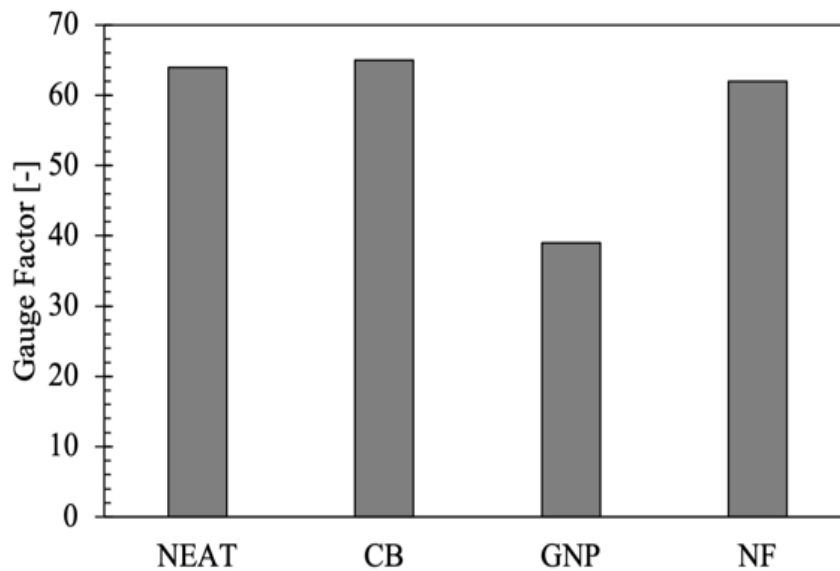


Figure 5-8 Gauge factors obtained from electromechanical tests on all the samples

Table 6 summarizes the results of the electromechanical tests, comparing the values of initial electrical resistance, GF and Sensor Response, defined as the product of the two previous features (Equation (6)):

$$SR = GF \cdot R_0 = -\frac{\Delta R/R_0}{\epsilon} = -\frac{\Delta R}{\epsilon} \quad (4)$$

where ΔR is the incremental variation in electrical resistance of the composites, R_0 is the initial internal electrical resistance, GF is the gauge factor and ϵ is the axial strain, considered positive in compression. Table 5-5 confirms that the nano-materials with highest sensitivity are the composites with CB and NF. These last samples also appear to be the best performing ones in the analyses of the linearity of the signals, as reported in Figure 5-9. The results appear consistent with those obtained in previous research on cement composites with carbon-based fillers obtained with similar preparation procedures [31,33,49,50], even if some deviations are observed, which is due to the different setup and shape of the samples.

Table 5-5 Initial resistance R_0 , Gauge Factor GF, Sensor Response SR and linearity of the tested samples

Sample	R_0 [Ω]	GF	SR [Ω]	R^2 [-]
NEAT	3.02E + 05	64	1.93E + 07	0.8577
CB	2.21E + 05	65	1.43E + 07	0.9852
GNP	2.55E + 05	39	0.98E + 07	0.9636
NF	2.36E + 05	62	1.46E + 07	0.9825

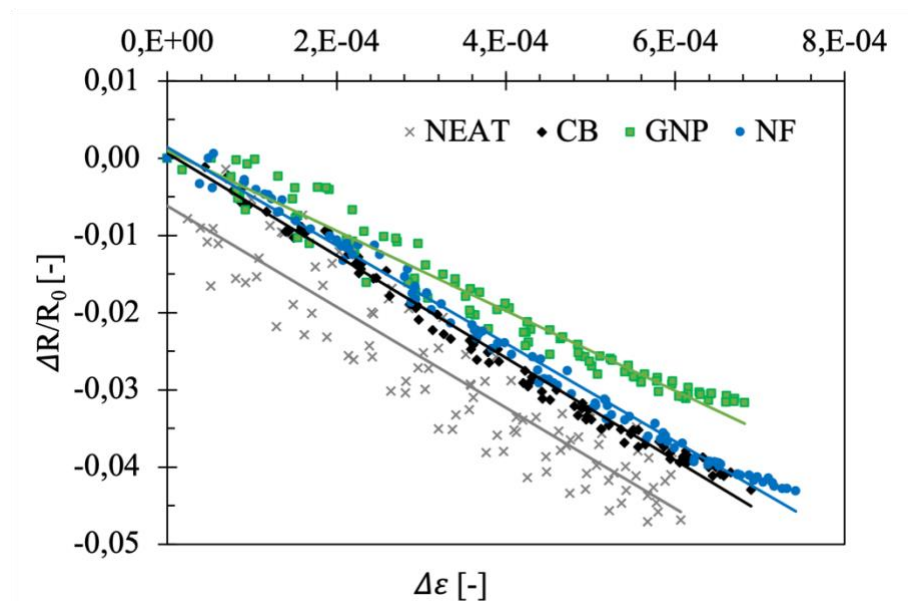


Figure 5-9 Analysis of the linearity of the signals

Figure 5-10 shows, for all the sensors, the variation of fractional change in electrical resistance versus strain, for loading and unloading phases of the triangular cyclical loads. The results exhibit the enhanced performance of the nano-modified samples in comparison to the normal samples. The graphs also report the values of the hysteresis areas of all the samples: the numerical comparison indicates that the presence of nano

carbon fillers in the composite determines the reduction in the non-linear behavior and in the hysteresis.

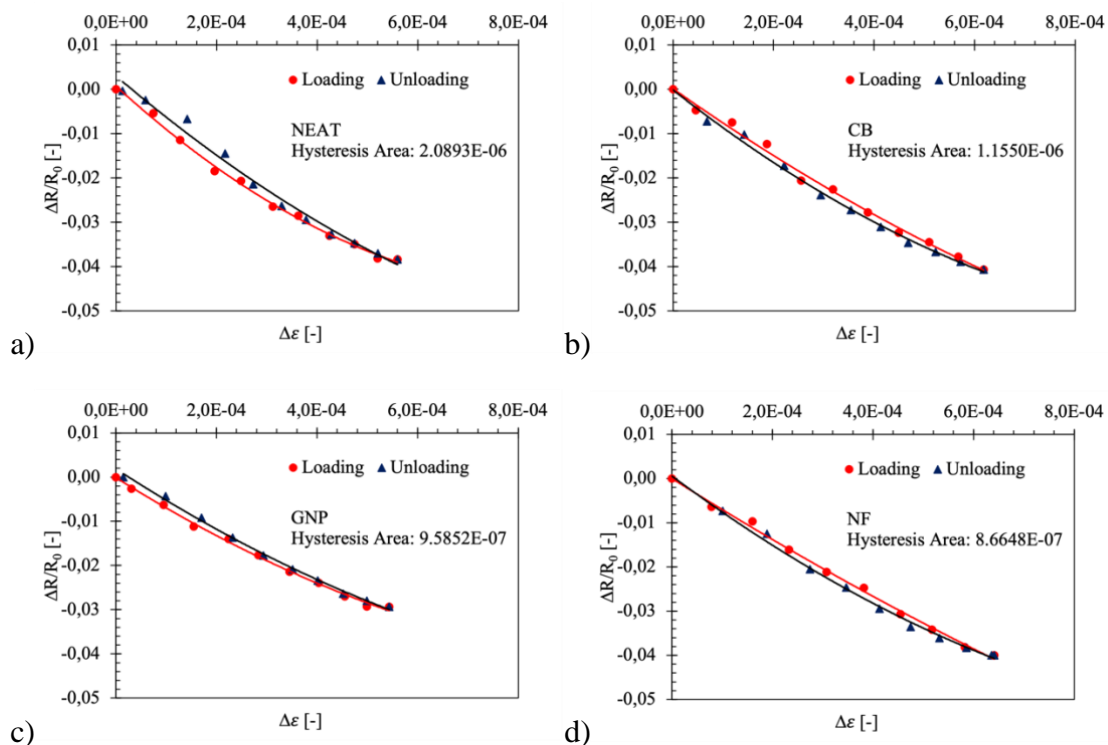


Figure 5-10 Fractional change in electrical resistance vs. applied strain for loading and unloading phase under cyclic compression loads for samples: (a) NEAT, (b) with carbon black (CB), (c) with graphite nanoplatelets (GNP), (d) with carbon nanofibers (NF)

5.2.5 Conclusions

This research has presented the investigation of the physical, mechanical and electromechanical properties of low environmental impact alkali-activated slag (AAS) cement-based mortars doped with different carbon-based nanofillers, i.e., nanotubes, nanofibers, carbon black and graphene nano-platelets. The development of these types of nano-modified materials is quite recent, but their possible applications appear promising. As a matter of fact, literature on doped AAS composites is still scarce, above all for smart conductive materials. The samples investigated in this research are produced by adding the same percentage of fillers, namely 1% of the weight of the slag. The mixes with carbon fillers exhibit acceptable workability, density and mechanical performances, albeit slightly lower than those characterizing the plain material. Electrical and electromechanical tests demonstrate the good performance of the nano-modified samples in sensing changes in stresses and strains. The composites with CB and CNF appear the

most promising for applications in the monitoring of civil engineering structures and infrastructures.

5.3 Experimental research on self-cleaning capability of alkali-activated slag mortars

Building materials are deeply subjected to atmospheric factors and aging, therefore good aesthetical and surface properties are required [230]. A façade of a building exposed to vehicular traffic has an average duration of 3 years, therefore it requires continuous maintenance to be aesthetically pleasant. Moreover, the subways and tunnels, according to Italian standard [231], should have a sufficient chromatic value to guarantee adequate brightness. For this reason, they are subject to very high maintenance costs with also annoying consequences for the periodic construction sites responsible for the redevelopment of internal structures walls. Furthermore, the initial reflectance of porous materials is not always restored through cleaning techniques [232]. Consequently, the addition of nanoparticles of titanium dioxide is an advantageous alternative to maintain the aesthetic properties of building façade, as they are able to provide self-cleaning properties to the materials. A self-cleaning surface is defined as a surface that is capable of cleaning itself through a natural phenomenon without involving manual labor. Self-cleaning in building materials has the potential to keep building surfaces clean with a reduction in the maintenance [233]. In the 1970s Fujishima and Honda [234] discovered the photochemistry of TiO_2 , reporting the photocatalytic splitting of water in titanium dioxide. However, the applications of titanium dioxide photocatalysts to construction materials began towards the end of the 1980s. Over the years, thanks to the advances of knowledge on the subject, TiO_2 has been implemented in various commonly used materials, such as concrete, mortars, paints, tile and glass, used both for new buildings and for the restructuring of civil infrastructures. The addition of titanium dioxide in commonly used materials is one of the most important examples that derive from the application of nanotechnology on different fields, including the construction and civil infrastructures. The addition of titanium dioxide, thanks to its photocatalysis, gives cementitious materials self-cleaning and anti-pollution aspect, in order to obtain aesthetic, economic and in some cases even environmental comfort benefits. The evolution of this

product stems from the need to obtain a material capable of preserving its aesthetic characteristics, therefore of color, over time, without suffering the daily aggression of the substances that dirty it. Starting from this concept, after years of research and development, it has also obtained significant advantages in terms of pollution reduction and antibacterial properties. Obviously the two characteristics of self-cleaning of the façade and anti-pollution of the air are closely related to each other. In fact, the NO_x and organic compounds that diffuse through the porous surface bond to the titanium dioxide nanoparticles. Subsequently, the absorption of UV light by the TiO₂ incorporated in the cement mixture leads to its photoactivation and the consequent degradation of pollutants such as NO and NO₂, absorbed on the particles and transformed into nitric acid. Finally, the rain removes nitric acid in the form of harmless nitrate ions, which are used, for example, to fertilize the soil. During the last years, many studies have investigated the photocatalytic activity of TiO₂ applied on different materials, in the field of new construction technologies and for cultural heritage preservation [109,235–238]. Some studies have shown that the addition of nanomaterials in Portland cement pastes, mortars and geopolymers could contribute to the enhancement of mechanical and chemical properties [239]. Sumesh et al. [240] have shown that the nano-particles incorporation in cement composite has performed better compared to the samples without nano-materials. This behavior is attributed to the combined effects of pozzolanic activity and filler effect of nano-particles which form denser microstructures. On other hand, the nano-materials reduce the workability of the mixtures, because of the very fine particle size as well as significantly high surface area of nano-materials. Furthermore, Llano-Guerrero et al. [241] have shown that titanium dioxide nanoparticles can accelerate early hydration of Portland cement, improving compressive and flexural strengths, abrasion resistance and providing excellent mechanical properties to construction materials. Pozo-Antonio [242] demonstrated that Portland-based mixtures manufactured with the addition of titanium dioxide nanoparticles show self-cleaning properties. In fact, after thirty days with FESEM, FTIR and colour spectrophotometry it is possible to observe a slightly self-cleaning effect for lime-based mortars and Portland cement. Nevertheless, only few papers investigated the addition of the titanium dioxide in two-part alkali activated mixtures. Yang et al. [243] studied the effect of the addition of TiO₂ nanoparticles in alkali-activated fly ash on the mechanical properties, reporting that the nanoparticles

promote the formation of reaction products, resulting in fewer cracks, denser microstructures and improving carbonation resistance. Chen et al. [244] have noted that the setting time in cement mixtures was shorter for the samples with higher nano-TiO₂ contents. This behavior is caused by the increase in viscosity and therefore solidification occurred earlier due to the rapid consumption of free water that fills the gaps. Finally, Maiti et al. [245] affirm that fly ash-based mortars exhibit photocatalytic properties: increasing the quantity of titanium dioxide increases the rate of degraded pollutant. Also, with the decrease in particle size of TiO₂, the photocatalytic degradation efficiency increases. Based on the literature survey described above, there is a lack of studies on the use of one-part alkali-activated slag as self-cleaning materials. The purpose of this research is to evaluate the self-cleaning activity of one-part alkali-activated slag-based mortars manufactured by adding different percentages by weight of titanium dioxide. The photocatalytic properties of the materials have been evaluated through natural and accelerated tests. In particular, in the latter, their ability to discolor rhodamine B and methylene blue, applied to their surfaces and submitted to artificial sunlight have been studied.

5.3.1 Materials

The alkali activated mortars were manufactured by using a ground granulated blast furnace slag (GGBFS) with 28-day pozzolanic activity index equal to 0.76 (according to EN 196-5) as a precursor and an alkaline powder as activator. In particular, sodium metasilicate pentahydrate, potassium hydroxide and sodium carbonate with relative mass ratio of 7:3:1 were used as activators in accordance with previous studies [69,118,161]. Moreover, two different Portland cement mortars were manufactured as reference by using a Type I Portland cement CEM I 52.5R (GC) and a Type I white Portland cement (WC). The physical properties of binder and the laser granulometry were reported in the previous chapters.

Five different natural siliceous sands (Table 5-6) with maximum size of 2.5 mm were used as aggregates. A superplasticizer based on ester of methacrylic acid monomer (PCE) having 1000 g/mol side chain length was used. Finally, a powder of titanium dioxide was used. TiO₂ powder had a particle size ranging from 150 to 400 nm and having purity higher than 92%.

Table 5-6 Physical properties of aggregates

Aggregate Size [mm]	Specific Mass [kg/dm ³]	Water Absorption s.s.d. [wt%]	Dosage [wt% vs Total Aggregates]
0.00/0.25	2.41	1.20	25
0.25/0.50	2.70	0.76	30
0.50/1.00	2.58	0.77	25
1.00/1.50	2.63	0.93	10
1.50/2.50	2.62	1.02	10

5.3.2 Mixtures, preparation and samples curing

Three different one-part alkali-activated slag-based mortars were produced by varying the activator/precursor ratio between 8 and 16. In addition, two cementitious mortars manufactured with Portland cement (grey or white cement) were used as control mixtures to evaluate the effectiveness of color change. In all mixes, the water/binder (w/b) were fixed at 0.55 and the sand/binder (s/b) of mortars were fixed at 3.00. Furthermore, a superplasticizer at 0.5 wt% vs. cement mass used in order to ensure a thixotropic consistency of cement-based mortar. Finally, a second set of mortars including 1%, 3% and 5% of titanium dioxide on weight of cement were also made.

Cement-based mixtures were manufactured according to EN 196-1, while alkali activated mortars were prepared in accordance with the “Dry mixing method” reported in [246].

Table 5-7 Composition of mortars. WC: White cement-based mortars; GC: Portland cement-based mortars; S: Alkali-activated slag-based mortars (The number indicates the activator to slag ratio by mass; the number after the hyphen indicates the percentage of TiO₂).

[g]	WC	GC	GGBFS	Activators	Aggregates	Water	Superplasticizer	TiO ₂	w/b
WC-0	500				1500	275	2.25	--	0.55
WC-1	500				1500	275	2.25	5	0.55
WC-3	500				1500	275	2.25	15	0.55
WC-5	500				1500	275	2.25	25	0.55
GC-0		500			1500	275	2.25	--	0.55
GC-1		500			1500	275	2.25	5	0.55
GC-3		500			1500	275	2.25	15	0.55
GC-5		500			1500	275	2.25	25	0.55
S8-0			500	40	1500	275		--	0.55
S8-1			500	40	1500	275		5	0.55
S8-3			500	40	1500	275		15	0.55
S8-5			500	40	1500	275		25	0.55
S12-0			500	54	1500	275		--	0.55
S12-1			500	54	1500	275		5	0.55
S12-3			500	54	1500	275		15	0.55
S12-5			500	54	1500	275		25	0.55
S16-0			500	72	1500	275		--	0.55
S16-1			500	72	1500	275		5	0.55
S16-3			500	72	1500	275		15	0.55
S16-5			500	72	1500	275		25	0.55

5.3.3 *Experimental Setup*

5.3.3.1 *Fresh and Elasto-Mechanical Properties*

The workability, the specific mass at fresh state and the air content were detected in accordance with EN 1015-3, EN 1015-6 and 1015-7, respectively. Moreover, the setting time was determined using Vicat's apparatus in accordance with EN 196-1. Specific mass at hardened state, flexural and compressive strength were determined at 1, 7, 28 and 270 days from casting (EN 1015-11). Finally, dynamic modulus of elasticity of mixtures was estimated by means of Ultrasonic Digital Indicator Tester at 1, 7 and 28 days in accordance with EN 12504-4.

5.3.3.2 *Accelerated photocatalyst tests*

Self-cleaning capability of photocatalytic mortars was determined by monitoring the discoloration of organic dyes (Rhodamine B (RhB) – UNI 11259:2016) and methylene blue (MB)). Experiments were carried out for both dyes according to the procedure given in the standard UNI 11259:2016 with some modification. While the standard recommends a solution with a concentration of $0.1 \text{ g/L} \pm 0.005 \text{ g/L}$, the current study used a solution with a concentration equal to 1 g/L , in such a way as to have a more homogeneous distribution of color on the surface. According to UNI 11259 standard, after spraying the mixtures with an aqueous solution of organic dyes, they were left to dry in a dark environment for 24 h. Subsequently, the samples were exposed to artificial sunlight setting a UV radiation. The color variation was measured after 4 and 24 hours of exposure to UV light by studying the a^* coordinate or b^* coordinate, related to red/green or yellow/blue hues. The percentage of discoloration was expressed with the coordinate of dominant color of dye a^* or b^* for RhB and MB, respectively.

$$a\% \text{ of color change RhB} = [(a_0^* - a_t^*) / a_0^*] \cdot 100$$

$$b\% \text{ of color change MB} = [(b_0^* - b_t^*) / b_0^*] \cdot 100$$

where a_0^* and b_0^* are the color intensity coordinates of specimens before the UV irradiation, a_t^* and b_t^* are the color intensity coordinates of specimens at t hours of irradiation. For the colorimetric detection a portable spectrophotometer PCE-CSM 4 was used. Also, the tendency of the different mixtures to absorb and retain dust and other impurities deposited on the surface was observed by monitoring the discoloration of

carbon black in accordance with UNI 10792:1999. In particular, half of specimens was immersed for 30 seconds in an aqueous dispersion of 1% carbon black, then the specimens were washed under tap water for about 10 seconds, dried with an absorbent cloth and left to dry for 24 hours at a room temperature ($20^{\circ}\text{C} \pm 2^{\circ}\text{C}$). After 24 hours, the difference in brightness (ΔL) between the part of specimens that was immersed and the part that was not immersed was measured. Furthermore, the absorption of the different mixtures was calculated by immersing the specimens for 30 seconds in water; the absorption values was reported in g/m^2 .

5.3.3.3 Outdoor natural exposure

The specimens were exposed to the urban environment, on a rooftop of Laboratory of University of Bergamo for a period of 6 months. The samples were positioned with an inclination of 45° and were positioned facing both north and south; the different orientation was used to understand if the self-cleaning capability is influenced by the different solar exposure. Specimens were monitored approximately every 30 days, have been analyzed the individual color coordinates, in particular, the variation of brightness that represent the dirt accumulation on the surface. The data were compared with the meteorological data of the local environmental agency, ARPA (Regional Agency for Environmental Protection), which provides the daily data of rain (in millimeters) and overall integrated solar radiation.

5.3.4 Results and Discussion

5.3.4.1 Fresh state and Elasto-Mechanical Properties

The mixtures manufactured with the addition of titanium dioxide, regardless of the percentage, present the same workability of mortars manufactures without. Moreover, as expected, the increase in alkali content leads to an increase in the workability of the mixtures. This behavior is caused by the deflocculating and plasticizing effect promoted by the use of sodium silicate as activator that reduce the yield stress at early ages [29]. The addition of titanium dioxide determines a decrease in the setting time, in particular when increasing TiO_2 respect to cement mass, the initial and final setting time decreased (Figure 5-11). The variation in setting time occurs both in alkali activated slag mixtures and in Portland cement based mortars. Zhang et al. [247] reported that the nanoparticles

of titanium dioxide act as a setting accelerator. The precipitation of the hydrates could be promoted because the titanium dioxide nanoparticles act as seeds for the precipitation of the hydration products. The air content and the specific mass at fresh state of mortars without nano-TiO₂ are similar. The addition of titanium dioxide nanoparticles does not result in a significant change in specific mass at fresh state and in entrapped air, in fact, the variations are below 2 percent.

Table 5-8 Fresh properties of mortars manufactured

	Workability [mm]	Entrapped air [%]	Specific mass at fresh state [kg/m ³]	Specific mass at 28 days [kg/m ³]	Initial setting [min]	Final setting [min]
S8-0	180	5.2	2120	2085	300	580
S8-1	185	4.6	2135	2160	300	550
S8-3	180	5.2	2125	2180	300	530
S8-5	180	5.2	2140	2170	290	530
S12-0	195	4.9	2145	2180	190	430
S12-1	190	5.2	2140	2180	140	390
S12-3	190	5.1	2165	2190	130	410
S12-5	190	5.0	2155	2190	120	390
S16-0	200	4.0	2175	2215	170	360
S16-1	210	3.4	2190	2215	130	300
S16-3	200	3.8	2180	2220	120	300
S16-5	210	4.6	2190	2210	110	290
WC-0	165	6.0	2120	2140	180	310
WC-1	170	6.0	2130	2150	150	280
WC-3	170	5.5	2150	2200	150	280
WC-5	170	5.5	2145	2175	140	270
GC-0	150	6.4	2165	2260	170	230
GC-1	155	6.0	2165	2260	160	220
GC-3	150	6.3	2185	2250	150	220
GC-5	160	5.8	2165	2260	150	200

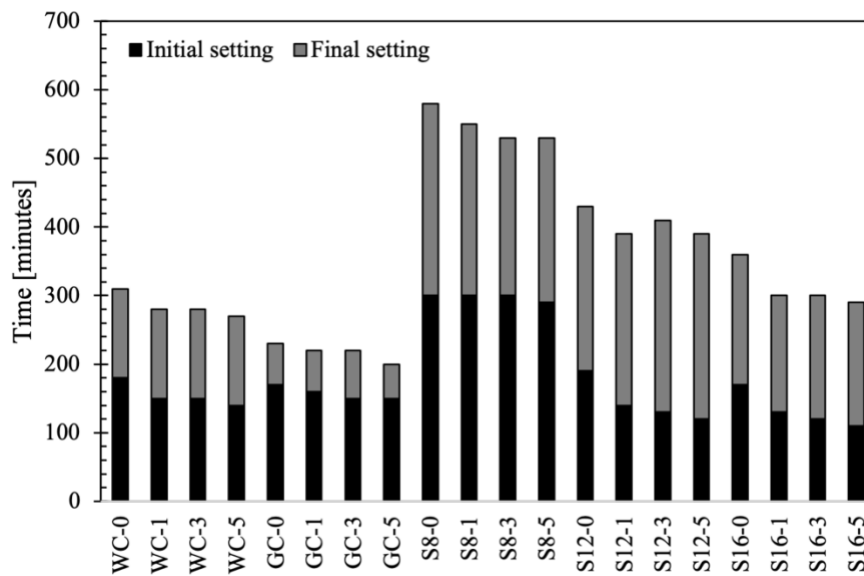


Figure 5-11 Initial and final setting time of mortars

Table 5-9 shows the compressive strength measured in prismatic specimens, it is possible to note that the mechanical properties, regardless of age, increase by increasing the percentage of activation of the mixtures, in agreement with what found in previous works [69,118]. In particular, after 28 days, S8 reaches a compressive strength close to 25 MPa, S12 of 35 MPa, S16 of 45 MPa, WC of 43 MPa and GC of 48 MPa. In all the system analyzed, the results indicated that the incorporation of titanium dioxide in mortars exhibited an enhancement in the compressive strength values. In some mixtures an increase of the compressive strength up to 20% is observed compared to the value of the conglomerate manufactured without the addition of titanium dioxide. Duan et al. [248] affirm that this behavior could be attributed to the micro-filling effect of the fine titanium dioxide which promotes the formation of denser microstructures and in this way improves the strength. Finally, it is possible to observe that the elastic modulus of mortars is not affected by the addition of titanium dioxide, but it depends on the binder used, as explained in the previous papers [118].

Table 5-9 Hardened properties of mortars manufactured

	Flexural strength [MPa]				Compressive strength [MPa]			
	1d	7d	28d	270d	1d	7d	28d	270d
S8-0	1.4 ± 0.3	3.6 ± 0.7	4.6 ± 1.3	5.5 ± 1.6	5.1 ± 0.7	16.0 ± 2.3	22.9 ± 2.7	33.2 ± 2.9
S8-1	1.5 ± 0.4	3.5 ± 0.9	5.0 ± 1.4	6.0 ± 1.3	5.8 ± 0.9	17.9 ± 1.9	25.8 ± 2.6	37.1 ± 2.6
S8-3	1.7 ± 0.2	3.8 ± 0.5	5.8 ± 1.7	6.2 ± 1.7	5.9 ± 1.3	18.8 ± 2.1	26.0 ± 2.4	38.9 ± 3.1
S8-5	1.8 ± 0.3	4.1 ± 0.4	6.4 ± 2.1	6.3 ± 1.8	5.6 ± 1.4	18.1 ± 2.4	25.0 ± 2.5	39.1 ± 3.9
S12-0	2.7 ± 0.8	4.9 ± 0.5	6.5 ± 1.4	8.1 ± 2.1	10.1 ± 1.3	23.8 ± 2.5	36.4 ± 2.7	51.1 ± 4.1
S12-1	2.8 ± 0.9	4.4 ± 0.9	6.9 ± 1.7	8.1 ± 2.4	10.1 ± 1.7	24.1 ± 2.3	35.3 ± 2.8	50.6 ± 3.9
S12-3	2.9 ± 0.5	4.6 ± 0.8	6.6 ± 1.7	8.3 ± 2.1	10.0 ± 2.1	24.6 ± 2.4	34.1 ± 2.6	51.7 ± 3.2
S12-5	3.1 ± 0.3	5.0 ± 0.9	6.2 ± 1.3	8.5 ± 2.2	10.5 ± 1.8	24.9 ± 2.4	36.4 ± 2.8	52.7 ± 2.9
S16-0	3.4 ± 0.2	6.0 ± 1.2	7.5 ± 1.9	8.1 ± 1.6	14.2 ± 2.3	31.3 ± 3.1	43.4 ± 3.5	57.4 ± 3.8
S16-1	3.2 ± 0.6	6.5 ± 1.4	8.3 ± 2.2	8.3 ± 1.9	14.0 ± 1.9	29.1 ± 2.9	40.7 ± 3.1	57.0 ± 2.5
S16-3	3.4 ± 0.8	6.6 ± 1.7	8.0 ± 2.1	8.1 ± 1.8	15.8 ± 3.1	32.4 ± 2.9	46.3 ± 3.3	61.2 ± 3.4
S16-5	4.3 ± 0.7	5.9 ± 1.9	8.6 ± 1.9	8.8 ± 1.9	16.1 ± 2.9	31.7 ± 3.2	43.7 ± 3.2	62.1 ± 4.1
WC-0	4.8 ± 0.7	6.7 ± 0.9	7.6 ± 2.4	8.0 ± 2.1	18.2 ± 2.3	35.1 ± 3.3	41.2 ± 2.8	48.9 ± 3.8
WC-1	4.6 ± 0.8	6.5 ± 1.4	7.9 ± 1.4	8.1 ± 2.3	17.1 ± 2.8	36.4 ± 3.8	41.6 ± 2.7	49.0 ± 3.1
WC-3	4.3 ± 0.9	6.7 ± 1.6	7.5 ± 2.1	8.2 ± 2.2	18.7 ± 2.5	39.3 ± 2.3	45.2 ± 2.9	49.0 ± 3.5
WC-5	4.4 ± 0.7	7.7 ± 2.1	8.0 ± 2.4	8.7 ± 2.2	19.3 ± 2.3	41.3 ± 3.3	45.3 ± 3.1	48.7 ± 3.4
GC-0	5.6 ± 1.2	6.9 ± 1.9	8.1 ± 1.7	8.2 ± 1.9	25.0 ± 3.1	42.1 ± 3.6	44.8 ± 3.6	48.8 ± 4.1
GC-1	5.7 ± 0.9	7.2 ± 2.1	8.0 ± 1.8	8.2 ± 1.9	25.7 ± 2.9	40.8 ± 3.5	45.7 ± 3.7	48.7 ± 2.9
GC-3	5.3 ± 1.3	7.1 ± 1.8	7.4 ± 2.1	7.9 ± 1.6	26.0 ± 3.3	44.0 ± 2.5	48.1 ± 3.5	48.9 ± 3.5
GC-5	5.4 ± 0.8	7.7 ± 2.4	8.4 ± 2.5	7.6 ± 1.7	26.8 ± 2.3	44.3 ± 2.6	49.5 ± 3.7	49.9 ± 3.4

Table 5-10 Elastic modulus of mortars manufactured

	Elastic modulus at 1d [GPa]	Elastic modulus at 7d [GPa]	Elastic modulus at 28d [GPa]
S8-0	16.8 ± 1.9	24.1 ± 1.9	25.9 ± 2.7
S8-1	18.9 ± 1.6	25.8 ± 1.6	27.7 ± 2.9
S8-3	18.3 ± 1.4	26.0 ± 1.5	27.6 ± 2.8
S8-5	17.6 ± 1.7	26.0 ± 1.8	28.1 ± 2.7
S12-0	23.0 ± 2.1	27.8 ± 1.9	29.9 ± 2.9
S12-1	23.1 ± 2.2	27.8 ± 1.8	30.2 ± 2.6
S12-3	23.1 ± 1.9	28.0 ± 1.7	30.6 ± 2.5
S12-5	23.4 ± 1.8	28.1 ± 2.1	30.8 ± 2.74
S16-0	24.8 ± 1.7	28.9 ± 2.1	31.3 ± 2.9
S16-1	24.6 ± 2.2	28.8 ± 2.4	31.7 ± 3.1
S16-3	24.7 ± 1.9	28.9 ± 2.5	31.9 ± 2.7
S16-5	25.1 ± 1.8	28.9 ± 2.2	31.6 ± 3.2
WC-0	25.3 ± 2.2	33.3 ± 2.7	35.2 ± 3.3
WC-1	25.8 ± 1.9	34.0 ± 2.6	35.3 ± 2.9
WC-3	25.7 ± 1.5	33.6 ± 2.4	35.3 ± 2.8
WC-5	25.8 ± 1.8	34.0 ± 2.3	35.1 ± 3.1
GC-0	26.4 ± 2.3	35.6 ± 3.2	36.5 ± 3.7
GC-1	26.2 ± 1.9	35.4 ± 2.9	36.1 ± 3.5
GC-3	26.8 ± 1.7	35.4 ± 2.8	35.7 ± 2.7
GC-5	27.0 ± 1.6	36.0 ± 2.7	36.1 ± 2.9

5.3.4.2 Accelerated photocatalyst test

The standard UNI 11259:2016 considered a photocatalytic material when $a_4 > 20\%$ and $a_{24} > 50\%$, where a_4 is the percentage of color change after 4 hours of irradiation and a_{24} is the percentage of color change after 24 hours of irradiation. However, this standard refers to white cementitious materials, for this reason in RhB test the value of a^* after 24 hours of permanence under UV lights is less than 50%. Figure 5-12 shows $a\%$ of RhB solution on standard and photoactive samples, it can be noted that all mixtures showed a good self-cleaning ability, even ground granulated blast furnace slag mixtures manufactured without the addition of titanium dioxide nanoparticles show a degradation of the a^* close to 10% after 24 hours under UV lights. De Gutiérrez et al. [249] attributed this behavior to the ability to attract and retain organic cationic species by the hydroxyl groups present on the surface of the alkali-activated mortars. Moreover, as expected, the increase in the percentage of TiO_2 increases the self-cleaning capacity of the conglomerates.

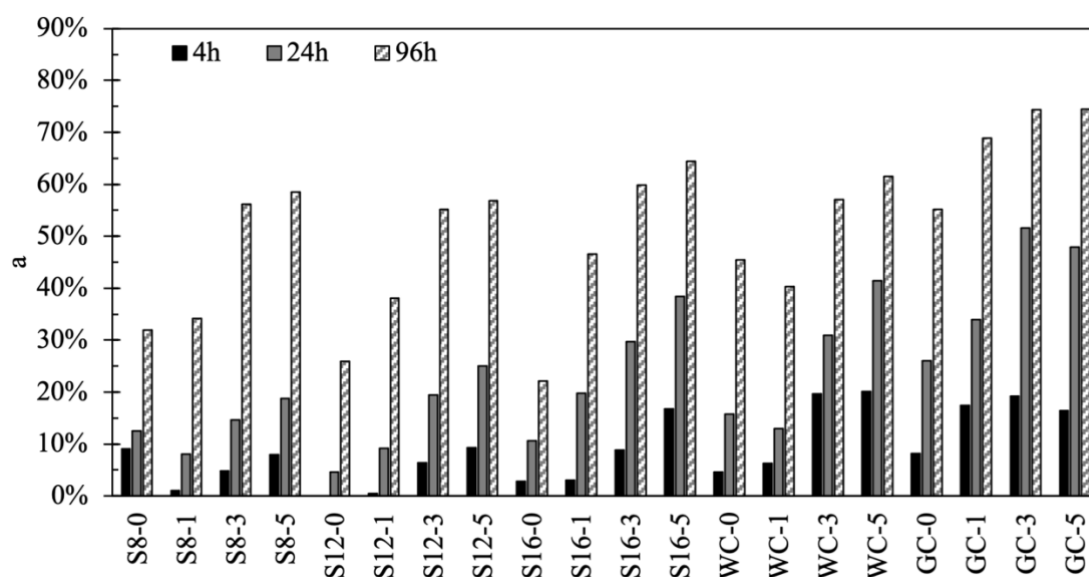


Figure 5-12 $a\%$ (extent of degradation) of RhB solution, previously deposited and dried on sample, under UV irradiation on standard and photoactive samples

Figure 5-13 shows $b\%$ of MB solution on standard and photoactive samples, it can be observed that not all specimens show photocatalytic capabilities, in fact, the mortars WC-0 have values of b_4 and b_{24} approximately equal to 0. On the contrary, the other mixtures have a good ability to degrade methylene blue solution, even small percentages

of TiO₂ allow to have photocatalytic materials ($b_{24} > 50\%$). Moreover, it is possible to observe that even with the blue methylene solution, increasing the percentage of the photocatalytic nanoparticles increases the self-cleaning capacity. In particular, b_{24} of S16-0 is equal to 23.5 and the R_{24} of s16-5 is equal to 76.3; the white cement mortars show a b_{24} of WC-0 and WC-5 equal to 1.4 and 71.0, respectively. Finally, it is possible to note that the conglomerates produced with a percentage of activator equal to 12 or 16 show very similar b_4 and b_{24} values, even higher than those of white cement mortars.

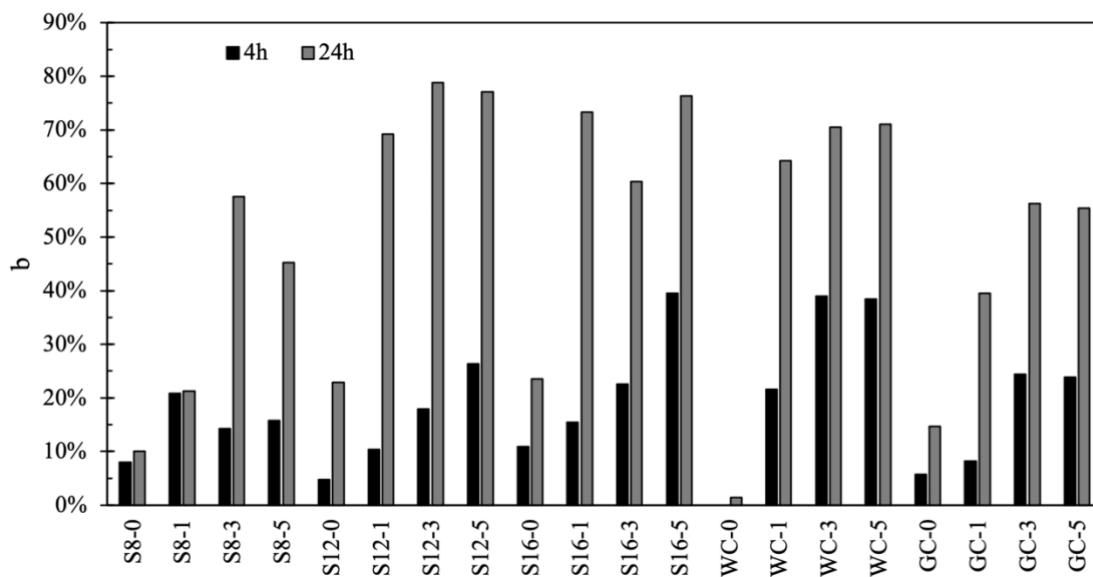


Figure 5-13 $b\%$ (extent of degradation) of MB solution, previously deposited and dried on samples, under UV irradiation on standard and photoactive samples

Comparison of the results obtained for both dyes in samples is given in Figure 5-14, where it can be seen that for no binder there is a good correlation between the values corresponding to RhB and MB at 4 h and 24 h. In fact, all the mortars have more degraded the MB dye than the RhB. The same behavior was found by Zhu et al. [250], who attribute the photodegradation efficiency to the photosensitization of dyes. In particular, superoxide radicals could form from the reaction of electron excited from dyes that have been ejected to the conduction band of photocatalyst and oxygen [251].

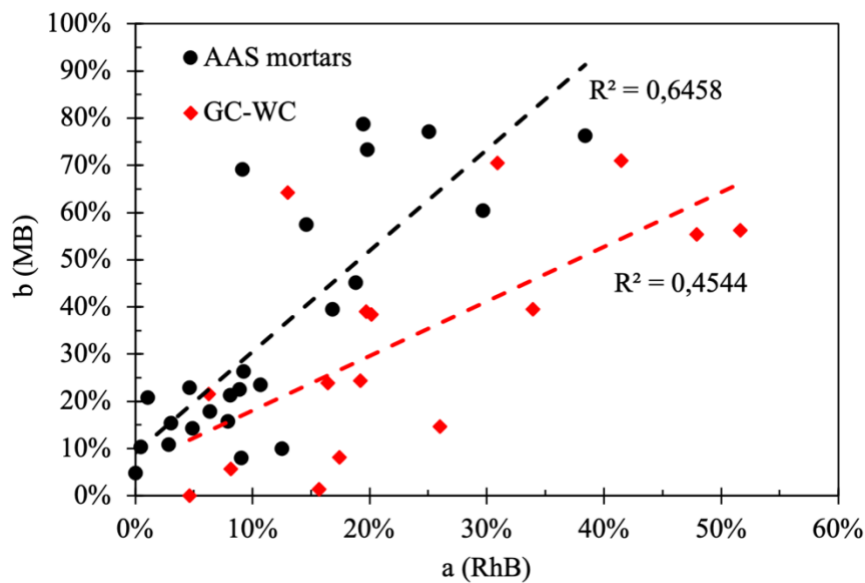


Figure 5-14 Comparison of the results obtained for both dyes in samples

The results of dirt pick-up are shown in Figure 5-15, each point is an average of 9 measurements (3 samples per type, 3 measurements on each sample). The test carried out according to the standard UNI 10792:1999 serves to establish a method for determining the tendency of mixtures to retain very fine pigment particles. This measurement was carried out to understand the tendency of the different mixtures to absorb and retain dust and other impurities deposited on the surface, and therefore to dirty it. It can be observed that the difference in brightness is not influenced by the presence of titanium dioxide, but varies according to the mixture. In ground granulated blast furnace slag-based mortars the difference in brightness is a function of the activation percentage: increasing the a/p ratio decreases the difference in brightness between the portion of the specimens immersed in the carbon black solution and the non-immersed one. This behavior is primarily attributable to the different absorption of mortars. Figure 5-16 shows the correlation between water absorption and the difference in brightness. It can be noted that the absorption of water does not depend on the percentage of titanium dioxide, but is a function of the binder: Portland-based mortars have a lower water absorption that one-part alkali-activated slag. Especially, the GC and WC mortars have similar compressive strength and equal ΔL , but completely different water absorption rates. The high absorption of AAS respect to OPC can be attributed to two main reasons. The first one is the large proportion of fine pores and from micro-cracks in the matrix that cause the high

pore connectivity of alkali activated slag, as reported by [252] and confirmed by optical microscopy observation on S8 sample (Figure 5-17). The second reason is the amount of moisture that can be absorbed by the excess dry salts that are formed during the drying process [253,254]. Furthermore, as expected as the percentage of alkali activators increases the absorption of water tends to decrease. In fact, Shariati et al. [255] noted that this behavior could be due to the fact that higher alkali content increased the alkalinity of the activator solution, which accelerated the dissolution of Si and Al complexes and led to an increase in C-S-H gel.

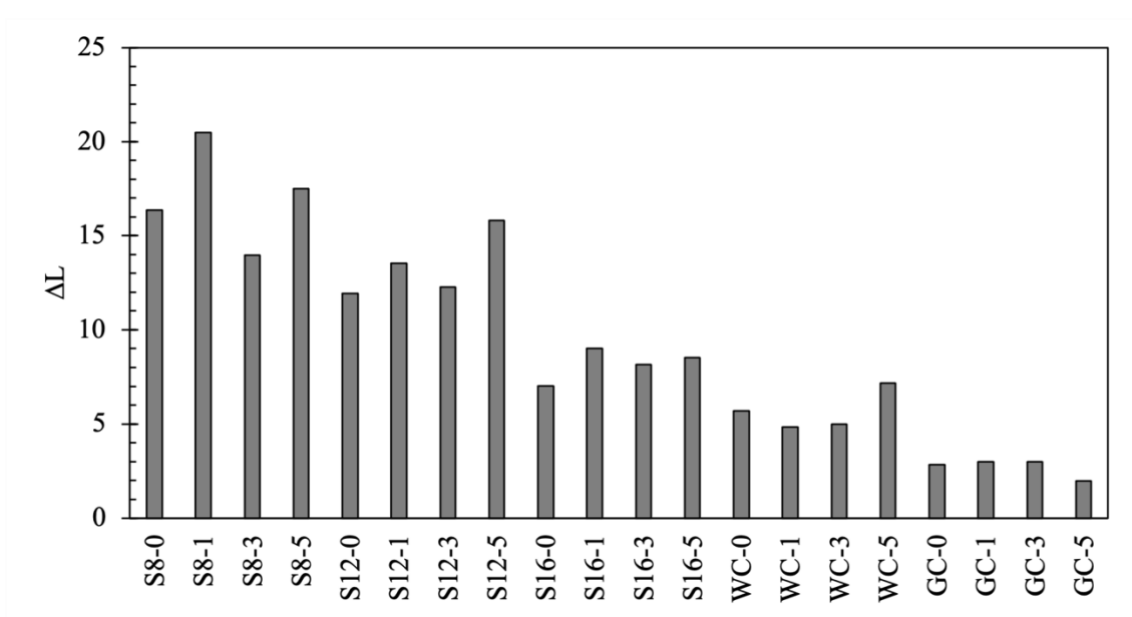


Figure 5-15 Difference in brightness (ΔL) between the part of mortar which was immersed in the carbon black solution and that not immersed

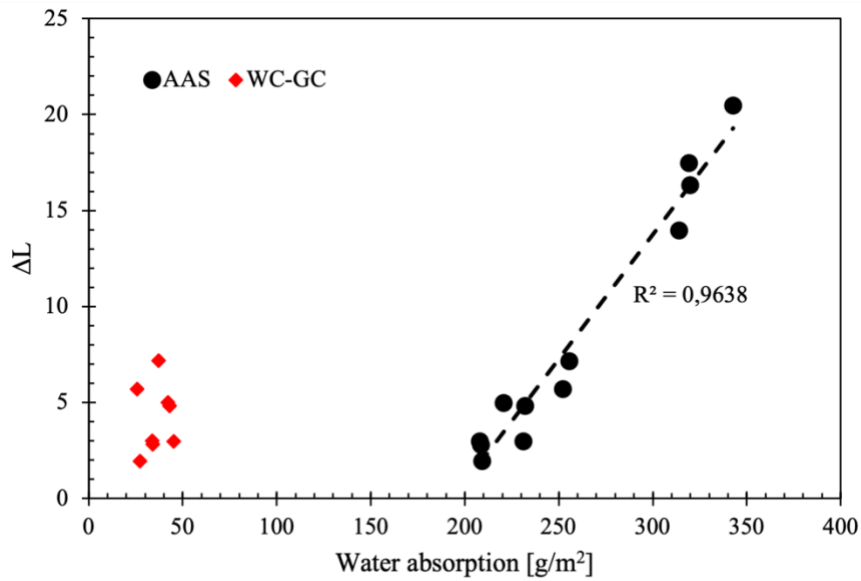


Figure 5-16 Correlation between water absorption and difference in brightness of mortars



Figure 5-17 Optical micrograph of S8

5.3.4.3 Outdoor natural exposure

The self-cleaning ability, induced by titanium dioxide, has been evaluated by exposing all the specimens to the urban environment for 6 months (from 2 March to 2 September 2021). The absorption of dust and pollutants could cause a difference in brightness. The results of lightness percent variation of the outdoor natural exposure are reported in Figure 5-18. The Figure 5-18 also shows the qualitative trend of daily precipitation and radiation in the exposure period. In this way, it is possible to identify

any rainy events that have contributed to the cleaning of the mixtures and the possibility of sunlight photoactivation. The data are reported as daily average value and daily cumulative value, for radiation and precipitation, respectively. The precipitation span from 0 mm/day to 40 mm/day, while solar radiation reaches a maximum of 300 W/m².

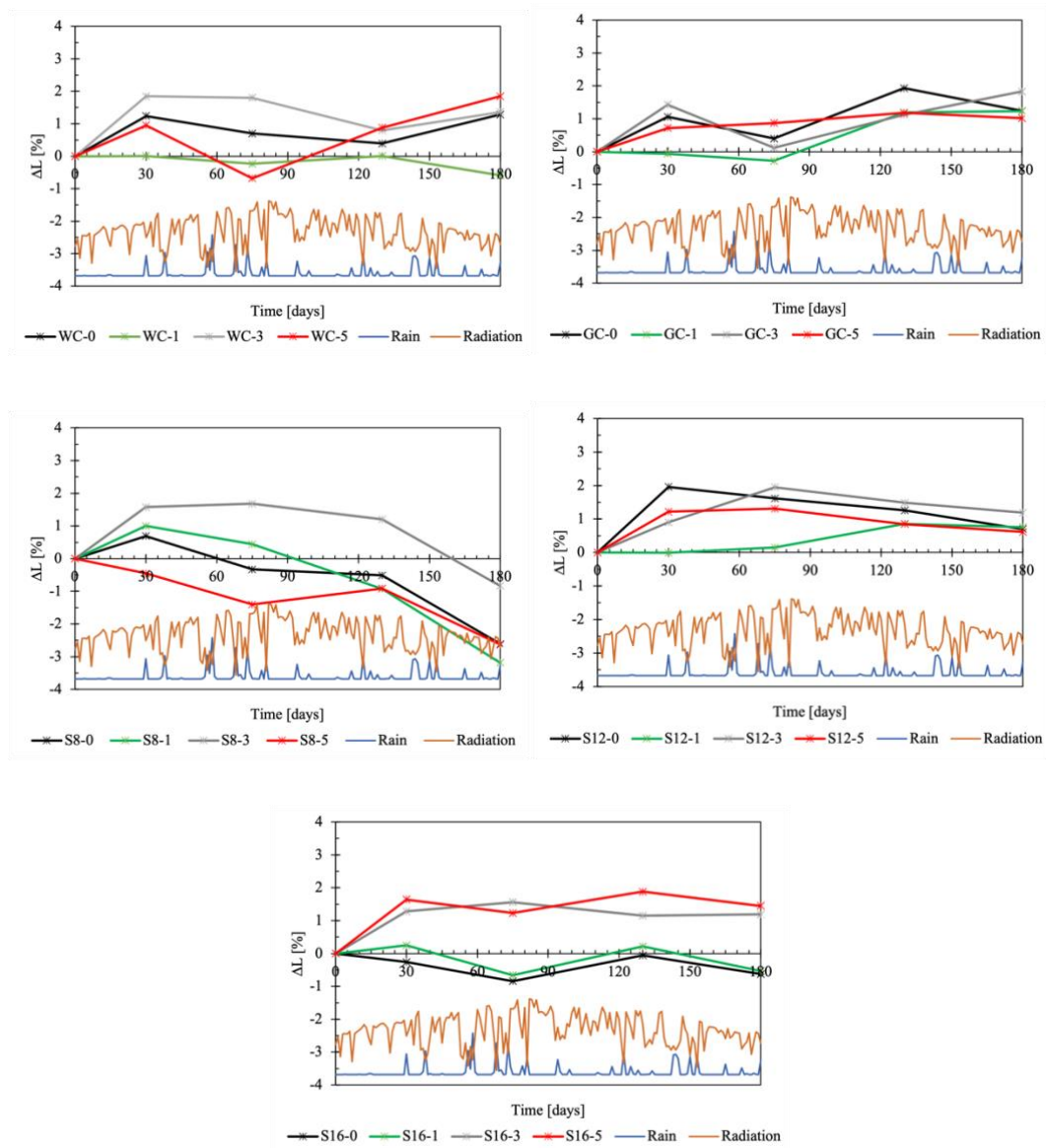
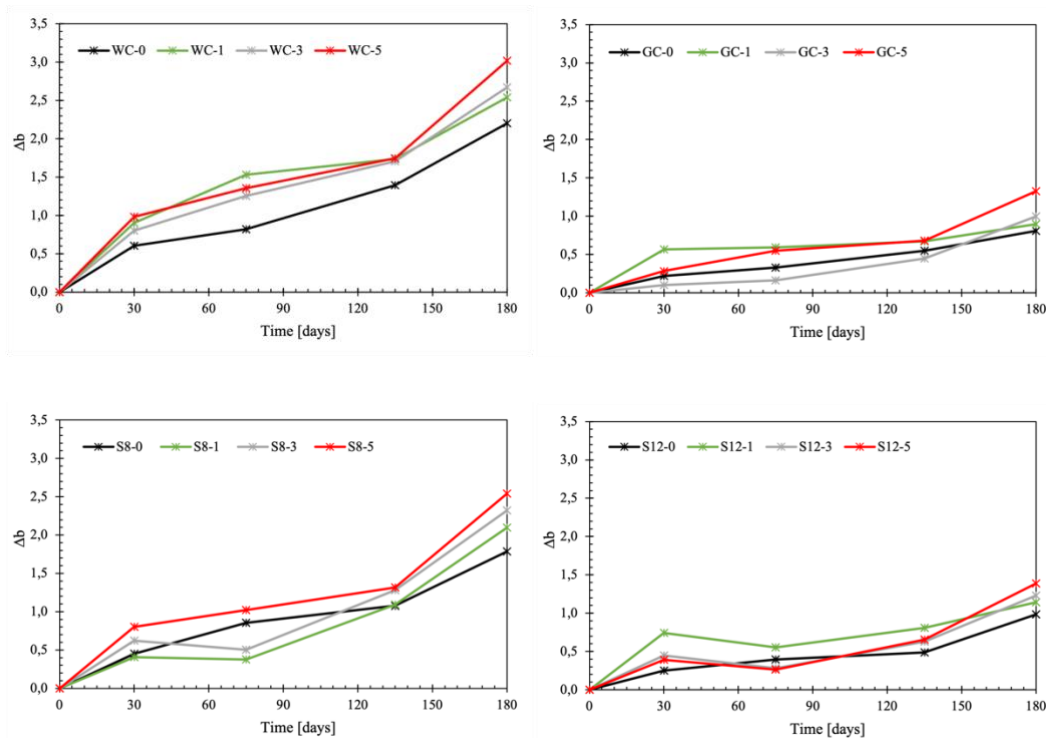


Figure 5-18 Lightness percent variation recorded on mortars during the 6 months

First of all, it is important underline that increasing the percentage of titanium dioxide increases the initial lightness of the mixture, whose L* values are 68.76 (WC-0), 71.03 (GC-0), 72.52 (S8-0), 69.86 (S12-0) and 66.73 (S16-0) against 69.41 (WC-5), 71.34 (GC-5), 76.64 (S8-5), 76.5 (S12-5) and 70.50 (S16-5), respectively (Appendix A and B). Furthermore, it can be observed that all the mixtures have not undergone an

important variation in brightness, in fact, all the specimens show a ΔL dissimilarity of at most 2%. Customarily the human eye is able to perceive a chromatic change equal to $\Delta L^* = 1$, anyway literature reports higher values of just noticeable difference (JND) by naked eye: 2.3 units [256] or a more generic 2-3 units range [257,258]. Finally, observing the experimental data (Appendix B) it can be affirmed that after six months of exposure there are no substantial differences in the L^* parameter of the north oriented mixtures compared to the south oriented ones. Furthermore, it can be deduced that a minor reduction in brightness variation of material containing titanium dioxide, respect to the same material without TiO_2 , is caused by the photocatalytic activity and not by a minor fouling of the surface. In fact, the data obtained through the standard UNI 10792 showed that the difference in brightness is not influenced by the presence of titanium dioxide.

Moreover, analyzing the color coordinates of the different mixtures, a marked increase in b^* was observed, as shown in figure 5-19. Peruchon et al [259] claim that this superficial yellowing can be caused by the mineralization of organic compounds previously absorbed on the surface. This may indirectly indicate that the mixtures, in addition to their self-cleaning characteristics, also contribute to the degradation of polluting compounds in the atmosphere.



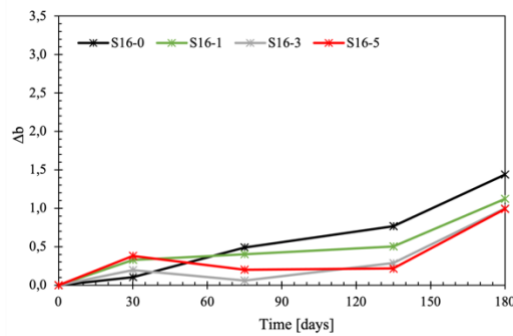


Figure 5-19 b^* variation of specimens

5.3.5 Conclusions

This experimental study was aimed at evaluating the self-cleaning potential of one-part alkali activated slag photoactive mortars manufactured with the addition of different percentage of titanium dioxide nanoparticles. The following conclusions can be drawn:

- The workability, the specific mass at fresh state and the entrapped air remain constant with the addition of TiO_2 . On the other hand, increasing the percentage of titanium dioxide decreases the initial and final setting time;
- The incorporation of nanoparticles leads to an enhancement in the compressive strength values. In some mixtures an increase of the compressive strength up to 20% is observed compared to the value of the conglomerate manufactured without the addition of titanium dioxide;
- Accelerated tests show that the alkali-activated slag mortars have a good self-cleaning capacity, in fact with 5% of TiO_2 it was observed a change up to 80% after 24 hours under UV lights with respect to the reference sample without photocatalyst;
- The test with carbon black solution shows that in all the mixtures the difference in brightness is not influenced by the presence of titanium dioxide;
- After 6 months of natural exposure in the urban environment of Bergamo, the mixtures do not show any significant variation in lightness, on the contrary they show an increase in the b^* coordinate.

Conclusions

This thesis is focused on the development and characterization of one-part alkali-activated slag mortars for traditional and innovative application. The main specific conclusions arisen from this PhD thesis are listed below:

- The key parameter that governed most of the properties both in fresh and hardened state of alkali-activated mixtures is the alkali content. In particular, the main reaction product are calcium silicate hydrates (C-S-H) and their concentration increase by increasing the alkali content. In general, the higher the alkali content, the higher the strength and the resistance in severe conditions. High alkali-content AAS mortars evidence a freeze-thaw resistance similar to that of blast furnace-based mixtures. Furthermore, the use of AEA enhances the freezing and thawing resistance of alkali-activated slag-based mortars without any strong reduction in compressive strength. The AAS mixtures are quasi-immune to expansive calcium oxychloride formation in presence of CaCl_2 -based deicing salts due to the negligible calcium hydroxide content. On the other hand, these conglomerates suffer from severe damages and high strength loss as a consequence of semi-immersion in 10 wt% Mg_2SO_4 solution due to decalcification of C-S-H gel and gypsum formation. Moreover, the resistance to carbonation of the AAS is related to its strength. In particular, mortars with compressive strength less than 25 MPa undergo rapid carbonation, which leads to reduction in strength. However, alkali-activated slags with compressive strength higher than 40 MPa undergo less carbonation and suffer a slight strength loss. Also, alkali-activated slag show higher acid corrosion resistance compared to Portland cement, due to the absence of portlandite and low Ca/Si ratio in the binder;
- An alkali-activated slag-based plaster is able to provide a structural reinforcement of stone masonry buildings (28-day compressive strength equal to 12 MPa) with a suitable rheology for a plaster. Moreover, the use of plastic bags for the storage of pre-packed plaster allows to solve the problems caused by the hygroscopic nature of the alkaline activators;

- Alkali-activated slag mortars are also suitable for producing intelligent mixtures. In particular, AAS cement-based mortars doped with different carbon-based nanofillers, i.e., nanotubes, nanofibers, carbon black and graphene nano-platelets, allow the realization of self-sensing mixtures. In fact, electrical and electromechanical tests demonstrate the good performance of the nano-modified samples in sensing changes in stressed and strains. The composites with CB and CNF appear the most promising for applications in the monitoring of civil engineering structures and infrastructures. Moreover, it is possible manufactured AAS self-cleaning mortars with the addition of small percentages of titanium dioxide. Especially, these mortars have a good self-cleaning capacity, in fact, with 5% of TiO_2 it was observed a color change up to 80% after 24 hours under UV lights with respect to the reference samples without photocatalyst.

References

- [1] J. Davidovits, Geopolymers and geopolymeric materials, *J. Therm. Anal.* 1989 352. 35 (1989) 429–441. doi:10.1007/BF01904446.
- [2] J.L. Provis, J.S.J. Van Deventer, *Geopolymers: structure, processing, properties and industrial applications*, Woodhead, 2009. [https://books.google.it/books?hl=en&lr=&id=NqjjAgAAQBAJ&oi=fnd&pg=PP1&dq=Geopolymers+:+structure,+processing,+properties+and+industrial+applications&ots=e2k77dumgt&sig=OJdkP_n2Sj1dliihja6ijsHjHMM&redir_esc=y#v=onepage&q=Geopolymers %3A structure%2C proces](https://books.google.it/books?hl=en&lr=&id=NqjjAgAAQBAJ&oi=fnd&pg=PP1&dq=Geopolymers+:+structure,+processing,+properties+and+industrial+applications&ots=e2k77dumgt&sig=OJdkP_n2Sj1dliihja6ijsHjHMM&redir_esc=y#v=onepage&q=Geopolymers%3A%20structure%20proces) (accessed July 21, 2021).
- [3] A. Fernández-Jiménez, F. Puertas, Alkali-activated slag cements: Kinetic studies, *Cem. Concr. Res.* 27 (1997) 359–368. doi:10.1016/S0008-8846(97)00040-9.
- [4] A. Fernandez-Jimenez, F. Puertas, A. Arteaga, Determination of Kinetic Equations of Alkaline Activation of Blast Furnace Slag by Means of Calorimetric Data, *J. Therm. Anal. Calorim.* 1998 523. 52 (1998) 945–955. doi:10.1023/A:1010172204297.
- [5] S.A. Bernal, J.L. Provis, V. Rose, R. Mejía De Gutierrez, Evolution of binder structure in sodium silicate-activated slag-metakaolin blends, *Cem. Concr. Compos.* 33 (2011) 46–54. doi:10.1016/J.CEMCONCOMP.2010.09.004.
- [6] P. Duxson, A. Fernández-Jiménez, J.L. Provis, G.C. Lukey, A. Palomo, J.S.J. van Deventer, Geopolymer technology: the current state of the art, *J. Mater. Sci.* 2006 429. 42 (2006) 2917–2933. doi:10.1007/S10853-006-0637-Z.
- [7] P. Duxson, J.L. Provis, Designing Precursors for Geopolymer Cements, *J. Am. Ceram. Soc.* 91 (2008) 3864–3869. doi:10.1111/J.1551-2916.2008.02787.X.
- [8] C. Shi, Krivenko; Pavel V., D. Roy, *Alkali-activated cements and concretes*, Taylor & Francis, 2006.
- [9] J.L. Provis, J.S.J. Van Deventer, *Geopolymers: structures, processing, properties and industrial applications*, Woodhead, 2009. doi:10.1533/9781845696382.

- [10] F. Pacheco-Torgal, J. Labrincha, C. Leonelli, A. Palomo, P. Chindapasirt, Handbook of alkali-activated cements, mortars and concretes, 2014.
- [11] D. Li, Z. Xu, Z. Luo, Z. Pan, L. Cheng, The activation and hydration of glassy cementitious materials, *Cem. Concr. Res.* 32 (2002) 1145–1152. doi:10.1016/S0008-8846(02)00755-X.
- [12] S.C. Pal, A. Mukherjee, S.R. Pathak, Investigation of hydraulic activity of ground granulated blast furnace slag in concrete, *Cem. Concr. Res.* 33 (2003) 1481–1486. doi:10.1016/S0008-8846(03)00062-0.
- [13] S.D. Wang, K.L. Scrivener, P.L. Pratt, Factors affecting the strength of alkali-activated slag, *Cem. Concr. Res.* 24 (1994) 1033–1043. doi:10.1016/0008-8846(94)90026-4.
- [14] S. Puligilla, P. Mondal, Role of slag in microstructural development and hardening of fly ash-slag geopolymer, *Cem. Concr. Res.* 43 (2013) 70–80. doi:10.1016/j.cemconres.2012.10.004.
- [15] S.-D. Wang, K.L. Scrivener, P.L. Pratt, Factors affecting the strength of alkali-activated slag, *Cem. Concr. Res.* 24 (1994) 1033–1043. doi:10.1016/0008-8846(94)90026-4.
- [16] J.L. Provis, P. Duxson, J.S.J. van Deventer, The role of particle technology in developing sustainable construction materials, *Adv. Powder Technol.* 21 (2010) 2–7. doi:10.1016/j.appt.2009.10.006.
- [17] F. Puertas, Cementos de escorias activadas alcalinamente: Situación actual y perspectivas de futuro, *Mater. Construcción.* 45 (1995) 53–64.
- [18] M.C.G. Juenger, F. Winnefeld, J.L. Provis, J.H. Ideker, Advances in alternative cementitious binders, *Cem. Concr. Res.* 41 (2011) 1232–1243.
- [19] F. Puertas, M. Palacios, H. Manzano, J.S. Dolado, A. Rico, J. Rodríguez, A model for the C-A-S-H gel formed in alkali-activated slag cements, *J. Eur. Ceram. Soc.* 31 (2011) 2043–2056. doi:10.1016/J.JEURCERAMSOC.2011.04.036.

- [20] A. Fernández-Jiménez, F. Puertas, I. Sobrados, J. Sanz, Structure of Calcium Silicate Hydrates Formed in Alkaline-Activated Slag: Influence of the Type of Alkaline Activator, *J. Am. Ceram. Soc.* 86 (2003) 1389–1394. doi:10.1111/J.1151-2916.2003.TB03481.X.
- [21] R. Taylor, I.G. Richardson, R.M.D. Brydson, Composition and microstructure of 20-year-old ordinary Portland cement–ground granulated blast-furnace slag blends containing 0 to 100% slag, *Cem. Concr. Res.* 40 (2010) 971–983. doi:10.1016/J.CEMCONRES.2010.02.012.
- [22] V.D. Glukhovskiy, Ancient, modern and future concretes, in: *First Int. Conf. Alkaline Cem. Concr.*, Kiev, 1994: pp. 1–8.
- [23] F. Puertas, Escorias de alto horno: composición y comportamiento hidráulico, *Mater. Construcción.* 43 (1993) 37–48. doi:10.3989/MC.1993.V43.I229.687.
- [24] S.P. Kang, S.J. Kwon, Effects of red mud and Alkali-Activated Slag Cement on efflorescence in cement mortar, *Constr. Build. Mater.* 133 (2017) 459–467. doi:10.1016/J.CONBUILDMAT.2016.12.123.
- [25] D. Tang, C. Yang, X. Li, X. Zhu, K. Yang, L. Yu, Mitigation of efflorescence of alkali-activated slag mortars by incorporating calcium hydroxide, *Constr. Build. Mater.* 298 (2021) 123873. doi:10.1016/J.CONBUILDMAT.2021.123873.
- [26] S.-D. Wang#, K.L. Scrivener, HYDRATION PRODUCTS OF ALKALI ACTIVATED SLAG CEMENT, *Cem. End Concr. Res.* 25 (1995) 561–571.
- [27] F. Puertas, C. Varga, M.M. Alonso, Rheology of alkali-activated slag pastes. Effect of the nature and concentration of the activating solution, *Cem. Concr. Compos.* 53 (2014) 279–288. doi:10.1016/J.CEMCONCOMP.2014.07.012.
- [28] F. Puertas, B. González-Fonteboa, I. González-Taboada, M.M. Alonso, M. Torres-Carrasco, G. Rojo, F. Martínez-Abella, Alkali-activated slag concrete: Fresh and hardened behaviour, *Cem. Concr. Compos.* 85 (2018) 22–31. doi:10.1016/J.CEMCONCOMP.2017.10.003.
- [29] A. Kashani, J.L. Provis, G.G. Qiao, J.S.J. Van Deventer, The interrelationship

- between surface chemistry and rheology in alkali activated slag paste, *Constr. Build. Mater.* 65 (2014) 583–591. doi:10.1016/J.CONBUILDMAT.2014.04.127.
- [30] J.L. Provis, J.S.J. Van Deventer, *Alkali Activated Materials - State-of-the-Art Report - Rilem - Tc 224-AAM*, 2014. doi:10.1007/978-94-007-7672-2.
- [31] X. Yang, W. Zhu, Q. Yang, The Viscosity Properties of Sodium Silicate Solutions, *J. Solut. Chem.* 2007 371. 37 (2007) 73–83. doi:10.1007/S10953-007-9214-6.
- [32] M. Palacios, S. Gismera, M.M. Alonso, J.B. d’Espinose de Lacaillerie, B. Lothenbach, A. Favier, C. Brumaud, F. Puertas, Early reactivity of sodium silicate-activated slag pastes and its impact on rheological properties, *Cem. Concr. Res.* 140 (2021) 106302. doi:10.1016/J.CEMCONRES.2020.106302.
- [33] S.A. Bernal, J.L. Provis, R.J. Myers, R.S. Nicolas, J.S.J. van Deventer, Role of carbonates in the chemical evolution of sodium carbonate-activated slag binders, *Mater. Struct.* 2014 483. 48 (2014) 517–529. doi:10.1617/S11527-014-0412-6.
- [34] H. Xu, J.L. Provis, J.S.J. van Deventer, P. V Krivenko, Characterization of aged slag concretes, *ACI Mater. J.* 105 (2008) 131.
- [35] O. Ozdemir, M.S. Çelik, Z.S. Nickolov, J.D. Miller, Water structure and its influence on the flotation of carbonate and bicarbonate salts, *J. Colloid Interface Sci.* 314 (2007) 545–551. doi:10.1016/J.JCIS.2007.05.086.
- [36] Y.J. Zhang, Y.L. Zhao, H.H. Li, D.L. Xu, Structure characterization of hydration products generated by alkaline activation of granulated blast furnace slag, *J. Mater. Sci.* 43 (2008) 7141–7147. doi:10.1007/s10853-008-3028-9.
- [37] R. Andersson, H.-E. Gram, Properties of alkali-activated slag concrete, *Nord. Concr. Res.* 6 (1987) 7–18.
- [38] J.J. Chang, A study on the setting characteristics of sodium silicate-activated slag pastes, *Cem. Concr. Res.* 33 (2003) 1005–1011.
- [39] S. Caijun, L. Yinyu, Investigation on some factors affecting the characteristics of alkali-phosphorus slag cement, *Cem. Concr. Res.* 19 (1989) 527–533.

doi:10.1016/0008-8846(89)90004-5.

- [40] A. Fernández-Jiménez, J.G. Palomo, F. Puertas, Alkali-activated slag mortars: Mechanical strength behaviour, *Cem. Concr. Res.* 29 (1999) 1313–1321. doi:10.1016/S0008-8846(99)00154-4.
- [41] M. Ben Haha, B. Lothenbach, G. Le Saout, F. Winnefeld, Influence of slag chemistry on the hydration of alkali-activated blast-furnace slag — Part I: Effect of MgO, *Cem. Concr. Res.* 41 (2011) 955–963. doi:10.1016/J.CEMCONRES.2011.05.002.
- [42] M. Ben Haha, B. Lothenbach, G. Le Saout, F. Winnefeld, Influence of slag chemistry on the hydration of alkali-activated blast-furnace slag - Part II: Effect of Al₂O₃, *Cem. Concr. Res.* 42 (2012) 74–83. doi:10.1016/j.cemconres.2011.08.005.
- [43] A.R. Sakulich, E. Anderson, C.L. Schauer, M.W. Barsoum, Influence of Si:Al ratio on the microstructural and mechanical properties of a fine-limestone aggregate alkali-activated slag concrete, *Mater. Struct.* 2009 437. 43 (2009) 1025–1035. doi:10.1617/S11527-009-9563-2.
- [44] M. Saedi, K. Behfarnia, H. Soltanian, The effect of the blaine fineness on the mechanical properties of the alkali-activated slag cement, *J. Build. Eng.* 26 (2019) 100897. doi:10.1016/J.JOBE.2019.100897.
- [45] S. Narimani Zamanabadi, S.A. Zareei, P. Shoaie, F. Ameri, Ambient-cured alkali-activated slag paste incorporating micro-silica as repair material: Effects of alkali activator solution on physical and mechanical properties, *Constr. Build. Mater.* 229 (2019) 116911. doi:10.1016/J.CONBUILDMAT.2019.116911.
- [46] C. Shi, R.L. Day, Some factors affecting early hydration of alkali-slag cements, *Cem. Concr. Res.* 26 (1996) 439–447. doi:10.1016/S0008-8846(96)85031-9.
- [47] M. Ben Haha, G. Le Saout, F. Winnefeld, B. Lothenbach, Influence of activator type on hydration kinetics, hydrate assemblage and microstructural development of alkali activated blast-furnace slags, *Cem. Concr. Res.* 41 (2011) 301–310. doi:10.1016/J.CEMCONRES.2010.11.016.

- [48] D. Nasr, A.H. Pakshir, H. Ghayour, The influence of curing conditions and alkaline activator concentration on elevated temperature behavior of alkali activated slag (AAS) mortars, *Constr. Build. Mater.* 190 (2018) 108–119. doi:10.1016/J.CONBUILDMAT.2018.09.099.
- [49] M. Hojati, F. Rajabipour, A. Radlińska, Drying shrinkage of alkali-activated cements: effect of humidity and curing temperature, *Mater. Struct.* 2019 526. 52 (2019) 1–14. doi:10.1617/S11527-019-1430-1.
- [50] I. Amer, M. Kohail, M.S. El-Feky, A. Rashad, M.A. Khalaf, A review on alkali-activated slag concrete, *Ain Shams Eng. J.* 12 (2021) 1475–1499. doi:10.1016/J.ASEJ.2020.12.003.
- [51] P.S. Deb, P. Nath, P.K. Sarker, The effects of ground granulated blast-furnace slag blending with fly ash and activator content on the workability and strength properties of geopolymer concrete cured at ambient temperature, *Mater. Des.* 62 (2014) 32–39. doi:10.1016/J.MATDES.2014.05.001.
- [52] G.S. Ryu, Y.B. Lee, K.T. Koh, Y.S. Chung, The mechanical properties of fly ash-based geopolymer concrete with alkaline activators, *Constr. Build. Mater.* 47 (2013) 409–418. doi:10.1016/J.CONBUILDMAT.2013.05.069.
- [53] P. Zhang, K. Wang, Q. Li, J. Wang, Y. Ling, Fabrication and engineering properties of concretes based on geopolymers/alkali-activated binders - A review, *J. Clean. Prod.* 258 (2020) 120896. doi:10.1016/J.JCLEPRO.2020.120896.
- [54] F.G. Collins, J.G. Sanjayan, Workability and mechanical properties of alkali activated slag concrete, *Cem. Concr. Res.* 29 (1999) 455–458. doi:10.1016/S0008-8846(98)00236-1.
- [55] P. Duxson, J.L. Provis, G.C. Lukey, S.W. Mallicoat, W.M. Kriven, J.S.J. Van Deventer, Understanding the relationship between geopolymer composition, microstructure and mechanical properties, *Colloids Surfaces A Physicochem. Eng. Asp.* 269 (2005) 47–58. doi:10.1016/J.COLSURFA.2005.06.060.
- [56] J. Wongpa, K. Kiattikomol, C. Jaturapitakkul, P. Chindapasirt, Compressive

- strength, modulus of elasticity, and water permeability of inorganic polymer concrete, *Mater. Des.* 31 (2010) 4748–4754. doi:10.1016/J.MATDES.2010.05.012.
- [57] B. Talling, P. Krivenko, Blast furnace slag-the ultimate binder, *Waste Mater. Used Concr. Manuf.* (1996) 235–289. doi:10.1016/B978-081551393-3.50008-9.
- [58] J.E. Oh, S.M. Clark, P.J.M. Monteiro, Does the Al substitution in C–S–H(I) change its mechanical property?, *Cem. Concr. Res.* 41 (2011) 102–106. doi:10.1016/J.CEMCONRES.2010.09.010.
- [59] E. Douglas, A. Bilodeau, V.M. Malhotra, Properties and Durability of Alkali-Activated Slag Concrete, *Mater. J.* 89 (1992) 509–516. doi:10.14359/1832.
- [60] F. Sajedi, H.A. Razak, The effect of chemical activators on early strength of ordinary Portland cement-slag mortars, *Constr. Build. Mater.* 24 (2010) 1944–1951. doi:https://doi.org/10.1016/j.conbuildmat.2010.04.006.
- [61] M. Komljenovic, Z. Bascarevic, N. Marjanovic, V. Nikolic, External sulfate attack on alkali-activated slag, *Constr. Build. Mater.* 49 (2013) 31–39. doi:10.1016/j.conbuildmat.2013.08.013.
- [62] J. Provis, J. van Deventer, Alkali Activated Materials State-of-the-Art Report, in: RILEM TC 224-AAM, Springer, London, UK, 2014: pp. 59–85.
- [63] J. DEJA, Carbonation aspects of alkali activated slag mortars and concretes, *Silic. Ind.* (2002).
- [64] Report Ance 2020, No Title, n.d.
- [65] N. Delatte, Failure, Distress and Repair of Concrete Structures, Woodhead Publishing, 2009. doi:10.1533/9781845697037.
- [66] Z. Zhang, X. Yao, H. Zhu, Potential application of geopolymers as protection coatings for marine concrete: II. Microstructure and anticorrosion mechanism, *Appl. Clay Sci.* 49 (2010) 7–12. doi:10.1016/J.CLAY.2010.04.024.
- [67] E. Gartner, Industrially interesting approaches to “low-CO₂” cements, *Cem.*

- Concr. Res. 34 (2004) 1489–1498. doi:10.1016/J.CEMCONRES.2004.01.021.
- [68] J.S.J. Van Deventer, J.L. Provis, P. Duxson, Technical and commercial progress in the adoption of geopolymer cement, *Miner. Eng.* 29 (2012) 89–104. doi:10.1016/J.MINENG.2011.09.009.
- [69] L. Coppola, D. Coffetti, E. Crotti, Pre-packed alkali activated cement-free mortars for repair of existing masonry buildings and concrete structures, *Constr. Build. Mater.* 173 (2018) 111–117. doi:10.1016/j.conbuildmat.2018.04.034.
- [70] K. Caldeira, M.E. Wickett, Anthropogenic carbon and ocean pH, *Nature.* 425 (2003) 365. doi:10.1038/425365a.
- [71] S. Solomon, G.-K. Plattner, R. Knutti, P. Friedlingstein, Irreversible climate change due to carbon dioxide emissions, *Proc. Natl. Acad. Sci.* 106 (2009) 1704–1709. doi:10.1073/pnas.0812721106.
- [72] National Centers for Environmental Information - National Oceanic and Atmosphere Administration Of USA, *Climate Monitoring Data*, (2021).
- [73] World Economic Forum, *The Global Risks Report 2020*, 2020.
- [74] Swiss Re Institute, *Natural catastrophes and man-made disasters in 2018: “secondary” perils on the frontline*, 2019.
- [75] M. Coronese, F. Lamperti, K. Keller, F. Chiaromonte, A. Roventini, Evidence for sharp increase in the economic damages of extreme natural disasters, *Proc. Natl. Acad. Sci. U. S. A.* 116 (2019) 21450–21455. doi:10.1073/pnas.1907826116.
- [76] National Climate Assessment, *Fourth National Climate Assessment, Volume II: Impacts, risks and adaptation in the United States*, 2018.
- [77] D. Le Bars, S. Drijfhout, H. De Vries, A high-end sea level rise probabilistic projection including rapid Antarctic ice sheet mass loss, *Environ. Res. Lett.* 12 (2017). doi:10.1088/1748-9326/aa6512.
- [78] T. Frederikse, M.K. Buchanan, E. Lambert, R.E. Kopp, M. Oppenheimer, D.J. Rasmussen, R.S.W. van de Wal, Antarctic Ice Sheet and emission scenario controls

- on 21st-century extreme sea-level changes, *Nat. Commun.* 11 (2020) 1–11. doi:10.1038/s41467-019-14049-6.
- [79] T. Slater, I.R. Lawrence, I.N. Ootosaka, A. Shepherd, N. Gourmelen, L. Jakob, P. Tepes, L. Gilbert, Review Article: Earth’s ice imbalance, *Cryosph. Discuss.* (2020) 1–21.
- [80] S.A. Kulp, B.H. Strauss, New elevation data triple estimates of global vulnerability to sea-level rise and coastal flooding, *Nat. Commun.* 10 (2019). doi:10.1038/s41467-019-12808-z.
- [81] H. Yang, G. Lohmann, W. Wei, M. Dima, M. Ionita, J. Liu, Intensification and poleward shift of subtropical western boundary currents in a warming climate, *J. Geophys. Res. Ocean.* 121 (2016) 4928–2945. doi:10.1002/2015JC011513.
- [82] J.C. Bowen, C.P. Ward, G.W. Kling, R.M. Cory, Arctic Amplification of Global Warming Strengthened by Sunlight Oxidation of Permafrost Carbon to CO₂, *Geophys. Res. Lett.* 47 (2020) 1–8. doi:10.1029/2020GL087085.
- [83] C. Plaza, E. Pegoraro, R. Bracho, G. Celis, K.G. Crummer, J.A. Hutchings, C.E. Hicks Pries, M. Mauritz, S.M. Natali, V.G. Salmon, C. Schädel, E.E. Webb, E.A.G. Schuur, Direct observation of permafrost degradation and rapid soil carbon loss in tundra, *Nat. Geosci.* 12 (2019) 627–631. doi:10.1038/s41561-019-0387-6.
- [84] The Intergovernmental Panel On Climate Change (IPCC) - United Nations, IPCC Special Report, 2018.
- [85] United Nations Environment Programme, Emission Gap Report 2019, 2019.
- [86] R. McSweeney, R. Pearce, Analysis: Just four years left of the 1.5C carbon budget, *Carbon Br.* (2017).
- [87] Global Alliance For Buildings And Construction - United Nations Environment Programme, 2020 Global Status Report For Buildings And Construction, 2020.
- [88] United Nations - Department of Economic And Social Affairs - Population Division, World Population Prospect 2019, 2019.

- [89] United Nations - Department of Economic And Social Affairs - Population Division, World Urbanization Prospect 2018, 2019.
- [90] U.S. Geological Survey, U.S. Department of Interior, Mineral Commodity Summaries 2020, 2020.
- [91] A. Sivakrishna, A. Adesina, P.O. Awoyera, K. Rajesh Kumar, Green concrete: A review of recent developments, *Mater. Today Proc.* 27 (2020) 54–58. doi:<https://doi.org/10.1016/j.matpr.2019.08.202>.
- [92] Organization for Economic and Co-operation and Development (OECD), Global Material Resources Outlook to 2060, 2018.
- [93] N. Cadavid-Giraldo, M.C. Velez-Gallego, A. Restrepo-Boland, Carbon emissions reduction and financial effects of a cap and tax system on an operating supply chain in the cement sector, *J. Clean. Prod.* 275 (2020). doi:[10.1016/j.jclepro.2020.122583](https://doi.org/10.1016/j.jclepro.2020.122583).
- [94] Global Carbon Project, CO2 emissions by country - 2019, (2020).
- [95] International Energy Agency (IEA), Cement, 2020.
- [96] P.J.M. Monteiro, S.A. Miller, A. Horvath, Towards sustainable concrete, *Nat. Mater.* 16 (2017) 698–699. doi:[10.1038/nmat4930](https://doi.org/10.1038/nmat4930).
- [97] U.S. Energy Information Administration (EIA), U.S. Energy Facts Explained, (2020).
- [98] L. Coppola, D. Coffetti, E. Crotti, G. Gazzaniga, T. Pastore, An Empathetic Added Sustainability Index (EASI) for cementitious based construction materials, *J. Clean. Prod.* 220 (2019) 475–482. doi:[10.1016/j.jclepro.2019.02.160](https://doi.org/10.1016/j.jclepro.2019.02.160).
- [99] E. Gartner, H. Hirao, A review of alternative approaches to the reduction of CO2 emissions associated with the manufacture of the binder phase in concrete, *Cem. Concr. Res.* 78 (2015) 126–142. doi:[10.1016/j.cemconres.2015.04.012](https://doi.org/10.1016/j.cemconres.2015.04.012).
- [100] J. de Brito, R. Kurda, The past and future of sustainable concrete: A critical review and new strategies on cement-based materials, *J. Clean. Prod.* (2020) 123558.

doi:10.1016/j.jclepro.2020.123558.

- [101] A. Hasanbeigi, L. Price, E. Lin, Emerging energy-efficiency and CO₂emission-reduction technologies for cement and concrete production: A technical review, *Renew. Sustain. Energy Rev.* 16 (2012) 6220–6238. doi:10.1016/j.rser.2012.07.019.
- [102] D. Coffetti, E. Crotti, G. Gazzaniga, M. Carrara, T. Pastore, L. Coppola, Pathways towards sustainable concrete, *Cem. Concr. Res.* 154 (2022) 106718. doi:10.1016/j.cemconres.2022.106718.
- [103] B. Han, L. Zhang, J. Ou, Smart and multifunctional concrete toward sustainable infrastructures, 2017. doi:10.1007/978-981-10-4349-9.
- [104] N. Makul, Advanced smart concrete - A review of current progress, benefits and challenges, *J. Clean. Prod.* 274 (2020) 122899. doi:10.1016/j.jclepro.2020.122899.
- [105] B. Han, Y. Wang, S. Dong, L. Zhang, S. Ding, X. Yu, J. Ou, Smart concretes and structures: A review, *J. Intell. Mater. Syst. Struct.* 26 (2015) 1303–1345. doi:10.1177/1045389X15586452.
- [106] P.N. Reddy, Structural health monitoring methods, dispersion of fibers, micro and macro structural properties, sensing, and mechanical properties of self-sensing concrete—A review, *Struct. Concr. J. FIB.* 22 (2021) 793–805.
- [107] H.V. Le, M.K. Kim, S.U. Kim, S.-Y. Chung, D.J. Kim, Enhancing self-stress sensing ability of smart ultra-high performance concretes under compression by using nano functional fillers, *J. Build. Eng.* 44 (2021) 102717. doi:10.1016/j.jobbe.2021.102717.
- [108] P.M. Carmona-Quiroga, S. Martínez-Ramírez, H.A. Viles, Efficiency and durability of a self-cleaning coating on concrete and stones under both natural and artificial ageing trials, *Appl. Surf. Sci.* 433 (2018) 312–320. doi:10.1016/j.apsusc.2017.10.052.
- [109] H. Dikkar, V. Kapre, A. Diwan, S.K. Sekar, Titanium dioxide as a photocatalyst to create self-cleaning concrete, *Mater. Today Proc.* 45 (2020) 4058–4062.

doi:10.1016/j.matpr.2020.10.948.

- [110] W. Zhang, Q. Zheng, A. Ashour, B. Han, Self-healing cement concrete composites for resilient infrastructures: A review, *Compos. Part B Eng.* 189 (2020) 107892. doi:10.1016/j.compositesb.2020.107892.
- [111] P. Kumar Jogi, T.V.S. Vara Lakshmi, Self healing concrete based on different bacteria: A review, *Mater. Today Proc.* 43 (2021) 1246–1252. doi:10.1016/j.matpr.2020.08.765.
- [112] C. Qian, T. Zheng, X. Zhang, Y. Su, Application of microbial self-healing concrete: Case study, *Constr. Build. Mater.* 290 (2021) 123226. doi:10.1016/j.conbuildmat.2021.123226.
- [113] D. Satyanarayana, R. Padmapriya, Performance of photocatalytic concrete blended with M-Sand, POFA and Titanium Dioxide, *Mater. Today Proc.* 44 (2021) 4919–4923. doi:10.1016/j.matpr.2020.11.949.
- [114] M. Somasri, B. Narendra Kumar, Graphene oxide as Nano material in high strength self-compacting concrete, *Mater. Today Proc.* 43 (2021) 2280–2289. doi:10.1016/j.matpr.2020.12.1085.
- [115] K.-S. Lauch, C. Desmettre, J.-P. Charron, New water permeability set-up and factors affecting concrete self-healing, *Constr. Build. Mater.* 294 (2021) 123595. doi:10.1016/j.conbuildmat.2021.123595.
- [116] A. Arabzadeh, M.A. Notani, A. Kazemiyan Zadeh, A. Nahvi, A. Sassani, H. Ceylan, Electrically conductive asphalt concrete: An alternative for automating the winter maintenance operations of transportation infrastructure, *Compos. Part B Eng.* 173 (2019) 106985. doi:10.1016/j.compositesb.2019.106985.
- [117] W. Schmidt, M. Alexander, V. John, Education for sustainable use of cement based materials, *Cem. Concr. Res.* 114 (2018) 103–114. doi:10.1016/j.cemconres.2017.08.009.
- [118] L. Coppola, D. Coffetti, E. Crotti, G. Gazzaniga, T. Pastore, The durability of one-part alkali activated slag-based mortars in different environments, *Sustainability*.

12 (2020) 3561.

- [119] F. Pacheco-Torgal, Z. Abdollahnejad, A.F. Camões, M. Jamshidi, Y. Ding, Durability of alkali-activated binders: A clear advantage over Portland cement or an unproven issue?, *Constr. Build. Mater.* 30 (2012) 400–405. doi:10.1016/J.CONBUILDMAT.2011.12.017.
- [120] F. Shahrajabian, K. Behfarnia, The effects of nano particles on freeze and thaw resistance of alkali-activated slag concrete, *Constr. Build. Mater.* 176 (2018) 172–178. doi:10.1016/j.conbuildmat.2018.05.033.
- [121] H. Tan, X. Deng, X. He, J. Zhang, X. Zhang, Y. Su, J. Yang, Compressive strength and hydration process of wet-grinded granulated blast-furnace slag activated by sodium sulfate and sodium carbonate, *Cem. Concr. Compos.* 97 (2019) 387–398. doi:10.1016/J.CEMCONCOMP.2019.01.012.
- [122] F. Shahrajabian, K. Behfarnia, The effects of nano particles on freeze and thaw resistance of alkali-activated slag concrete, *Constr. Build. Mater.* 176 (2018) 172–178. doi:10.1016/J.CONBUILDMAT.2018.05.033.
- [123] Y. Fu, L. Cai, W. Yonggen, Freeze-thaw cycle test and damage mechanics models of alkali-activated slag concrete, *Constr. Build. Mater.* 25 (2011) 3144–3148. doi:10.1016/j.conbuildmat.2010.12.006.
- [124] L. Cai, H. Wang, Y. Fu, Freeze-thaw resistance of alkali-slag concrete based on response surface methodology, *Constr. Build. Mater.* 49 (2013) 70–76. doi:10.1016/j.conbuildmat.2013.07.045.
- [125] V. Elfmarkova, P. Spiesz, H.J.H. Brouwers, Determination of the chloride diffusion coefficient in blended cement mortars, *Cem. Concr. Res.* 78 (2015) 190–199. doi:10.1016/J.CEMCONRES.2015.06.014.
- [126] P. Awoyera, A. Adesina, Durability Properties of Alkali Activated Slag Composites: Short Overview, (n.d.). doi:10.1007/s12633-019-00199-1.
- [127] M. Criado, J.L. Provis, Alkali Activated Slag Mortars Provide High Resistance to Chloride-Induced Corrosion of Steel, *Front. Mater.* 0 (2018) 34.

doi:10.3389/FMATS.2018.00034.

- [128] Q. Ma, S. V. Nanukuttan, P.A.M. Basheer, Y. Bai, C. Yang, Chloride transport and the resulting corrosion of steel bars in alkali activated slag concretes, *Mater. Struct.* 2015 499. 49 (2015) 3663–3677. doi:10.1617/S11527-015-0747-7.
- [129] D. Bondar, Q. Ma, M. Soutsos, M. Basheer, J.L. Provis, S. Nanukuttan, Alkali activated slag concretes designed for a desired slump, strength and chloride diffusivity, *Constr. Build. Mater.* 190 (2018) 191–199. doi:10.1016/J.CONBUILDMAT.2018.09.124.
- [130] I. Ismail, S.A. Bernal, J.L. Provis, R. San Nicolas, D.G. Brice, A.R. Kilcullen, S. Hamdan, J.S.J. Van Deventer, Influence of fly ash on the water and chloride permeability of alkali-activated slag mortars and concretes, *Constr. Build. Mater.* 48 (2013) 1187–1201. doi:10.1016/j.conbuildmat.2013.07.106.
- [131] T. Bakharev, J.G. Sanjayan, Y.B. Cheng, Sulfate attack on alkali-activated slag concrete, *Cem. Concr. Res.* 32 (2002) 211–216. doi:10.1016/S0008-8846(01)00659-7.
- [132] A.M. Neville, *Properties of concrete*, Longman London, 1995.
- [133] I. Ismail, S.A. Bernal, J.L. Provis, S. Hamdan, J.S.J. Van Deventer, Microstructural changes in alkali activated fly ash/slag geopolymers with sulfate exposure, *Mater. Struct. Constr.* 46 (2013) 361–373. doi:10.1617/s11527-012-9906-2.
- [134] S.A. Bernal, J.L. Provis, B. Walkley, R. San Nicolas, J.D. Gehman, D.G. Brice, A.R. Kilcullen, P. Duxson, J.S.J. Van Deventer, Gel nanostructure in alkali-activated binders based on slag and fly ash, and effects of accelerated carbonation, *Cem. Concr. Res.* 53 (2013) 127–144. doi:10.1016/J.CEMCONRES.2013.06.007.
- [135] J. He, Q. Gao, Y. Wu, J. He, X. Pu, Study on improvement of carbonation resistance of alkali-activated slag concrete, *Constr. Build. Mater.* 176 (2018) 60–67. doi:10.1016/J.CONBUILDMAT.2018.04.117.
- [136] F. Puertas, M. Palacios, T. Vázquez, Carbonation process of alkali-activated slag mortars, *J. Mater. Sci.* 41 (2006) 3071–3082. doi:10.1007/s10853-005-1821-2.

- [137] H. Ye, R. Cai, Z. Tian, Natural carbonation-induced phase and molecular evolution of alkali-activated slag: Effect of activator composition and curing temperature, *Constr. Build. Mater.* 248 (2020) 118726. doi:10.1016/J.CONBUILDMAT.2020.118726.
- [138] T. Bakharev, J.G. Sanjayan, Y.-B. Cheng, Resistance of alkali-activated slag concrete to carbonation, (n.d.).
- [139] S.A. Bernal, R. San Nicolas, J.L. Provis, R. Mejía De Gutiérrez, J.S.J. Van Deventer, Natural carbonation of aged alkali-activated slag concretes, *Mater. Struct. Constr.* 47 (2014) 693–707. doi:10.1617/s11527-013-0089-2.
- [140] A. Mellado, M.I. Pérez-Ramos, J. Monzó, M.V. Borrachero, J. Payá, Resistance to acid attack of alkali-activated binders: Simple new techniques to measure susceptibility, *Constr. Build. Mater.* 150 (2017) 355–366. doi:10.1016/J.CONBUILDMAT.2017.05.224.
- [141] S.A. Bernal, E.D. Rodríguez, R.M. de Gutiérrez, J.L. Provis, Performance of alkali-activated slag mortars exposed to acids, [Http://Dx.Doi.Org/10.1080/21650373.2012.747235](http://dx.doi.org/10.1080/21650373.2012.747235). 1 (2012) 138–151. doi:10.1080/21650373.2012.747235.
- [142] D.C.C. Joseph Davidovits John H. Paterson, Douglas J. Ritcey, Geopolymeric concretes For Environmental Protection, *Concr. Int.* 12 (n.d.).
- [143] B.M. Mithun, M.C. Narasimhan, Performance of alkali activated slag concrete mixes incorporating copper slag as fine aggregate, *J. Clean. Prod.* 112 (2016) 837–844. doi:10.1016/J.JCLEPRO.2015.06.026.
- [144] C. Shi, Strength, pore structure and permeability of alkali-activated slag mortars, *Cem. Concr. Res.* 26 (1996) 1789–1799. doi:10.1016/S0008-8846(96)00174-3.
- [145] Z. Sun, X. Lin, A. Vollpracht, Pervious concrete made of alkali activated slag and geopolymers, *Constr. Build. Mater.* 189 (2018) 797–803. doi:10.1016/J.CONBUILDMAT.2018.09.067.
- [146] S.A. Bernal, R. Mejía de Gutiérrez, A.L. Pedraza, J.L. Provis, E.D. Rodriguez, S.

- Delvasto, Effect of binder content on the performance of alkali-activated slag concretes, *Cem. Concr. Res.* 41 (2011) 1–8.
- [147] M. Rostami, K. Behfarnia, The effect of silica fume on durability of alkali activated slag concrete, *Constr. Build. Mater.* 134 (2017) 262–268. doi:10.1016/J.CONBUILDMAT.2016.12.072.
- [148] E. Rodríguez, S. Bernal, R.M. de Gutiérrez, F. Puertas, Alternative concrete based on alkali-activated slag, *Mater. Construcción.* 58 (2008) 53–67. doi:10.3989/MC.2008.V58.I291.104.
- [149] P. Shoaie, P. Ghassemi, F. Ameri, H.R. Musaei, C. Chee Ban, T. Ozbakkaloglu, Comparative study on the effect of fiber type and content on the fire resistance of alkali-activated slag composites, *Constr. Build. Mater.* 288 (2021) 123136. doi:10.1016/J.CONBUILDMAT.2021.123136.
- [150] R. Cai, H. Ye, Clinkerless ultra-high strength concrete based on alkali-activated slag at high temperatures, *Cem. Concr. Res.* 145 (2021) 106465. doi:10.1016/J.CEMCONRES.2021.106465.
- [151] R. Mejía de Gutiérrez, J. Maldonado, C. Gutiérrez, Resistencia a temperaturas elevadas de escorias activadas alcalinamente, *Mater. Construcción.* 54 (2004) 87–92. doi:10.3989/mc.2004.v54.i276.257.
- [152] M. Guerrieri, J. Sanjayan, F. Collins, Residual strength properties of sodium silicate alkali activated slag paste exposed to elevated temperatures, *Mater. Struct.* 43 (2010) 765–773. doi:10.1617/s11527-009-9546-3.
- [153] M. Mastali, A. Alzaza, K.M. Shaad, P. Kinnunen, Z. Abdollahnejad, B. Woof, M. Illikainen, Using Carbonated BOF Slag Aggregates in Alkali-Activated Concretes, *Mater.* 2019, Vol. 12, Page 1288. 12 (2019) 1288. doi:10.3390/MA12081288.
- [154] C. Shi, Z. Shi, X. Hu, R. Zhao, L. Chong, A review on alkali-aggregate reactions in alkali-activated mortars/concretes made with alkali-reactive aggregates, *Mater. Struct.* 2014 483. 48 (2015) 621–628. doi:10.1617/S11527-014-0505-2.
- [155] S. Al-Otaibi, Durability of concrete incorporating GGBS activated by water-glass,

- Constr. Build. Mater. 22 (2008) 2059–2067.
doi:10.1016/J.CONBUILDMAT.2007.07.023.
- [156] C. You-zhi, P. Xin-cheng, Y. Chang-hui, D. Qing-jun, Alkali aggregate reaction in alkali slag cement mortars, *J. Wuhan Univ. Technol. Sci. Ed.* 2002 173. 17 (2002) 60–62. doi:10.1007/BF02838542.
- [157] Z. Shi, C. Shi, S. Wan, Z. Ou, Effect of alkali dosage on alkali-silica reaction in sodium hydroxide activated slag mortars, *Constr. Build. Mater.* 143 (2017) 16–23. doi:10.1016/J.CONBUILDMAT.2017.03.125.
- [158] L. Coppola, D. Coffetti, E. Crotti, A. Marini, C. Passoni, T. Pastore, Lightweight cement-free alkali-activated slag plaster for the structural retrofit and energy upgrading of poor quality masonry walls, *Cem. Concr. Compos.* 104 (2019) 103341. doi:10.1016/j.cemconcomp.2019.103341.
- [159] A. Allahverdi, E. Najafi Kani, S. Esmailpoor, Effects of Silica Modulus and Alkali Concentration on Activation of Blast-Furnace Slag, *Iran. J. Mater. Sci. Eng.* 5 (2008) 32–35.
- [160] R. Bayuaji, A.K. Yasin, T.E. Susanto, M.S. Darmawan, S. Darmawan, A review in geopolymers binder with dry mixing method (geopolymer cement), *AIP Conf. Proc.* 1887 (2017) 20042. doi:10.1063/1.5003513.
- [161] L. Coppola, D. Coffetti, E. Crotti, S. Candamano, F. Crea, G. Gazzaniga, T. Pastore, The combined use of admixtures for shrinkage reduction in one-part alkali activated slag-based mortars and pastes, *Constr. Build. Mater.* 248 (2020). doi:10.1016/j.conbuildmat.2020.118682.
- [162] C. Qiao, P. Suraneni, J. Weiss, Phase diagram and volume change of the $\text{Ca}(\text{OH})_2$ - CaCl_2 - H_2O system for varying $\text{Ca}(\text{OH})_2/\text{CaCl}_2$ molar ratios, *J. Mater. Civ. Eng.* 30 (2018). doi:10.1061/(ASCE)MT.1943-5533.0002145.
- [163] L. Coppola, D. Coffetti, E. Crotti, One-Part Alkali-Activated Slag Cement for Conservation of Existing Structures, *ACI Spec. Publ.* 330 (2018) 107–122.
- [164] D. Coffetti, Alternative binders as milestone of 3R strategy for sustainable

- construction materials, PhD Thesis, University of Bergamo, 2019.
doi:10.13140/RG.2.2.26173.31201.
- [165] H. Ye, C. Cartwright, F. Rajabipour, A. Radlińska, Understanding the drying shrinkage performance of alkali-activated slag mortars, *Cem. Concr. Compos.* 76 (2017) 13–24.
- [166] H. Ye, A. Radlińska, Shrinkage mechanisms of alkali-activated slag, (2016).
doi:10.1016/j.cemconres.2016.07.001.
- [167] I. Galan, L. Perron, F.P. Glasser, Impact of chloride-rich environments on cement paste mineralogy, *Cem. Concr. Res.* 68 (2015) 174–183.
doi:10.1016/j.cemconres.2014.10.017.
- [168] R.J. Myers, S.A. Bernal, J.L. Provis, Phase diagrams for alkali-activated slag binders, *Cem. Concr. Res.* 95 (2017) 30–38.
doi:10.1016/j.cemconres.2017.02.006.
- [169] R.J. Myers, B. Lothenbach, S.A. Bernal, J.L. Provis, Thermodynamic modelling of alkali-activated slag cements, *Appl. Geochemistry.* 61 (2015) 233–247.
doi:10.1016/j.apgeochem.2015.06.006.
- [170] D.W. Law, A.A. Adam, T.K. Molyneaux, I. Patnaikuni, Durability assessment of alkali activated slag (AAS) concrete, *Mater. Struct. Constr.* 45 (2012) 1425–1437.
doi:10.1617/s11527-012-9842-1.
- [171] A. Steffens, D. Dinkler, H. Ahrens, Modeling carbonation for corrosion risk prediction of concrete structures, *Cem. Concr. Res.* 32 (2002) 935–941.
doi:10.1016/S0008-8846(02)00728-7.
- [172] Z. Shi, C. Shi, S. Wan, N. Li, Z. Zhang, Effect of alkali dosage and silicate modulus on carbonation of alkali-activated slag mortars, *Cem. Concr. Res.* 113 (2018) 55–64. doi:10.1016/j.cemconres.2018.07.005.
- [173] N. Li, N. Farzadnia, C. Shi, Microstructural changes in alkali-activated slag mortars induced by accelerated carbonation, *Cem. Concr. Res.* 100 (2017) 214–226. doi:10.1016/j.cemconres.2017.07.008.

- [174] M. Castellote, C. Andrade, X. Turrillas, J. Campo, G.J. Cuello, Accelerated carbonation of cement pastes in situ monitored by neutron diffraction, *Cem. Concr. Res.* 38 (2008) 1365–1373.
- [175] H.W. Song, S.J. Kwon, Permeability characteristics of carbonated concrete considering capillary pore structure, *Cem. Concr. Res.* 37 (2007) 909–915.
- [176] S.A. Bernal, R.M. de Gutierrez, J.L. Provis, V. Rose, Effect of silicate modulus and metakaolin incorporation on the carbonation of alkali silicate-activated slags, *Cem. Concr. Res.* 40 (2010) 898–907. doi:10.1016/j.cemconres.2010.02.003.
- [177] N. Li, N. Farzadnia, C. Shi, Microstructural changes in alkali-activated slag mortars induced by accelerated carbonation, *Cem. Concr. Res.* 100 (2017) 214–226. doi:10.1016/J.CEMCONRES.2017.07.008.
- [178] K. Il Song, J.K. Song, B.Y. Lee, K.H. Yang, Carbonation characteristics of alkali-activated blast-furnace slag mortar, *Adv. Mater. Sci. Eng.* 2014 (2014). doi:10.1155/2014/326458.
- [179] F. Matalkah, T. Salem, P. Soroushian, Acid resistance and corrosion protection potential of concrete prepared with alkali aluminosilicate cement, *J. Build. Eng.* 20 (2018) 705–711. doi:10.1016/J.JOBE.2018.08.001.
- [180] T. Bakharev, J.G. Sanjayan, Y.B. Cheng, Resistance of alkali-activated slag concrete to acid attack, *Cem. Concr. Res.* 33 (2003) 1607–1611. doi:10.1016/S0008-8846(03)00125-X.
- [181] N.K. Lee, H.K. Lee, Influence of the slag content on the chloride and sulfuric acid resistances of alkali-activated fly ash/slag paste, *Cem. Concr. Compos.* 72 (2016) 168–179. doi:10.1016/J.CEMCONCOMP.2016.06.004.
- [182] N. De Belie, J. Monteny, A. Beeldens, E. Vincke, D. Van Gemert, W. Verstraete, Experimental research and prediction of the effect of chemical and biogenic sulfuric acid on different types of commercially produced concrete sewer pipes, *Cem. Concr. Res.* 34 (2004) 2223–2236. doi:10.1016/J.CEMCONRES.2004.02.015.

- [183] L. Gu, T. Bennett, P. Visintin, Sulphuric acid exposure of conventional concrete and alkali-activated concrete: Assessment of test methodologies, *Constr. Build. Mater.* 197 (2019) 681–692. doi:10.1016/J.CONBUILDMAT.2018.11.166.
- [184] R.R. Lloyd, J.L. Provis, J.S.J. van Deventer, Acid resistance of inorganic polymer binders. 1. Corrosion rate, *Mater. Struct.* 2011 451. 45 (2011) 1–14. doi:10.1617/S11527-011-9744-7.
- [185] T.A. Aiken, J. Kwasny, W. Sha, M.N. Soutsos, Effect of slag content and activator dosage on the resistance of fly ash geopolymer binders to sulfuric acid attack, *Cem. Concr. Res.* 111 (2018) 23–40. doi:10.1016/J.CEMCONRES.2018.06.011.
- [186] S.A. Bernal, R. Mejía De Gutiérrez, J.L. Provis, Engineering and durability properties of concretes based on alkali-activated granulated blast furnace slag/metakaolin blends, *Constr. Build. Mater.* 33 (2012) 99–108. doi:10.1016/J.CONBUILDMAT.2012.01.017.
- [187] I. Ismail, S.A. Bernal, J.L. Provis, R. San Nicolas, D.G. Brice, A.R. Kilcullen, S. Hamdan, J.S.J. Van Deventer, Influence of fly ash on the water and chloride permeability of alkali-activated slag mortars and concretes, *Constr. Build. Mater.* 48 (2013) 1187–1201. doi:10.1016/J.CONBUILDMAT.2013.07.106.
- [188] I. Ismail, S.A. Bernal, J.L. Provis, S. Hamdan, J.S.J. van Deventer, Drying-induced changes in the structure of alkali-activated pastes, *J. Mater. Sci.* 2013 489. 48 (2013) 3566–3577. doi:10.1007/S10853-013-7152-9.
- [189] S. Aydin, B. Baradan, Effect of activator type and content on properties of alkali-activated slag mortars, *Compos. Part B Eng.* 57 (2014) 166–172. doi:10.1016/J.COMPOSITESB.2013.10.001.
- [190] S. Andrejkovičová, C. Alves, A. Velosa, F. Rocha, Bentonite as a natural additive for lime and lime–metakaolin mortars used for restoration of adobe buildings, *Cem. Concr. Compos.* 60 (2015) 99–110. doi:10.1016/J.CEMCONCOMP.2015.04.005.
- [191] M. Shuller, R. Atkinson, J. Noland, Structural evaluation of historic masonry

- buildings, *APT Bull. J. Preserv. Technol.* 26 (1995) 51–61.
- [192] L. Binda, A. Saisi, C. Tiraboschi, Investigation procedures for the diagnosis of historic masonries, *Constr. Build. Mater.* 14 (2000) 199–233. doi:10.1016/S0950-0618(00)00018-0.
- [193] A. Borri, M. Corradi, G. Castori, A. De Maria, A method for the analysis and classification of historic masonry, *Bull. Earthq. Eng.* 13 (2015) 2647–2665. doi:10.1007/s10518-015-9731-4.
- [194] M.R. Valluzzi, F. Da Porto, C. Modena, Behavior and modeling of strengthened three-leaf stone masonry walls, *Mater. Struct. Constr.* 37 (2004) 184–192. doi:10.1617/13977.
- [195] P.B. Lourenço, N. Mendes, L.F. Ramos, D. V. Oliveira, Analysis of masonry structures without box behavior, *Int. J. Archit. Herit.* 5 (2011) 369–382. doi:10.1080/15583058.2010.528824.
- [196] M. Rota, A. Penna, G. Magenes, A framework for the seismic assessment of existing masonry buildings accounting for different sources of uncertainty, *Earthq. Eng. Struct. Dyn.* 43 (2014) 1045–1066. doi:10.1002/eqe.2386.
- [197] B. Silva, A.E. Pigouni, M.R. Valluzzi, C. Modena, Calibration of analytical formulations predicting compressive strength in consolidated three-leaf masonry walls, *Constr. Build. Mater.* 64 (2014) 28–38. doi:10.1016/j.conbuildmat.2014.04.044.
- [198] A. Avorio, A. Borri, G. Cangi, Riparazione e consolidamento degli edifici in muratura, in: *Man. per La Riabil. e La Ricostr. Post Sismica Degli Edif.*, DEI editio, Rome, 1999.
- [199] E. Giuriani, A. Marini, Experiences from the Northern Italy 2004 earthquake: vulnerability assessment and strengthening of historic churches, in: *Proc. VI Int. Conf. Struct. Anal. Hist. Constr. SAHC - Bath*, 2008: pp. 13–24.
- [200] E.P. Giuriani, A. Marini, M. Preti, Thin-folded Shell for the Renewal of Existing Wooden Roofs, *Int. J. Archit. Herit.* 10 (2016) 797–816.

doi:10.1080/15583058.2015.1075626.

- [201] L. Ferrario, A. Marini, P. Riva, E. Giuriani, Traditional and innovative techniques for the seismic strengthening of barrel vaulted structures subjected to rocking of the abutments, in: Proc. ATC-SEI Conf. Improv. Seism. Perform. Exist. Build. Other Struct. - San Fr., American Society of Civil Engineers, Reston, VA, 2009. doi:10.1061/41084(364)122.
- [202] M. Corradi, A. Borri, G. Castori, R. Sisti, Shear strengthening of wall panels through jacketing with cement mortar reinforced by GFRP grids, Compos. Part B Eng. 64 (2014) 33–42. doi:10.1016/j.compositesb.2014.03.022.
- [203] S. Cominelli, E. Giuriani, A. Marini, Mechanisms governing the compressive strength of unconfined and confined rubble stone masonry, Mater. Struct. Constr. 50 (2017) 10. doi:10.1617/s11527-016-0905-6.
- [204] A. Borri, M. Corradi, R. Sisti, C. Buratti, E. Belloni, E. Moretti, Masonry wall panels retrofitted with thermal-insulating GFRP-reinforced jacketing, Mater. Struct. Constr. 49 (2016) 3957–3968. doi:10.1617/s11527-015-0766-4.
- [205] M.R. Veiga, A.L. Velosa, A.C. Magalhães, Evaluation of mechanical compatibility of renders to apply on old walls based on a restrained shrinkage test, Mater. Struct. 2006 4010. 40 (2006) 1115–1126. doi:10.1617/S11527-006-9209-6.
- [206] M.T. Freire, M. do R. Veiga, A. Santos Silva, J. de Brito, Restoration of ancient gypsum-based plasters: Design of compatible materials, Cem. Concr. Compos. 120 (2021) 104014. doi:10.1016/J.CEMCONCOMP.2021.104014.
- [207] R. Veiga, Air lime mortars: What else do we need to know to apply them in conservation and rehabilitation interventions? A review, Constr. Build. Mater. 157 (2017) 132–140. doi:10.1016/J.CONBUILDMAT.2017.09.080.
- [208] A. Isebaert, L. Van Parys, V. Cnudde, Composition and compatibility requirements of mineral repair mortars for stone – A review, Constr. Build. Mater. 59 (2014) 39–50. doi:10.1016/J.CONBUILDMAT.2014.02.020.
- [209] L. Schueremans, Ö. Cizer, E. Janssens, G. Serré, K. Van Balen, Characterization

- of repair mortars for the assessment of their compatibility in restoration projects: Research and practice, *Constr. Build. Mater.* 25 (2011) 4338–4350. doi:10.1016/J.CONBUILDMAT.2011.01.008.
- [210] Y. Wang, Y. Cao, Y. Ma, S. Xiao, J. Hu, H. Wang, Fresh and hardened properties of alkali-activated fly ash/slag binders: effect of fly ash source, surface area, and additives, <https://doi.org/10.1080/21650373.2021.1932637>. (2021). doi:10.1080/21650373.2021.1932637.
- [211] M. Almakhadmeh, A.M. Soliman, Effects of mixing water temperatures on properties of one-part alkali-activated slag paste, *Constr. Build. Mater.* 266 (2021) 121030. doi:10.1016/J.CONBUILDMAT.2020.121030.
- [212] J. Zhang, C. Shi, Z. Zhang, Z. Ou, Durability of alkali-activated materials in aggressive environments: A review on recent studies, *Constr. Build. Mater.* 152 (2017) 598–613.
- [213] R. Narayan Swamy, Dynamic Poisson's ratio of portland cement paste, mortar and concrete, *Cem. Concr. Res.* 1 (1971) 559–583. doi:10.1016/0008-8846(71)90060-3.
- [214] B. Joseph, G. Mathew, Influence of aggregate content on the behavior of fly ash based geopolymer concrete, *Sci. Iran.* 19 (2012) 1188–1194. doi:10.1016/J.SCIENT.2012.07.006.
- [215] R. Arellano-Aguilar, O. Burciaga-Díaz, A. Gorokhovskiy, J.I. Escalante-García, Geopolymer mortars based on a low grade metakaolin: Effects of the chemical composition, temperature and aggregate:binder ratio, *Constr. Build. Mater.* 50 (2014) 642–648. doi:10.1016/J.CONBUILDMAT.2013.10.023.
- [216] W. Chen, Y. Xie, B. Li, B. Li, J. Wang, N. Thom, Role of aggregate and fibre in strength and drying shrinkage of alkali-activated slag mortar, *Constr. Build. Mater.* 299 (2021) 124002. doi:10.1016/J.CONBUILDMAT.2021.124002.
- [217] Y. Alrefaei, J.G. Dai, Tensile behavior and microstructure of hybrid fiber ambient cured one-part engineered geopolymer composites, *Constr. Build. Mater.* 184

- (2018) 419–431. doi:10.1016/J.CONBUILDMAT.2018.07.012.
- [218] B. Nematollahi, J. Sanjayan, J. Qiu, E.H. Yang, High ductile behavior of a polyethylene fiber-reinforced one-part geopolymer composite: A micromechanics-based investigation, *Arch. Civ. Mech. Eng.* 17 (2017) 555–563. doi:10.1016/J.ACME.2016.12.005.
- [219] S.F.A. Shah, B. Chen, S.Y. Oderji, M. Aminul Haque, M.R. Ahmad, Comparative study on the effect of fiber type and content on the performance of one-part alkali-activated mortar, *Constr. Build. Mater.* 243 (2020) 118221. doi:10.1016/J.CONBUILDMAT.2020.118221.
- [220] T. Bakharev, J.G. Sanjayan, Y.B. Cheng, Effect of admixtures on properties of alkali-activated slag concrete, *Cem. Concr. Res.* 30 (2000) 1367–1374.
- [221] Y. Wang, M. Zhou, J. Shan, F. Xu, Y. Yang, Influences of carboxyl methyl cellulose on performances of mortar, *J. Wuhan Univ. Technol. Sci. Ed.* 2007 221. 22 (2007) 108–111. doi:10.1007/S11595-005-1108-0.
- [222] R.J. Thomas, S. Peethamparan, Alkali-activated concrete: Engineering properties and stress–strain behavior, *Constr. Build. Mater.* 93 (2015) 49–56.
- [223] X.H. Yuan, W. Chen, Z.A. Lu, H. Chen, Shrinkage compensation of alkali-activated slag concrete and microstructural analysis, *Constr. Build. Mater.* 66 (2014) 422–428. doi:10.1016/j.conbuildmat.2014.05.085.
- [224] H. Ye, A. Radlińska, Shrinkage mitigation strategies in alkali-activated slag, *Cem. Concr. Res.* 101 (2017) 131–143. doi:10.1016/j.cemconres.2017.08.025.
- [225] N. Ranjbar, M. Mehrli, A. Behnia, A.J. Pordsari, M. Mehrli, U.J. Alengaram, M.Z. Jumaat, A Comprehensive Study of the Polypropylene Fiber Reinforced Fly Ash Based Geopolymer, *PLoS One.* 11 (2016) e0147546. doi:10.1371/JOURNAL.PONE.0147546.
- [226] A.M. Rashad, The effect of polypropylene, polyvinyl-alcohol, carbon and glass fibres on geopolymers properties, <https://doi.org/10.1080/02670836.2018.1514096>. 35 (2018) 127–146.

doi:10.1080/02670836.2018.1514096.

- [227] J. Guo, Z. Yang, C. Gao, Effect of Polypropylene Fiber on Properties of Aeolian-Sand Mortar, *IOP Conf. Ser. Mater. Sci. Eng.* 472 (2019) 012087. doi:10.1088/1757-899X/472/1/012087.
- [228] Y. Xu, H. Chen, P. Wang, Effect of Polypropylene Fiber on Properties of Alkali-Activated Slag Mortar, *Adv. Civ. Eng.* 2020 (2020). doi:10.1155/2020/4752841.
- [229] E. Barrios, D. Fox, Y.Y.L. Sip, R. Catarata, J.E. Calderon, N. Azim, S. Afrin, Z. Zhang, L. Zhai, Nanomaterials in Advanced, High-Performance Aerogel Composites: A Review, *Polym.* 2019, Vol. 11, Page 726. 11 (2019) 726. doi:10.3390/POLYM11040726.
- [230] M.Z. Guo, A. Maury-Ramirez, C.S. Poon, Self-cleaning ability of titanium dioxide clear paint coated architectural mortar and its potential in field application, *J. Clean. Prod.* 112 (2016) 3583–3588. doi:10.1016/j.jclepro.2015.10.079.
- [231] DLGS 264/06, (n.d.).
- [232] C. Ferrari, A. Gholizadeh Touchaei, M. Sleiman, A. Libbra, A. Muscio, C. Siligardi, H. Akbari, Effect of aging processes on solar reflectivity of clay roof tiles, *Adv. Build. Energy Res.* 8 (2014) 28–40. doi:10.1080/17512549.2014.890535.
- [233] A. Zhao, J. Yang, E.H. Yang, Self-cleaning engineered cementitious composites, *Cem. Concr. Compos.* 64 (2015) 74–83. doi:10.1016/j.cemconcomp.2015.09.007.
- [234] A. Fujishima, K. Honda, Electrochemical photolysis of water at a semiconductor electrode, *Nature.* 238 (1972) 37–38. doi:10.1038/238037a0.
- [235] M.V. Diamanti, R. Paolini, M. Rossini, A.B. Aslan, M. Zinzi, T. Poli, M.P. Pedferri, Long term self-cleaning and photocatalytic performance of anatase added mortars exposed to the urban environment, *Constr. Build. Mater.* 96 (2015) 270–278. doi:10.1016/j.conbuildmat.2015.08.028.
- [236] M. V. Diamanti, B. Del Curto, M. Ormellese, M.P. Pedferri, Photocatalytic and

- self-cleaning activity of colored mortars containing TiO₂, *Constr. Build. Mater.* 46 (2013) 167–174. doi:10.1016/j.conbuildmat.2013.04.038.
- [237] A. Folli, C. Pade, T.B. Hansen, T. De Marco, D.E. MacPhee, TiO₂ photocatalysis in cementitious systems: Insights into self-cleaning and depollution chemistry, *Cem. Concr. Res.* 42 (2012) 539–548. doi:10.1016/j.cemconres.2011.12.001.
- [238] E. Jimenez-Relinque, J.R. Rodriguez-Garcia, A. Castillo, M. Castellote, Characteristics and efficiency of photocatalytic cementitious materials: Type of binder, roughness and microstructure, *Cem. Concr. Res.* 71 (2015) 124–131. doi:10.1016/j.cemconres.2015.02.003.
- [239] T. Alomayri, Experimental study of the microstructural and mechanical properties of geopolymer paste with nano material (Al₂O₃), *J. Build. Eng.* 25 (2019) 100788. doi:10.1016/j.jobbe.2019.100788.
- [240] M. Sumesh, U.J. Alengaram, M.Z. Jumaat, K.H. Mo, M.F. Alnahhal, Incorporation of nano-materials in cement composite and geopolymer based paste and mortar – A review, *Constr. Build. Mater.* 148 (2017) 62–84. doi:10.1016/j.conbuildmat.2017.04.206.
- [241] E.A. Llano-Guerrero, L.Y. Gómez-Zamorano, E. Jiménez-Relinque, Effect of the addition of TiO₂ nanoparticles in alkali-activated materials, *Constr. Build. Mater.* 245 (2020) 118370. doi:10.1016/j.conbuildmat.2020.118370.
- [242] J.S. Pozo-Antonio, A. Dionísio, Self-cleaning property of mortars with TiO₂ addition using real diesel exhaust soot, *J. Clean. Prod.* 161 (2017) 850–859. doi:10.1016/J.JCLEPRO.2017.05.202.
- [243] L.Y. Yang, Z.J. Jia, Y.M. Zhang, J.G. Dai, Effects of nano-TiO₂ on strength, shrinkage and microstructure of alkali activated slag pastes, *Cem. Concr. Compos.* 57 (2015) 1–7. doi:10.1016/j.cemconcomp.2014.11.009.
- [244] J. Chen, S.C. Kou, C.S. Poon, Hydration and properties of nano-TiO₂ blended cement composites, *Cem. Concr. Compos.* 34 (2012) 642–649. doi:10.1016/j.cemconcomp.2012.02.009.

- [245] M. Maiti, M. Sarkar, S. Maiti, M.A. Malik, S. Xu, Modification of geopolymer with size controlled TiO₂ nanoparticle for enhanced durability and catalytic dye degradation under UV light, *J. Clean. Prod.* 255 (2020) 120183. doi:10.1016/j.jclepro.2020.120183.
- [246] R. Bayuaji, A.K. Yasin, T.E. Susanto, M.S. Darmawan, A review in geopolymer binder with dry mixing method (geopolymer cement), in: *AIP Conf. Proc.*, American Institute of Physics Inc., 2017: p. 20022. doi:10.1063/1.5003505.
- [247] R. Zhang, X. Cheng, P. Hou, Z. Ye, Influences of nano-TiO₂ on the properties of cement-based materials: Hydration and drying shrinkage, *Constr. Build. Mater.* 81 (2015) 35–41. doi:10.1016/J.CONBUILDMAT.2015.02.003.
- [248] P. Duan, C. Yan, W. Luo, W. Zhou, Effects of adding nano-TiO₂ on compressive strength, drying shrinkage, carbonation and microstructure of fluidized bed fly ash based geopolymer paste, *Constr. Build. Mater.* 106 (2016) 115–125. doi:10.1016/j.conbuildmat.2015.12.095.
- [249] R. Mejía de Gutiérrez, M.A. Villaquirán-Cacedo, L.A. Guzmán-Aponte, Alkali-activated metakaolin mortars using glass waste as fine aggregate: Mechanical and photocatalytic properties, *Constr. Build. Mater.* 235 (2020) 117510. doi:10.1016/J.CONBUILDMAT.2019.117510.
- [250] Q. Zhu, N. Liu, N. Zhang, Y. Song, M.S. Stanislaus, C. Zhao, Y. Yang, Efficient photocatalytic removal of RhB, MO and MB dyes by optimized Ni/NiO/TiO₂ composite thin films under solar light irradiation, *J. Environ. Chem. Eng.* 6 (2018) 2724–2732. doi:10.1016/J.JECE.2018.04.017.
- [251] Y. Yang, X.J. Li, J.T. Chen, L.Y. Wang, Effect of doping mode on the photocatalytic activities of Mo/TiO₂, *J. Photochem. Photobiol. A Chem.* 163 (2004) 517–522. doi:10.1016/J.JPHOTOCHEM.2004.02.008.
- [252] F. Collins, J.G. Sanjayan, Effect of pore size distribution on drying shrinking of alkali-activated slag concrete, *Cem. Concr. Res.* 30 (2000) 1401–1406. doi:10.1016/S0008-8846(00)00327-6.

- [253] Q. Li, K. Yang, C. Yang, An alternative admixture to reduce sorptivity of alkali-activated slag cement by optimising pore structure and introducing hydrophobic film, *Cem. Concr. Compos.* 95 (2019) 183–192. doi:10.1016/J.CEMCONCOMP.2018.11.004.
- [254] A.R. Brough, A. Atkinson, Sodium silicate-based, alkali-activated slag mortars: Part I. Strength, hydration and microstructure, *Cem. Concr. Res.* 32 (2002) 865–879. doi:10.1016/S0008-8846(02)00717-2.
- [255] M. Shariati, A. Shariati, N.T. Trung, P. Shoaie, F. Ameri, N. Bahrami, S.N. Zamanabadi, Alkali-activated slag (AAS) paste: Correlation between durability and microstructural characteristics, *Constr. Build. Mater.* 267 (2021) 120886. doi:10.1016/J.CONBUILDMAT.2020.120886.
- [256] R. Sharma, Gaurav; Bala, Digital color imagining handbook, CRC Press, 2002.
- [257] M. Mahy, L. Van Eycken, A. Oosterlinck, Evaluation of Uniform Color Spaces Developed after the Adoption of CIELAB and CIELUV, *Color Res. Appl.* 19 (1994) 105–121. doi:10.1111/J.1520-6378.1994.TB00070.X.
- [258] B. Sundqvist, T. Morén, H. Als Roh, The influence of wood polymers and extractives on wood colour induced by hydrothermal treatment *Kurz-Originalia AE Brief Originals*, 60 (2002) 375–376. doi:10.1007/s00107-002-0320-2.
- [259] L. Peruchon, E. Puzenat, A. Girard-Egrot, L. Blum, J.M. Herrmann, C. Guillard, Characterization of self-cleaning glasses using Langmuir–Blodgett technique to control thickness of stearic acid multilayers: Importance of spectral emission to define standard test, *J. Photochem. Photobiol. A Chem.* 197 (2008) 170–176. doi:10.1016/J.JPHOTOCHEM.2007.12.033.

ANNEX A

The results reported in this PhD thesis were published in the following (from newest to oldest):

- Coffetti D., Cabrini, Crotti E., Gazzaniga G., Lorenzi S., Pastore T., Coppola L., “Durability of mortars manufactured with low-carbon binders exposed to calcium chloride-based de-icing salts”, *Crystals*, under review;
- Coffetti D., Crotti E., Gazzaniga G., Carrara M., Pastore P., Coppola L., “Pathways towards sustainable concrete”, *Cement Concrete Research*, 154 (2022), 106718;
- D’Alessandro A., Coffetti, D., Crotti E., Coppola L., Meoni A., Ubertini F., “Self-sensing properties of green Alkali-activated binders with carbon-based nanoinclusions”, *Sustainability*, 2020, 12(23), pp 1-13, 9916;
- Coppola L., Coffetti D., Crotti E., Gazzaniga G., Pastore T., “Durability of one-part alkali-activated slag-based mortars in different environments”, *Sustainability*, 2020, 12(9), 3561.

Moreover, the following papers were further published by the author in the field of construction materials (from newest to oldest):

- Coffetti, D., Crotti E., Gazzaniga G., Gottardo R., Pastore T., Coppola L., “Protection of concrete structures: Performance analysis of different commercial products and systems”, *Materials*, 2021, 14(13), 3719;
- Coppola L., Coffetti D., Crotti E., Candamano S., Crea F., Gazzaniga G., Pastore T., “The combined use of admixtures for shrinkage reduction in one-part alkali activated slag-based mortars and pastes”, *Construction and Building Materials*, 2020, 248, 118682;
- Coppola L., Coffetti D., Crotti E., Gazzaniga G., Pastore T., “Chloride diffusion in concrete protected with a silane-based corrosion inhibitor”, *Materials*, 2020, 13(8), 2001;
- Coppola L., Coffetti D., Crotti E., Dell’Aversano R., Gazzaniga G., Pastore T., “Influence of lithium carbonate and sodium carbonate on physical and elastic properties and on carbonation resistance of calcium sulphoaluminate-based

mortars”, *Applied Sciences*, 2020, 10(1), 176;

- Coppola L., Coffetti D., Crotti E., Dell’Aversano R., Gazzaniga G., “The influence of heat and steam curing on the properties of one-part fly ash/slag alkali activated materials: Preliminary results”, *AIP Conference Proceedings*, 2019, 2196, 020038;
- Coppola L., Coffetti D., Crotti E., Marini A., Passoni C., Pastore T., “Lightweight cement-free alkali-activated slag plaster for the structural retrofit and energy upgrading of poor quality masonry walls”, *Cement and Concrete Composites*, 2019, 104, 103341;
- Coppola L., Coffetti D., Crotti E., Gazzaniga G., Pastore T., “An Empathetic Added Sustainability Index (EASI) for cementitious based construction materials”, *Journal of Cleaner Production*, 2019, 2020, pp. 475-482;
- Coppola L., Coffetti D., Crotti E., “An holistic approach to a sustainable future in concrete construction”, *IOP Conference Series: Materials Science and Engineering*, 2018, 442(1), 012024;
- Coppola L., Coffetti D., Crotti E., Pastore T., “CSA-based Portland-free binders to manufacture sustainable concretes for jointless slabs in ground”, *Construction and Building Materials*, 2018, 187, pp. 691-698;
- Coppola L., Crotti E., et al. “Binders alternative to Portland cement and waste management for sustainable construction – Part 2”, *Journal of Applied Biomaterials and Functional Materials*, 2018, 16(4), pp. 207-221;
- Coppola L., Crotti E., et al. “Binders alternative to Portland cement and waste management for sustainable construction – Part 1”, *Journal of Applied Biomaterials and Functional Materials*, 2018, 16(3), pp. 186-202;
- Coppola L., Coffetti D., Crotti E., Forni D., Cadoni E., “Fiber reinforced mortars based on free Portland-CSA binders under high stress rate”, *EPJ Web of Conferences*, 2018, 183, 04013;
- Coppola L., Coffetti D., Crotti E., “Pre-packed alkali-activated cement-free mortars for repair of existing masonry buildings and concrete structures”, *Construction and Building Materials*, 2018, 173, pp. 111-117;
- Coppola L., Coffetti D., Crotti E., “Innovative carboxylic acid waterproofing admixtures for self-sealing watertight concretes”, *Construction and Building Materials*, 2018, 171, pp 817-824;

- Coppola L., Coffetti D., Crotti E., “Use of tartaric acid for the production of sustainable Portland-free CSA-based mortars”, *Construction and Buildings Materials*, 2018, 171, pp. 243-249;
- Coppola L., Coffetti D., Crotti E., “Plain and ultrafine fly ashes for environmentally friendly construction materials”, *Sustainability*, 2018, 10(3), 874;
- Coppola L., Coffetti D., Crotti E., “One-part alkali-activated slag cement for conservation of existing structures”, *ACI Special Publication*, 2018, 330, pp. 107-121;
- Coppola L., Coffetti D., Crotti E., “Environmentally friendly concretes manufactured with CSA cement”, *ACI Special Publication*, 2018, 326;
- Coppola L., Coffetti D., Crotti E., “Rheological and physical performance of mortars manufactured with plain and ultrafine fly ashes”, *ACI Special Publication*, 2018, 326;
- Coppola L., Coffetti D., Crotti E., “CSA-based mortars manufactured with tartaric acid-based retarder”, *ACI Special Publication*, 2018, SP 329, pp. 373-388.

Finally, the monograph was further published by the author in the field of construction materials:

- Coppola L., Buoso A., Coffetti D., Crotti E., “Valutazione della collaudabilità delle strutture in c.a. e c.a.p e accertamento delle responsabilità dell’impresa e del fornitore di calcestruzzo – Manuale d’uso per il calcolo della resistenza strutturale e potenziale in accord a NTC 2018, line guida e norma UNI EN 13791:2019”, *Dario Flaccovio Editore*, ISBN 9788857911748, pp. 164, 2020.

ANNEX B

Table B - 1 Color intensity coordinates of WC specimens exposed South

		WC-0	WC-1	WC-3	WC-5
0 days	L	80.73	83.18	82.41	81.40
	A	0.58	0.56	0.52	0.22
	B	2.78	2.40	2.78	2.38
30 days	L	81.97	83.19	84.26	82.35
	A	0.83	0.79	0.76	0.48
	B	3.38	3.30	3.58	3.36
75 days	L	81.43	82.95	84.21	80.72
	A	0.82	1.23	0.92	0.69
	B	3.60	3.93	4.03	3.73
135 days	L	81.12	83.19	83.21	82.28
	A	0.88	0.98	0.92	0.67
	B	4.17	4.13	4.48	4.12
180 days	L	82.01	82.59	83.77	83.25
	A	1.14	0.91	1.00	0.80
	B	4.98	4.43	5.45	5.40

Table B - 2 Color intensity coordinates of WC specimens exposed North

		WC-0	WC-1	WC-3	WC-5
0 days	L	82.2	82.84	83.65	81.02
	A	0.79	0.15	0.27	0.20
	B	2.56	2.24	2.65	1.39
30 days	L	82.33	83.18	83.73	82.53
	A	2.92	0.84	0.89	0.67
	B	3.41	3.13	3.82	3.13
75 days	L	83.72	83.17	83.8	82.82
	A	0.82	0.71	0.93	1.36
	B	3.01	3.39	3.95	3.71
135 days	L	84.2	82.62	84.43	83.57
	A	1.11	0.88	0.88	0.72
	B	3.51	4.10	4.48	4.09
180 days	L	84.32	81.96	83.79	83.40
	A	0.89	0.94	1.06	0.92
	B	3.64	4.91	6.15	6.31

Table B - 3 Color intensity coordinates of GC specimens exposed South

		GC-0	GC-1	GC-3	GC-5
0 days	L	69.5	68.7	70.26	70.56
	A	-0.27	-0.34	-0.25	-0.23
	B	0.65	0.70	0.71	0.69
30 days	L	70.56	68.64	71.69	71.28
	A	-0.20	0.27	-9.80	-0.14
	B	0.87	1.26	0.81	0.97
75 days	L	69.9	68.42	70.38	71.43
	A	-0.16	-0.18	-0.18	0.05
	B	0.98	1.45	1.33	1.32
135 days	L	71.43	69.89	71.38	71.74
	A	-0.21	-0.09	-0.29	-0.14
	B	0.63	1.58	1.15	1.45
180 days	L	70.74	69.94	72.09	71.58
	A	-0.20	-0.17	-0.16	-0.12
	B	1.46	1.59	1.70	2.02

Table B - 4 Color intensity coordinates of GC specimens exposed North

		GC-0	GC-1	GC-3	GC-5
0 days	L	68.66	68.04	70.91	70.52
	A	-0.46	-0.45	-0.34	-0.27
	B	1.03	1.48	1.04	1.07
30 days	L	68.38	69.07	68.68	71.18
	A	-0.01	0.07	-0.15	0.15
	B	0.79	1.52	1.37	1.67
75 days	L	69.68	69.01	71.07	71.04
	A	-0.29	-0.20	-0.23	0.09
	B	0.47	1.62	1.29	1.79
135 days	L	69.16	70.18	71.93	72.51
	A	0.13	0.02	-0.07	0.38
	B	0.90	1.76	1.61	2.02
180 days	L	69.54	68.86	71.50	74.13
	A	-0.23	-0.23	-0.04	0.07
	B	1.20	1.91	2.42	2.14

Table B - 5 Color intensity coordinates of S8 specimens exposed South

		S8-0	S8-1	S8-3	S8-5
0 days	L	72.96	73.37	76.03	78.08
	A	1.84	1.67	1.37	1.15
	B	7.28	7.04	6.16	5.84
30 days	L	73.65	74.37	77.61	77.63
	A	1.95	1.83	1.88	1.47
	B	7.73	7.45	6.78	6.65
75 days	L	72.63	73.81	77.71	76.68
	A	2.07	1.80	1.51	1.47
	B	8.14	7.42	6.66	6.87
135 days	L	72.45	72.45	77.23	77.17
	A	1.97	1.93	1.59	1.45
	B	8.36	8.13	7.44	7.16
180 days	L	70.35	70.19	75.20	75.45
	A	2.07	2.14	1.76	1.74
	B	9.07	9.14	8.05	8.38

Table B - 6 Color intensity coordinates of S8 specimens exposed North

		S8-0	S8-1	S8-3	S8-5
0 days	L	71.92	73.6	75.27	76.56
	A	1.88	1.30	1.20	1.05
	B	7.60	7.07	6.58	6.16
30 days	L	72.95	73.8	76.67	77.81
	A	2.21	1.81	1.64	1.30
	B	7.79	7.48	6.91	6.25
75 days	L	72.11	72.76	76.87	76.71
	A	2.35	1.75	1.54	1.33
	B	8.43	7.93	6.84	6.68
135 days	L	70.59	72.8	75.14	76.64
	A	2.06	1.99	1.81	1.50
	B	8.85	8.11	7.45	7.18
180 days	L	68.90	69.48	73.34	73.60
	A	2.28	1.96	2.13	1.78
	B	9.92	9.26	8.45	8.96

Table B - 7 Color intensity coordinates of S12 specimens exposed South

		S12-0	S12-1	S12-3	S12-5
0 days	L	75.49	76.99	76.28	79.51
	A	1.70	1.52	1.40	1.11
	B	7.04	6.40	5.95	5.30
30 days	L	77.45	76.98	77.18	80.73
	A	1.68	2.02	1.43	1.28
	B	7.29	7.14	6.40	5.69
75 days	L	77.11	77.14	78.23	80.82
	A	1.72	1.64	1.33	1.15
	B	7.44	6.95	6.23	5.56
135 days	L	76.75	77.85	77.77	80.36
	A	1.69	1.93	1.46	1.24
	B	7.53	7.20	6.58	5.95
180 days	L	76.19	75.26	77.47	80.12
	A	1.80	2.16	1.44	1.25
	B	8.02	7.97	7.18	6.69

Table B - 8 Color intensity coordinates of S12 specimens exposed North

		S12-0	S12-1	S12-3	S12-5
0 days	L	74.54	76.05	76.38	78.93
	A	1.41	1.24	1.10	0.90
	B	6.90	6.54	6.16	5.59
30 days	L	75.57	77.69	77.34	80.19
	A	1.79	1.47	1.47	1.22
	B	7.19	6.80	6.45	5.86
75 days	L	76.05	77.86	77.37	80.71
	A	1.62	1.49	1.63	1.14
	B	7.45	6.89	6.70	5.91
135 days	L	75.74	77.09	78.35	79.62
	A	1.90	1.82	1.49	1.23
	B	7.73	7.16	6.62	6.30
180 days	L	75.91	76.87	78.05	78.97
	A	1.72	1.61	1.56	1.34
	B	8.25	7.83	7.32	7.51

Table B - 9 Color intensity coordinates of S16 specimens exposed South

		S16-0	S16-1	S16-3	S16-5
0 days	L	78.18	79.46	77.72	79.81
	A	1.36	1.38	1.23	1.20
	B	6.29	6.30	5.60	5.29
30 days	L	77.92	79.71	79.00	81.45
	A	1.56	1.50	1.30	1.36
	B	6.40	6.63	5.80	5.67
75 days	L	77.34	78.8	79.28	81.04
	A	1.80	1.82	1.21	1.14
	B	6.78	6.70	5.66	5.18
135 days	L	78.12	79.68	78.87	81.69
	A	1.62	1.47	1.12	1.30
	B	7.06	6.80	5.89	5.51
180 days	L	77.55	78.93	78.91	81.26
	A	1.63	1.53	1.42	1.40
	B	7.73	7.42	6.60	6.28

Table B - 10 Color intensity coordinates of S16 specimens exposed North

		S16-0	S16-1	S16-3	S16-5
0 days	L	75.94	77.83	77.69	80.64
	A	1.18	1.17	1.05	1.09
	B	5.98	6.84	6.11	5.86
30 days	L	76.63	79.61	78.48	81.36
	A	1.46	1.42	1.30	1.26
	B	6.42	6.85	6.05	5.55
75 days	L	77.57	78.49	78.14	78.79
	A	3.22	1.32	1.13	1.12
	B	7.59	6.84	5.84	5.95
135 days	L	77.2	78.99	79.05	80.68
	A	1.60	1.48	1.27	1.25
	B	7.19	7.01	6.05	5.86
180 days	L	76.84	77.57	79.91	80.76
	A	1.71	1.65	1.40	1.53
	B	7.82	7.84	6.62	6.65